EPA-460/3-76-008-a
March 1976

STUDY ON OXIDES OF NITROGEN AND CARBON FORMATION IN DIESEL ENGINES - FINAL REPORT

U.S. ENVIRONMENTAL PROTECTION AGENCY
Office of Air and Waste Management
Office of Mobile Source Air Pollution Control
Emission Control Technology Division
Ann Arbor, Michigan 48105

EPA-460/3-76-008-a

STUDY ON OXIDES OF NITROGEN AND CARBON FORMATION IN DIESEL ENGINES - FINAL REPORT

by

C.J. Kau, T.J. Tyson, and M.P. Heap

Ultrasystems, Inc.
2400 Michelson Drive
Irvine, California 92664

Contract No. 68-01-0436

EPA Project Officers: J.L. Bascunana and G.D. Kittredge

Prepared for

COORDINATING RESEARCH COUNCIL, INC.
30 Rockefeller Plaza
New York, N. Y. 10020

APRAC CAPE 20-71

and

ENVIRONMENTAL PROTECTION AGENCY
Office of Air and Waste Management
Office of Mobile Source Air Pollution Control
Emission Control Technology Division
Ann Arbor, Michigan 48105

March 1976

This report is issued by the Environmental Protection Agency to report technical data of interest to a limited number of readers. Copies are available free of charge to Federal employees, current contractors and grantees, and nonprofit organizations - as supplies permit - from the Air Pollution Technical Information Center, Environmental Protection Agency. Research Triangle Park, North Carolina 27711; or, for a fee, from the National Technical Information Service, 5285 Port Royal Road, Springfield, Virginia 22161.

This report was furnished to the Environmental Protection Agency by Ultrasystems, Inc., Irvine, California, in fulfillment of Contract No. 68-01-0436. The contents of this report are reproduced herein as received from Ultrasystems, Inc. The opinions, findings, and conclusions expressed are those of the author and not necessarily those of the Environmental Protection Agency. Mention of company or product names is not to be considered as an endorsement by the Environmental Protection Agency.

Publication No. EPA-460/3-76-008-a

ACKNOWLEDGEMENTS

This report presents the outcome of almost four year's work and many individuals have contributed to the final product. The authors would like to express their thanks to several present and former Ultrasystems staff members, G. P. Carver, C. McComis, K. Maloney, L. J. Muzio, C. H. Waldman and R. P. Wilson, Jr., for their efforts in the early stages of the model's development and in the conduct of the experimental investigations.

The CAPE 20-71 Steering Committee of the Coordinating Research Council and the EPA originally defined the project and guided the work to it's final outcome. The ultimate value of this project is largely due to the Committee, without whose help and criticism it would have been difficult to complete. The authors sincerely acknowledge their gratitude to the following individuals who have served on the Steering Committee during the lifetime of the project:

F. J. Hills, Committee Chairman	Mobil Research & Development Corporation
J. L. Bascunana	Environmental Protection Agency
N. G. Beck	International Harvester
T. C. Belian	Coordinating Research Council
J. E. Bennethum	General Motors Research Laboratory
G. L. Borman	University of Wisconsin
W. L. Brown	Caterpillar Tractor
J. C. Hoelzer	International Harvester
G. D. Kittredge	Environmental Protection Agency
G. A. Lavoie	Ford Motor Company
D. F. Merrion	General Motors-Detroit Diesel Allison
P. C. Meurer	International Harvester
J. M. Perez	Caterpillar Tractor
S. M. Shahed	Cummins Engine
A. D. Tuteja	General Motors-Detroit Diesel Allison
A. V. Wilson	Cummins Engine
A. E. Zengel	Coordinating Research Council

TABLE OF CONTENTS

1.0 SUMMARY

A modular model describing the processes of energy release and pollutant formation in direct injection diesel engines has been developed and tested. The model consists of separate modules describing the following processes:

- Cylinder thermodynamics and heat transfer;
- Fuel injection and spray characterization;
- Air spray entrainment and droplet vaporization;
- Ignition delay;
- Air product mixing;
- Heat release;
- Nitric oxide formation;
- Soot formation and oxidation.

It was recognized at an early stage of development that a model of this type must be able to evolve with time. Consequently, the total package was constructed to ensure that any of the modules listed above could be readily updated as more definitive information becomes available. In essence, the present model provides a framework which can be readily used by other workers, after simple modification, for their own specific purposes.

The model contains a considerable number of empirical constants which have been divided into two groups:

- Those constants whose values are perhaps not universal, but which remain unaffected by gross changes in engine design, or do not strongly influence predictions of pollutant formation.
- Those constants which require adjustment to allow accurate predictions and which will require a certain degree of readjustment if the model is used outside its original frame of reference.

A sensitivity study has been carried out to ascertain the influence coefficients of these adjustable constants on nitrogen oxide and soot formation.

Experience gained during the development of the model and during subsequent application has highlighted two areas of major importance:

- Macromixing. The results of the sensitivity study indicated that the most sensitive parts of the model are those parameters related to fuel/air mixing.
- Spherical droplet diffusion flames. The model suggests that non-premixed heat release regions can not be adequately described by single droplet diffusion flames.

Chemistry inherently sets the lower limit on pollutant formation in diesel engines, however, it is not the governing mechanism. Macromixing, fuel and air contacting on the macroscale is the limiting mechanism. Consequently, it is not surprising that those parameters included in the model which influence fuel/air mixing have the strongest influence on pollutant formation.

Two regions are identified in the model which appear to be of major importance from the aspect of NO formation:

- Those regions where combustion products are well mixed on a scale which is small compared to the total volume of that region, and therefore, local gradients can be neglected. The NO formation rate is calculated by a non-equilibrium homogeneous model based upon extended Zeldovich kinetics.
- Those regions in the vicinity of fuel droplets which allow the formation of spherical diffusion flames. These regions are typified by steep gradients, and molecular diffusion plays a strong role.

Calculations indicate that the total exhaust NO level is dominated by NO produced in the former regions. In the model as it now stands, droplet diffusion flames do not contribute a significant fraction of the total NO production under normal diesel operating conditions. This can be attributed to:

- A large fraction of the droplets are contained within rich zones which cannot support spherical diffusion flames;

- The droplet lifetime is restricted to the time period close to top dead center where the available volume is small and, therefore, the volume available for the single flame is small, thus minimizing the total flame surface area;
- The droplet environment contains NO which will reduce the net rate of NO formation.

Model predictions have been compared with experimental data generated in a single cylinder diesel engine for the following operation and engine parameters:

- Load (or overall air/fuel ratio)
- Fuel injection timing
- Engine speed
- Compression ratio
- Exhaust gas recirculation
- Air swirl
- Fuel nozzle diameter
- Turbocharge.

Based upon comparison with single cylinder test data, it is concluded that the overall predictive capability of the model with respect to pressure history and exhaust NO level is adequate. However, its ability to predict exhaust soot emissions can only be considered fair. The model includes an arbitrary empirical relationship describing carbon formation in fuel rich regions since a more fundamental understanding of the chemistry of carbon formation is not presently available.

Experience with the model indicates that several minor modifications are possible which will improve and extend the model; these include:

- modifications to the equilibrium species tables to allow fuels of different hydrogen/carbon ratios to be easily treated and to extend these tables to higher pressures and richer mixtures;
- limits can be imposed on the equilibrium assumptions to enable carbon monoxide and hydrocarbon emissions to be included;

- the ignition model can be extended to more adequately reflect the fuel history; and
- mixing between burning zones can be included.

Four areas have been identified in which the model is deficient and which require more extensive work to include in the model:

- fuel injection schedules can rarely be approximated by a constant injection rate. The present model is limited to a constant fuel injection rate;
- the model considers that the jet behaves throughout its lifetime as a steady state jet, the influence of the transient nature of the jet is neglected;
- fuel/air mixing dictate pollutant emission levels and a more realistic mixing model which reflects the three dimensionality of the process and which includes fuel vapor segregation should be included. An effort must be made to ascertain the degree to which the well-ordered jet structure is maintained throughout the cycle; and
- as other components in the model are improved, the deficiencies in the equilibrium heat release model will become more apparent and some kinetic overlay will be called for.

In conclusion, it should be recognized that the model has only been compared against one set of single cylinder engine data. Before further improvements are made to the model, more extensive tests will be required to fully uncover both the weaknesses and the strong points in the model. Modifications should also be made to the basic model to allow prechamber engines to be accommodated.

2.0 INTRODUCTION

This report presents the culmination of three years effort to provide diesel engine designers with an analytical tool to aid in the development of clean, efficient diesel engines. The initial phase of this program was concerned with the construction and operation of a single cylinder engine to provide data on pollutant formation and to give some insight into the mechanism of pollutant formation. Experimental information was generated with which to test the analytical model to be developed in a later phase. The successful completion of this work has been adequately described by Wilson et al[1]. The second phase of the work, namely the construction, modification and exercise of a mathematical model to predict pollutant formation in a diesel engine is described in this report.

The general objective of the total study was to provide industry with a working computerized tool to aid engine development. This tool was to be developed in an iterative manner in conjunction with diagnostic experiments planned to provide information on the phenomena occurring within the cylinder during combustion. The model development included in this report is confined to direct injection engines, although the experimental investigations described by Wilson et al[1] include data on prechamber configurations. At the initiation of the project is was hoped that the model development would include both configurations. However, the realities of modeling such a complex process as intermittent combustion in a compression ignition engine dictated otherwise. The progress of combustion and, therefore, energy release and pollutant formation is dominated by the fuel/air mixing process. Since the mixing processes are entirely different in the two configurations, this would necessitate two separate models. Constraints imposed by time and budget precluded the development of two models and it was decided to concentrate the modeling effort on direct injection engines. The constraints stated above also prevented application of the model to other engine geometries and multi-cylinder engines.

3.0 THE METHODOLOGY OF DIESEL ENGINE MODELING

Diesel engines are a fact, they operate satisfactorily in all manner of equipment. A significant reason for attempting to develop an analytical model describing the processes occurring within a diesel engine can be that such a model lies on the critical path to the construction of a more efficient, cleaner engine. As a design tool the analytical model is at present in its infancy. The complex interaction of physical and chemical processes occurring in a diesel engine involve phenomena which are not completely understood at present. However, each small advance in the state-of-the-art of modeling helps to build what can be a powerful tool in the hands of engine designers.

The mathematical simulation along will not enable improved diesel engines to be built. Development and prototype testing, rejection and redesign are mandatory. However, the availability of an analytical model which will guide this iterative process could greatly reduce development costs. This is particularly applicable to attempts to reduce pollutant emissions through engine redesign without incurring the penalty of increased fuel consumption. Pollutant formation in diesel engines is controlled by several interrelated parameters which mades complete redesign based upon intuition difficult. An accurate analytical model which has been tested and the range of applicability established, will help to guide this intuition, thus saving valuable experimental test resources.

Before presenting the detailed mathematical formulation, a qualitative description of the model developed during this program will be given and contrasted with other models.

3.1 Review of Existing Models

Wilson et al[1] reviewed, in considerable detail, the characteristics of the various models which predate the present model. However, a concise description of their salient features will be presented to allow an adequate comparison to be made with the new Ultrasystems' model.

- The NREC (Northern Research and Engineering Corporation) Model [Bastress, Chang and Dix[2]]

This model includes a prescribed heat release schedule which has two stages:

- an initial premixed triangular distribution;
- a secondary Gaussian distribution.

In both of these stages the fuel-air ratios over which heat release takes place are specified. Random mixing is assumed to account for subsequent dilution of the combustion products and Zeldovich kinetics are used to describe NO production. The model requires the arbitrary specification of six parameters: a fuel vaporization rate, fuel burning rate, dilution rate, an overall heat transfer coefficient, a mean air-fuel ratio for heat release, and an air-fuel ratio excursion parameter for the premixed heat release schedule. One major disadvantage of the NREC approach is that there is no link between the value of these parameters and the actual physical processes. Such a link will be necessary if the model is to be used to assess the effect of design changes which influence the details of the combustion process.

- The CAV Model [Khan, Greeves, and Probert[3], and Khan and Greeves[4]]

The CAV Model represents an advance from the previous model in that it includes a fuel spray model. The spray is modeled by a conical free jet which impinges upon a plane wall, thus simulating the impact of the fuel jet on the piston bowl. Experimentally determined ignition delays are input as is a triangular premixed heat release distribution. The pre-exponential constant in the modified Zeldovich NO formation mechanism was increased by a factor of 5.37 over the literature value in order to match experimental exhaust data. This model also includes an Arrhenius type expression to allow soot formation to be predicted.

- The Cummins Model [Shahed, Chiu and Yumlu[5], and Shahed, Chiu and Lyn (6)]

A preliminary version of Cummins Model (Shahed et al[5]) correctly represented the cycle thermodynamics, but ignored mixing and spray

combustion. An empirical burning law based on the work of Lyn[7] and an empirical ignition delay correlation based on data of Lyn and Valdmanis[8,9] were used and it was assumed that heat release took place under stoichiometric conditions and the subsequent mixing between stoichiometric packages of combustion products and excess air was not included. The NO model is also based upon the Zeldovich mechanism with adjusted rate constants to correctly predict experimental data.

The latest version of the Cummins model contains considerable improvements over the preliminary model, particularly in the areas of mixing and fuel spray combustion. The formulae describing unsteady jet mixing were obtained via curve fitting experimental data obtained for various engine operating conditions and geometry (e.g., various chamber pressures, temperatures, swirl levels, injection pressures and hole sizes). The stoichiometric burning and non-dilution mixing assumptions were totally discarded. Thus, a more precise mathematical representation of the NO formation processes, which is capable of reflecting the important effects of local oxygen concentration history on NO formation has been included.

3.2 A Qualitative Description of the Ultrasystems' Model

The Ultrasystems' model of pollutant formation in diesel engines has been developed along the guidelines set down by Wilson et al[1]. However, there are important differences in the details of the various model components. The model was developed recognizing that the complexity of the process will not allow the total elimination of all empirical constants from the analytical expressions. The initial concept of eliminating all arbitrarily assigned constants has not been achieved. Certain adjustable constants have been included and these are discussed in detail in a later section. The aim of this section is to describe the model in qualitative terms before the mathematical formulation is presented in Section 4.

Figure 3-1 presents a general view of the various components of the model which has been constructed in such a way that any of these components can be modified as additional information becomes available. The model simulates conditions occurring in the cylinder of a four stroke direct injection

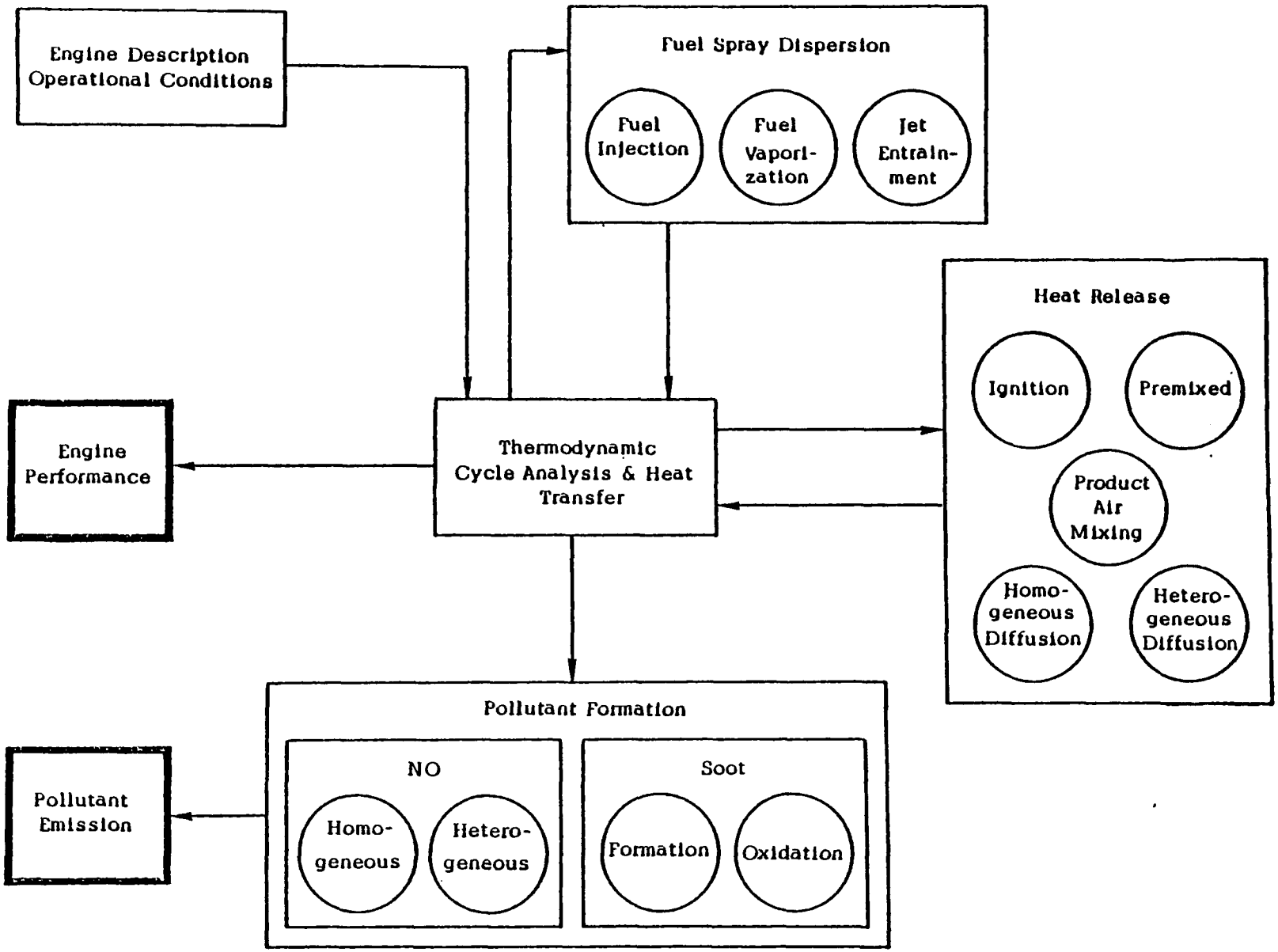

Fig. 3-1 Elements of the Ultrasystems Model

diesel engine from the crank angle degree of intake valve closure to the angle at which the exhaust valve opens. The model is built around the thermodynamic cycle and heat transfer analysis components which both receives and supplies information to and from the other components of the model. The interaction of the separate modules can be seen in Figure 3-1.

Fuel Spray Dispersion

In the fuel spray dispersion module the fuel jet is modeled as though it were a steady axisymmetric unconfined wall jet. Figure 3-2 shows a pictorial representation of the initial stages of the jet before impact. The fuel injection schedule is considered to be uniform and the fuel forms droplets of a specified size distribution immediately upon injection. In order to ascertain the subsequent history of all the fuel elements in 1° crank angle intervals it is considered to be distributed equally between four shells. Thus, each element of fuel can be denoted, both by its age and by its initial location in the jet. The fuel jet entrains air in the manner prescribed by well-established theories of turbulent jet mixing. Thus, the total mass in each shell will increase and those shells on the periphery of jet will have fuel air ratios lower than those shells on the jet axis.

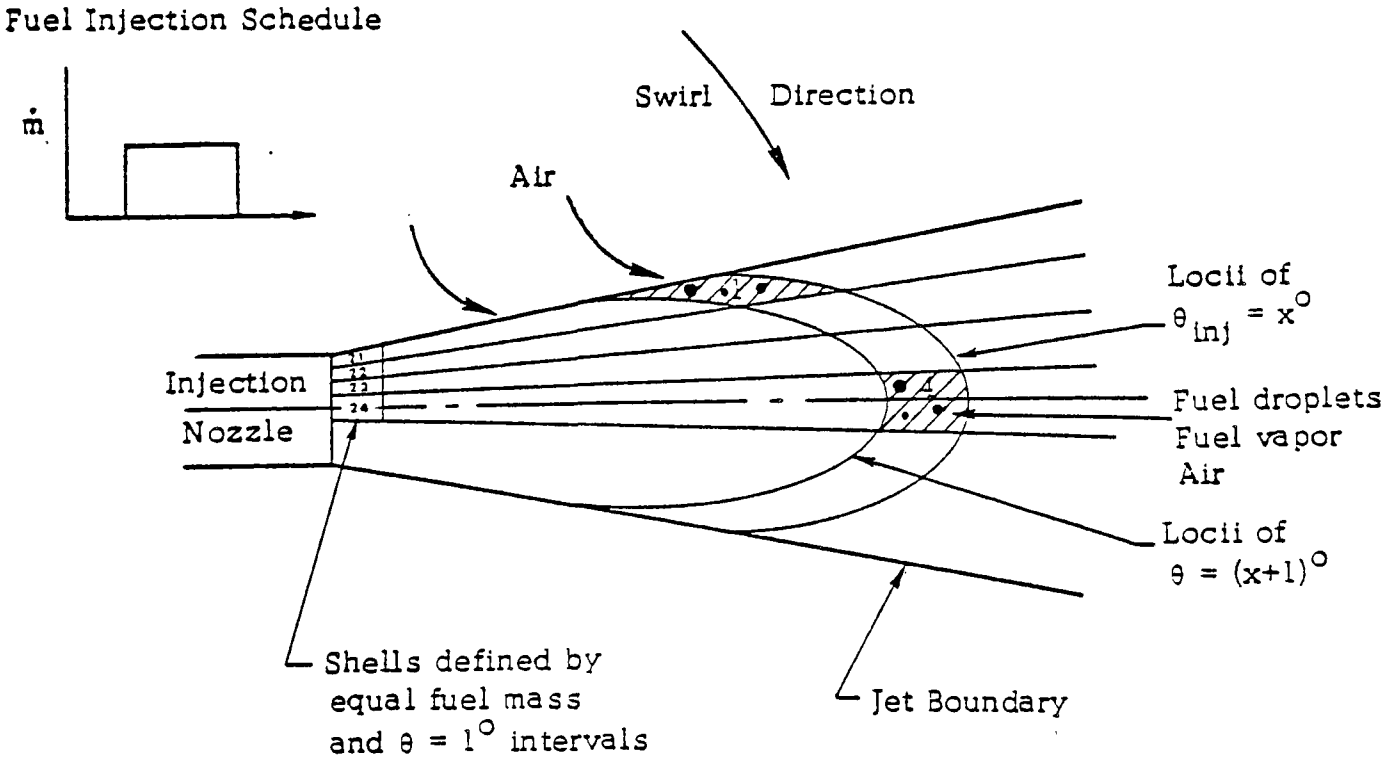

Figure 3-2. Pictorial Representation of the Fuel Jet

During the entrainment stage, the fuel droplets are treated as a single component hydrocarbon compound which will begin to vaporize when a stable wet bulb temperature is obtained. The rate of evaporation is influenced by the swirl velocity of the air sweeping through the jet, thus as the fuel element passes along the jet, its vaporization rate is increased, both by virtue of the increase in temperature of its environment, and also because of the increased angular velocity. The fuel that is vaporized remains in the parent shell. Thus, immediately before ignition the fuel jet consists of parcels of fuel, all mixing with air, which contain droplets in various stages of vaporization. The multi-orifice fuel injector is handled by dividing the total available air equally between the separate jets and assuming all jets are exactly similar.

Quite obviously, this is a very simple picture of a complex process which ignores all three dimensional effects, non-steady phenomena and influence of confinement. Several omissions should be enumerated:

- Cross flow — the swirl introduced with the air charge increases entrainment, but the jet remains axisymmetric. With sufficiently high swirl velocities the cross flow effects will deflect the jet axis and distort the circular section into a kidney shape (see Figure 3-3). Air entrainment will be different on the upwind and downwind sides. There is the possibility that vapor and small droplets will migrate in the direction of the cross flow.
- Non-steady jet — no attempt is made to include the transient effects of an intermittent jet, i.e., the nature of the leading and the trailing edges.
- Three dimensional effects — the jets exist in a finite and continuously changing space. The jet impact upon the piston bowl is not normal to a plane surface.
- Jet interaction — at no time are the fuel jets considered to interact.

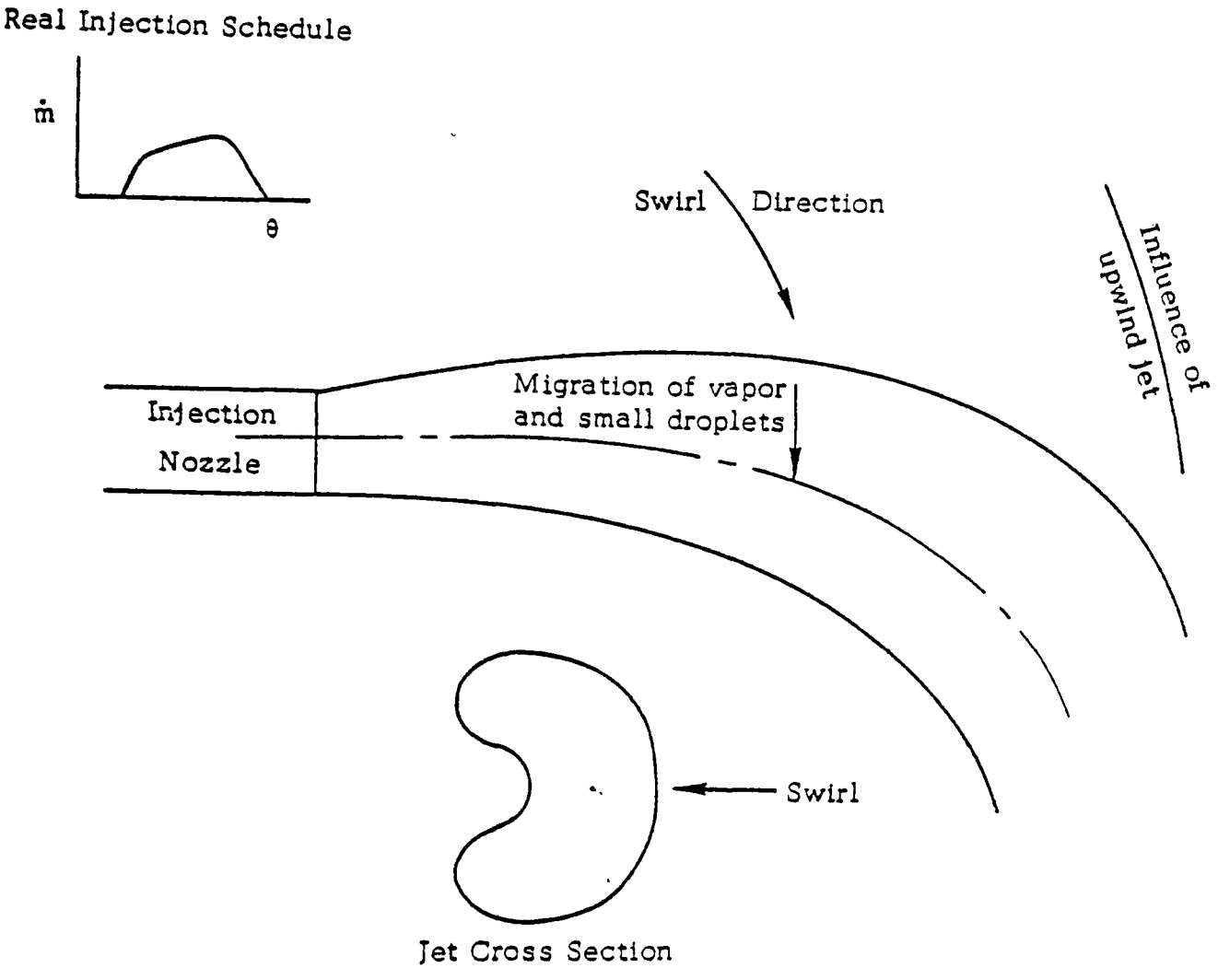

Figure 3-3. Schematic Showing Simplified Cross Flow Effects

Heat Release

The complex chemistry of ignition is not included in the model. A shell containing air and fuel vapor will ignite when an empirical ignition criterion has been satisfied. This criterion depends upon the properties of the fuel and the average pressure and temperature over the period of time before ignition takes place. Once ignited the vapor reacts with the air producing equilibrium combustion products. Initial heat release rates were too slow when a turbulent flame speed model was used to ignite other shells. An improved simulation has been achieved by allowing successive ignition in other shells when they also satisfy the ignition criteria.

Once ignition has occurred, the location of that shell is no longer tracked in space, but only in time. Mass transfer between air and zones containing combustion products and vaporizing fuel droplets is no longer considered to be controlled by the turbulent jet mixing model. All the air is assumed to be equally available to all the parcels of fuel and the mixing rate is dependent upon the mass of air available and the mass of each package of burned products. Air is vitiated with combustion products, but no provision is made for mixing to take place between packages of products. This random mixing process is related to the turbulence properties of the air charge, but it still includes an empirical constant.

The mechanism of heat release depends upon the state of the fuel and oxygen availability. The chemistry of hydrocarbon combustion is not included. Ignited fuel vapor, or fuel vaporizing in a rich zone is immediately transformed into equilibrium products. Droplets vaporizing in oxygen rich atmospheres can support spherical diffusion flames. No criterion is included for flame blow-off or the production of wake flames.

Pollutant Formation

The model does not consider that the pollutant species, nitric oxide and soot are in chemical equilibrium. The rates of formation and destruction of these species are calculated from simple kinetic considerations assuming that the species involved in their production and oxidation are in equilibrium. Extensive reviews of the kinetic mechanism of NO formation in combustion processes are available in the literature[10]. The model includes the following reactions:

$$N_2 + O \rightleftharpoons NO + N$$

$$N + O_2 \rightleftharpoons NO + O$$

which is usually referred to as the Zeldovich mechanism. This approach does not include any coupling of the hydrocarbon chemistry with the nitric oxide formation, either in terms of superequilibrium atom concentrations, or Fenimore type reactions[11], e.g.,

$$N_2 + CH \rightleftharpoons HCN + N$$

Once NO has been formed in lean zones, it could be reduced in rich zones by such reactions as[12]

$$NO + CH \longrightarrow HCO + N$$

which would allow the formation of nitrogen by

$$N + NO \longrightarrow N_2 + O$$

Although NO_2 has been observed both in flat flames and turbulent diffusion flames, no attempt has been made to allow for the formation of NO_2 within the cylinder. This might occur by the reaction of NO with HO_2 and its presence in the exhaust would depend upon the quench rate since the high temperatures would favor its conversion to NO.

The model allows for the formation of NO both in the homogeneous burned gas zones and during droplet combustion. The spherical droplet diffusion flames were originally included because it was believed that diffusion zones of this type were characteristic of the regions of pollutant formation in diesel engines. Also, mathematical analyses were available for single droplets contained in an infinite environment. Initial calculations indicated that these analyses gave the "improbable" situation that the flame volume was greater than the avilable cylinder volume. Consequently, the diffusion flame analysis was modified to include a bounded environment "filling up" with combustion products.

The model for soot formation is similar to that used earlier by other workers. The only difference is in the definition of zonal equivalence ratio to include both reacted and unreacted oxygen. Oxidation of soot is also included.

4.0 DETAILED DESCRIPTION OF A MODEL TO PREDICT POLLUTANT FORMATION IN DIESEL ENGINES

The physical and chemical processes controlling heat release and pollutant formation in diesel engines are extremely complex. The model, described in detail in this section, has been developed upon the premise that many of these processes can be decoupled from each other and, therefore, the total process can be subdivided into several tractable components. Although each of these components contains certain simplifying assumptions to make them mathematically amenable, every effort has been made to ensure that they retain their physical significance. Thus, a modular model has been developed which reflects the present state-of-the-art but which will allow any of its components to be updated independently as an improved understanding of the controlling phenomena is achieved. The separate components of the model are:

- The cycle thermodynamics and heat transfer
- Fuel injection and spray characterization
- Air spray entrainment and droplet vaporization
- Ignition delay
- Air product mixing
- Combustion
- Nitric oxide formation
- Soot formation and oxidation

A complete description of symbols, superscripts and subscripts included in these various components is given in Section 8, Nomenclature.

Cycle Thermodynamics and Heat Transfer

The cycle thermodynamic analysis serves as the skeleton upon which the separate components of the whole model are assembled and it describes the thermodynamic state of the cylinder contents during the compression and expansion processes for that period of the cycle when both the intake and the exhaust valves are closed.

At any instant the cylinder contents, which may be either gaseous or liquid, are considered to exist in separate zones:

> Air zone: the mixture of fresh air, recirculated exhaust gas (if any) and residual gas. Subsequent to ignition the "air" zone is vitiated and mixed with the burning gas zone. The properties related to this zone are identified by subscript "a".

Vaporizing liquid fuel zone: for thermodynamic purposes, all the pre-ignition liquid fuel is considered to exist in one single zone. This zone is identified by subscript "fl".

Burning liquid fuel zone: all the post-ignition liquid fuel, which is either engulfed by combustion products or diffusion flame envelopes is considered to exist in one single zone which is identified by the subscript "flb".

Fuel vapor zone: thermodynamically, all the vaporized fuel (either mixed or unmixed with air) is considered to exist in a single zone prior to ignition, designated by the subscript "fv". This approach might well introduce errors into the calculation of the thermodynamic properties during the ignition delay. However, it is considered that these errors will have little influence on overall pollutant predictions.

Burning zones: the zones which contain the combustion products are identified by subscripts which indicate both the time of ignition and the proximity to the fuel spray axis at the time of ignition (see Figure 3-2). Each burning zone is subsequently fed either by the combustion products generated by diffusion flames or by fuel vapor (when conditions do not allow diffusion flames to be established) from the fuel droplets engulfed by the zone itself. Although mass transfer between burning zones and the air zone, i.e., dilution and vitiation, is taken into consideration, the mass transfer between burning zones is not considered. Burning zones are signified by double subscript "bm,I".

The basic assumptions contained in the cycle thermodynamics model are:

- pressure is uniform throughout the cylinder;
- each zone is considered to be thermodynamically homogeneous;
- each zone radiates independently to the cylinder wall (i.e., radiative exchange between zones is not considered);
- the kinetic energy of the fluid within the cylinder is neglected except when it is required to characterize the velocity of the cylinder contents;
- the sole source of heat necessary for fuel vaporization is provided by the "air" zone;
- the specific heat of both the vapor and liquid fuel is constant;
- a "mixed burned" assumption is used to account for the combustion of the premixed air and vaporized fuel and equilibrium combustion products are formed immediately following ignition;

- the thermodynamic properties and species concentration (except those of nitric oxides and soot) of the "air" and burning zones are assumed to be in their equilibrium state based upon the zonal temperature, equivalence ratio and the pressure.

It should be stressed that the zones above are conceptual and although their total volume at any instant is that of the cylinder volume, their physical shape is irrelevant. The mass transfer between each of the zones is calculated by other relevant model components. Thus, the rate of liquid fuel vaporization is controlled by the fuel vaporization model, which relates to the physical process. However, for thermodynamic purposes, once vaporized all of that fuel is assumed to exist in one hypothetical zone. Figure 4-1 presents a pictorial representation of the cylinder contents showing the mass transfer between the various zones. The basic mathematical formula describing the thermodynamic state of these zones can be expressed by the following set of conservation equations.

Basic Energy Conservation Equations

Following the first law of thermodynamics, the basic energy conservation equations can be written as:

"Air"

$$\overline{\dot{m}_a u_a} = -h_a \dot{m}_D - [h_a \dot{m}_{apb}] + \Sigma h_{bm,I} \dot{m}_{v,I} - P \overline{\dot{\forall}_a V} - (\forall_a \dot{Q}_c + \dot{q}_{ra} + \dot{q}_{el}) + (h_{fj} - u_{fj}) \dot{m}_{fj} \qquad (4\text{-}1)$$

The last term represents the pumping work and kinetic energy dissipation associated with the injection of the fuel into the air which is generally negligible and is included only for self-consistency.

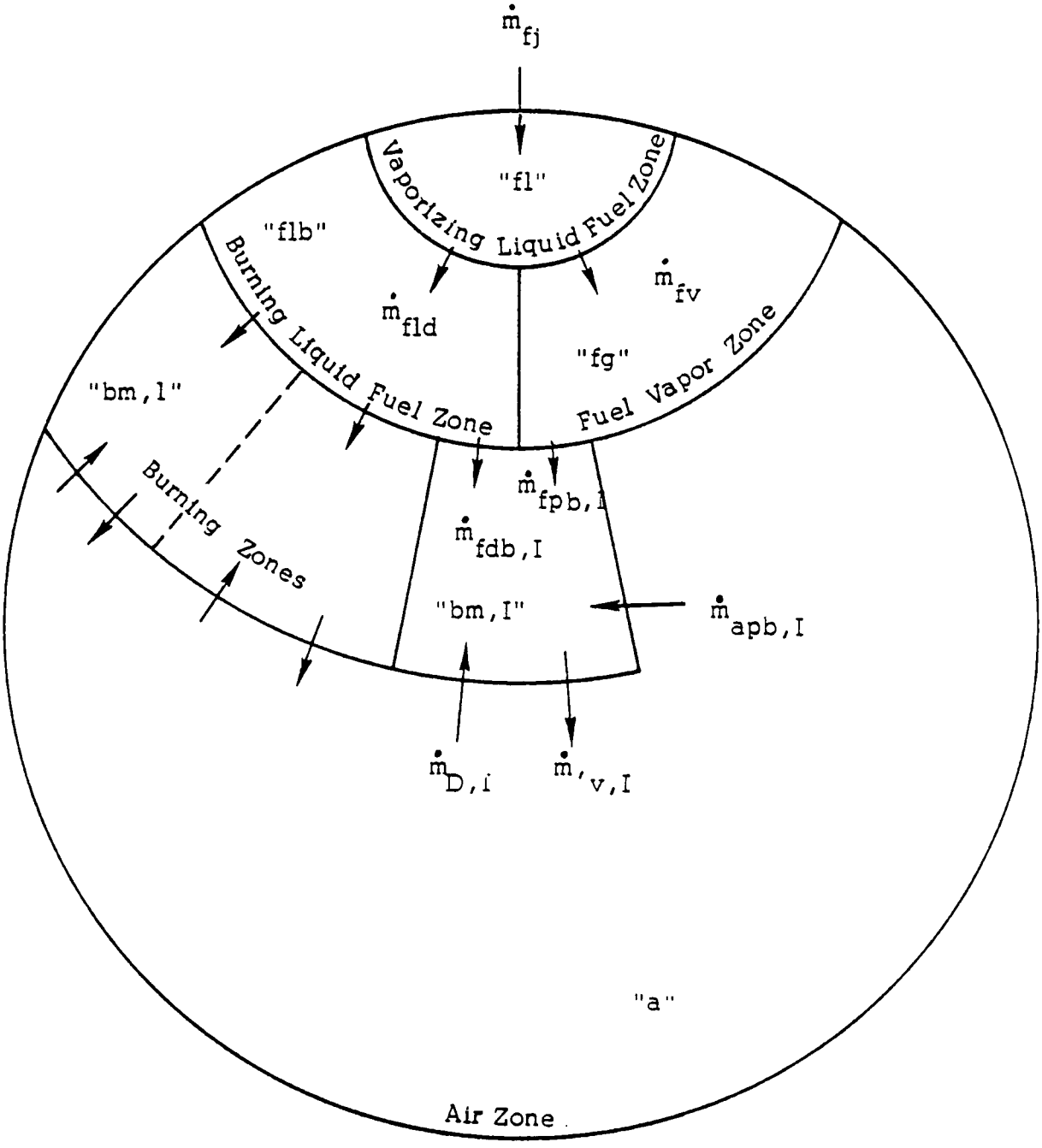

Figure 4-1 Conceptual Zones of Cylinder Contents

Liquid Fuel (Vaporizing)

$$\dot{\overline{m_{fl}\, u_{fl}}} = u_{fj}\,\dot{m}_{fj} - h_{fv}\,\dot{m}_{fv} - u_{fl}\,\dot{m}_{fld} + \dot{q}_{e1} \tag{4-2}$$

Liquid Fuel (Burning)

$$\dot{\overline{m_{flb}\, u_{flb}}} = u_{fl}\,\dot{m}_{fld} - h_{fd}\,\dot{m}_{fdb} + \dot{q}_{e2} \tag{4-3}$$

Fuel Vapor

$$\dot{\overline{m_{fg}\, u_{fg}}} = h_{fv}\dot{m}_{fv} - [h_{fg}\,\dot{m}_{fpb}] - P\,\dot{\overline{\beta_{fg} V}} - (\gamma_{fg}\dot{Q}_c + \dot{q}_{rfg}) \tag{4-4}$$

Burning Systems

$$\dot{\overline{m_{bm,I}\, u_{bm,I}}} = h_a\dot{m}_{D,I} + h_{fd}\dot{m}_{fdb,I} + [h_a\dot{m}_{apb,I} + h_{fg}\dot{m}_{fpb,I}] - h_{bm,I}\dot{m}_{v,I} - P\,\dot{\overline{\beta_{bm,I} V}} - (\gamma_{bm,I}\dot{Q}_c + \dot{q}_{rbm,I} + \dot{q}_{e2,I}) \tag{4-5}$$

Here dot represents the time rate of change in crank angles (i.e., $d/d\theta$).

The relative zonal volumes of gaseous systems to the total cylinder volume under uniform pressure, are defined by

$$\beta_a = \frac{m_a\, R_a\, T_a}{PV} \tag{4-6}$$

$$\beta_{fg} = \frac{m_{fg} R_{fg} T_{fg}}{PV} \tag{4-7}$$

$$\beta_{bm,I} = \frac{m_{bm,I} R_{bm,I} T_{bm,I}}{PV} \tag{4-8}$$

The instantaneous total volume of the engine cylinder is computed by:

$$V(\theta) = V_c + \frac{\pi}{4} D_e^2 R_w \left(1 - \cos\theta + \frac{R_L - \sqrt{R_L^2 - R_W^2 \sin^2\theta}}{R_W}\right) \tag{4-9}$$

The fraction factors for zonal convective heat transfer rate are evaluated by:

$$\gamma_a = \frac{(T_a - T_w)\ \beta_a^{2/3}}{B} \tag{4-10}$$

$$\gamma_{fg} = \frac{(T_{fg} - T_w)\ \beta_{fg}^{2/3}}{B} \tag{4-11}$$

$$\gamma_{bm,I} = \frac{(T_{bm,I} - T_w)\ \beta_{bm,I}^{2/3}}{B} \tag{4-12}$$

where normalizations were made by B, which is

$$B = (T_a - T_w)\ \beta_a^{2/3} + (T_{fg} - T_w)\ \beta_{fg}^{2/3} + \sum_I (T_{bm,I} - T_w)\ \beta_{bm,I}^{2/3} \tag{4-13}$$

and the mean cylinder wall temperature T_w, is used in above equations.

Mass Conservation Equation

The law of conservation of mass in each zone is described by the following mass rate balance equations:

"Air"

$$\dot{m}_a = \dot{m}_V - \dot{m}_D - \dot{m}_{apb} \tag{4-14}$$

Liquid Fuel (Vaporizing)

$$\dot{m}_{fl} = \dot{m}_{fj} - \dot{m}_{fv} - \dot{m}_{fld} \tag{4-15}$$

Liquid Fuel (Burning)

$$\dot{m}_{flb} = \dot{m}_{fld} - \dot{m}_{fdb} \tag{4-16}$$

Fuel Vapor

$$\dot{m}_{fg} = \dot{m}_{fv} - \dot{m}_{fpb} \tag{4-17}$$

Burning System

$$\dot{m}_{bm,I} = \dot{m}_{D,I} + \dot{m}_{fpb,I} + \dot{m}_{fpb,I} + \dot{m}_{apb,I} - \dot{m}_{v,I} \tag{4-18}$$

Equivalence Ratio

In order to determine the composition and theromodynamic properties of each zone, instantaneous equivalence ratios must be calculated. This can be achieved by maintaining separate accounts for the mass of pure air and the mass of fuel in each zone. The equivalence ratio of the "air" zone is governed by

$$\dot{\phi}_a = (m_{pa,a}\dot{m}_{f,a} - m_{f,a}\dot{m}_{pa,a}) \Big/ f_{os}\,\dot{m}^2_{pa,a} \tag{4-19}$$

where the total flux of fuel and pure air due to the various rate processes, i.e. vitiation, dilution and combustion can be expressed by:

$$\dot{m}_{f,a} = \sum \eta_I \dot{m}_{v,I} - \eta_a (\dot{m}_D + \dot{m}_{apb}) \tag{4-20}$$

$$\dot{m}_{pa,a} = \sum \alpha_I m_{v,I} - \alpha_a (\dot{m}_D + \dot{m}_{apb}) \tag{4-21}$$

Similarly, the equivalance ratio of the burning zone is governed by:

$$\dot{\varphi}_{bm,I} = (m_{pa,I}\dot{m}_{f,I} - m_{f,I}\dot{m}_{pa,I}) \Big/ f_{os}\,\dot{m}^2_{pa,I} \tag{4-22}$$

where

$$\dot{m}_{f,I} = \dot{m}_{fdb,I} + \dot{m}_{fpb,I} + \eta_a \dot{m}_{D,I} - \eta_I \dot{m}_{v,I}$$

$$\dot{m}_{pa,I} = \alpha_a \dot{m}_{D,I} - \alpha_I \dot{m}_{v,I} \tag{4-23}$$

and η and α are defined by:

$$\eta = \frac{f}{(1 + f)} \qquad (4\text{-}24)$$

$$\alpha = \frac{1}{(1 + f)}$$

Caloric Equations of State

The combustion products are assumed to be in thermodynamic and chemical equilibrium and the properties of the "air" and burning zones can be calculated based upon the pressure, the local temperature and the local equivalence ratio. Consequently, it is possible to express the internal energy and the gas constant of the combustion products and the "air" by the following general forms, i.e.,

$$U(P,T,\phi) = \frac{1}{1 + f_{os}\phi}\left\{\sum_{i=1}^{6} a_i T^{i-1} - \left(\sum_{i=1}^{6} b_i T^{i-1}\right)\phi\right.$$

$$+ \exp\left[d_1 + d_2\phi + d_3\phi^3 + (d_4 + d_5\phi + d_6\phi^3)\theta^{-1}\right.$$

$$\left.\left. + d_7 + d_8\phi + d_9\phi^3 + (d_{10} + d_{11}\phi)\theta^{-1} \ln P\right]\right\} \left(\frac{\text{cal}}{\text{gm}}\right) \qquad (4\text{-}25)$$

where

$$\theta = \frac{T}{1000}$$

and f_{os} is the stoichiometric air-fuel ratio based on the fuel used, and

$$R(P,T,\phi) = \frac{1}{1 + f_{os}\phi} \left\{ (r_1 + r_2\phi) + \exp\left[(r_3 + r_4\theta^{-1} + r_5 \ln P)\phi + (r_6 + r_7\theta^{-1} + r_8 \ln P)\right] \right\} \quad \left(\frac{\text{cal}}{\text{gm} - {}^{\circ}\text{K}}\right) \tag{4-26}$$

The polynomial coefficients a_i, b_i, d, and r_i can be obtained, for a particularly specified fuel composition by nonlinear least-square curve fitting of the calculated results from the NASA equilibrium program (Gordon and McBride[13]). The fuel consists of 50 percent n-heptane and 50 percent toluene and has a H/C ratio of approximately 1.7 and the coefficients which have been obtained are tabulated in Tables B-1 and B-2 in Appendix B for the range:

$$300 \leq T \leq 3500^{\circ}\text{K}$$
$$0.7 \leq P \leq 100 \text{ atm}$$
$$0.0 \leq \phi < 3.5$$

The fit is within 2 percent for lean mixtures, however there is a larger error of approximately 5 percent for very rich mixtures. Tables B-1 and B-2 must be modified for fuels of H/C ratio which differ significantly from 1.7

Over-all Conservation Equations

The overall energy conservation equation is obtained by summing up equations (4-1) through (4-5), i.e.,

$$\dot{m}_a u_a + \dot{m}_{fl} u_{fl} + \dot{m}_{flb} u_{flb} + \dot{m}_{fg} u_{fg} + \sum_I \dot{m}_{bn,I} u_{bm,I} \qquad (4\text{-}27)$$

$$= -\dot{P}V + h_{fj}\dot{m}_{fj} - \dot{Q}_c - \dot{Q}_r$$

where $\dot{Q}_r$ is the overall radiation loss from all zones, i.e.,

$$\dot{Q}_r = \dot{q}_{ra} + \dot{q}_{rfg} + \sum_I \dot{q}_{rbm,I} \qquad (4\text{-}28)$$

The over-all mass conservation equation is obtained by summing equations from (4-14) through (4-18), thus:

$$\dot{m}_a + \dot{m}_{fl} + \dot{m}_{flb} + \dot{m}_{fg} + \sum_I \dot{m}_{bm,I} = \dot{m}_{fj} \qquad (4\text{-}29)$$

The equation of state can be written as

$$\frac{PV}{J} = \sum_i m_i R_i T_i \qquad (4\text{-}30)$$

where

$i = a,\ fg,\ (bm,I)$

and J is the mechanical equivalent of heat.

Working Energy Conservation Equations

Internal energy and mass conservation relationships are expressed by polynomials, thus the energy conservation equations for the "air" and burning zones can be solved for the following temperate rate equations:

$$\dot{T}_a = A_a \dot{P} + B_a \tag{4-31a}$$

where

$$A_a = \frac{\left(m_a \frac{R_a T_a}{P} - \frac{\partial u_a}{\partial P} - T_a \frac{\partial R_a}{\partial P}\right)}{C_a}$$

$$B_a = \left\{ -\dot{m}_a \left(T_a \frac{\partial R_a}{\partial \varphi_a} + \frac{\partial u_a}{\partial \varphi_a}\right) \dot{\phi}_a + \Sigma (h_{bm,I} - h_a) \dot{m}_{V,I} - (\gamma_a \dot{Q}_c + \dot{q}_{ra} + \dot{q}_{el}) + (h_{fj} - u_{fl}) \dot{m}_{fj} \right\} / C_a$$

$$C_a = m_a \left(\frac{\partial u_a}{\partial T_a} + R_a + T_a \frac{\partial R_a}{\partial T_a} \right)$$

and

$$\dot{T}_{bm,I} = A_{bm,I} \dot{P} + B_{bm,I} \tag{4-31b}$$

where

$$A_{bm,I} = \frac{m_{bm,I} \left(\frac{R_{bm,I} T_{bm,I}}{P} + \frac{\partial U_{bm,I}}{\partial P} - T_{bm,I} \frac{\partial R_{bm,I}}{\partial P} \right)}{C_{bm,I}}$$

$$B_{bm,I} = \left(\frac{1}{C_{bm,I}}\right) x$$

$$\left\{ - m_{bm,I} \left(T_{bm,I} \frac{\partial R_{bm,I}}{\partial \phi_{bm,I}} + \frac{\partial U_{bm,I}}{\partial \phi_{bm,I}} \right) \dot{\phi}_{bm,I} + (h_a - h_{bm,I}) (\dot{m}_{D,I} + \dot{m}_{apb,I}) \right.$$

$$\left. + (h_{fd} - h_{bm,I}) \dot{m}_{fdb,I} + (h_{fg} - h_{bm,I}) \dot{m}_{fpb,I} - (\gamma_{bm,I} \dot{Q}_c + \dot{q}_{rbm,I} + \dot{q}_{e2,I}) \right\}$$

and

$$C_{bm,I} = m_{bm,I} \left(\frac{\partial U_{bm,I}}{\partial T_{bm,I}} + T_{bm,I} \frac{\partial R_{bm,I}}{\partial T_{bm,I}} + R_{bm,I} \right)$$

Similarly for fuel vapor we have

$$\dot{T}_{fg} = A_{fg} \dot{P} + B_{fg} \qquad (4\text{-}31c)$$

where

$$A_{fg} = \frac{R_{fg} T_{fg}}{P \left(c_{vfg} + R_{fg} \right)}$$

$$B_{fg} = \frac{(h_{fv} - h_{fg}) \dot{m}_{fv} - (\dot{\gamma}_{fg} \dot{Q}_c + \dot{q}_{rfg})}{m_{fg} (c_{vfg} + R_{fg})}$$

If Eqns (4-27) & (4-29) are introduced into the differentiated over-all equation of state, $\dot{p}$ can be written by

$$\dot{P} = \frac{\left\{ - \frac{P}{J} \dot{V} + \sum_I R_i T_i \dot{m}_i + \sum_I m_i T_i \frac{\partial R_i}{\partial \phi_i} \dot{\phi} + \sum_I m_i \left(R_i + T_i \frac{\partial R_i}{\partial T_i} \right) B_i \right\}}{\left\{ \frac{V}{J} - \sum m_i T_i \frac{\partial R_i}{\partial P} - \sum m_i \left(R_i + T_i \frac{\partial R_i}{\partial T_i} \right) A_i \right\}}$$

(4-31d)

where i = a, fg, (bm,I) and the volume rate is expressed by:

$$\dot{V} = \frac{\pi}{4} D_e^2 R_w \sin\theta \left(1 + \frac{R_w}{R_L} \frac{\cos\theta}{\sqrt{1 - \left(\frac{R_w}{R_l}\right)^2 \sin^2\theta}} \right)$$

Equations (4-31a) through 4-31c) are the working form of energy conversation equations.

Convective Heat Transfer

The gross convective heat transfer to the cylinder walls is expressed in a similar method to that used by Annand[14].

$$\dot{Q}_c = \left[A_c \frac{\kappa}{D_e} R_e^{B_c} A (\bar{T} - T_w) \right] \frac{dt}{d\theta} \qquad (4\text{-}32)$$

where

- κ is the mean thermal conductivity of cylinder gas
- R_e is the Reynolds number based on the mean piston velocity and cylinder bore
- $\bar{T}$ is the average gas temperature
- T_w is the average cylinder wall temperature
- A is the surface area of the cylinder chamber
- D_e is the bore

It should be noted that two empirical constants, A_c and B_c, have been introduced whose accepted values range from 0.17 to 0.49 for A_c, and $B_c = 0.7$[15,16].

Radiative Heat Transfer

The rate of radiative heat transfer from each zone to the cylinder wall is expressed by

$$\dot{q}_{rbm,I} = \left[A_I \bar{\alpha} \left(1 - e^{-KL_I} \right) \sigma \left(T_{bm,I}^4 - T_w^4 \right) \right] \frac{dt}{d\theta} \qquad (4\text{-}33)$$

K is a mean attenuation coefficient which will depend upon the concentration of radiating species (gases and particles), the number of particles, the particle cross section and the optical properties of those particles. McAuley[15] gives a value of K as 5.7×10^2 cm^3/gm x the zonal fuel concentration. L_I and A_I are the characteristic length and surface area of the zone respectively.

Similar expressions are also used for evaluation of the rate of radiative heat transfer from fuel vapor and "air" zones to the cylinder wall. However, they are negligible because of the very low zonal temperatures or the very low fuel concentration.

4.2 Fuel Injection and Spray Characterization

For the purposes of this work, the fuel jet is treated as an incompressible jet with a constant flow rate and the injection velocity is derived by:

$$v_{fjo} = \dot{m}_{fj}/(\rho_l A_{nozzle} C_D) \tag{4-34}$$

where $\dot{m}_{fj}$ the modified fuel flow rate is defined as

$$\dot{m}_{fj} = \frac{\text{mass of fuel injected per power stroke}}{\Delta\theta_{ing} N_{nozzle}} \tag{4-35}$$

It is assumed that the fuel spray breaks into droplets immediately upon injection and that the droplets have a specified size distribution. The drop-size distribution is described by an upper-limit distribution function, the fraction of the total fuel mass, having a dropsize within the interval $d_{i-1} \leq d \leq d_i$ being given by

$$G_i = \frac{\Delta m_1}{m_{tot}} = \frac{1}{2}\left\{ \text{erf}\left[\delta \ln\left(\frac{d_i}{d_{max} - d_i} \right) \right] - \text{erf}\left[\delta \ln\left(\frac{d_{i-1}}{d_{max} - d_{i-1}} \right) \right] \right\} \quad (4\text{-}36)$$

The maximum droplet size, d_{max}, is directly proportional to the nozzle diameter, and is inversely proportional to the product of the Weber and Reynolds numbers to the 1/4 power, and to the pressure of the cylinder air charge at the time of injection to the 1/5 power, i.e.,

$$d_{max} = C_{max} d_{nozzle}^{1/2} \sigma_l^{1/4} \Delta_P^{-3/8} \rho_l^{-1/8} \mu_l^{1/4} \rho_a^{-1/5} \quad (4\text{-}37)$$

where

Δ_P is the pressure difference across the injector orifice in (dyne/cm^2)

σ_l is the liquid surface tension in (gm/sec^2)

μ_l is the fuel viscosity in (gm/cm-sec)

d_{nozzle} is the nozzle diameter in (cm)

The two empirical parameters in the above expressions δ and C_{max}, have values of 0.85 and 37.5, respectively, which represent the best fit to experimental data by Lee[17].

4.3 Air Spray Entrainment and Droplet Vaporization

The analytical representation of the phenomena associated with the fuel spray dispersion is perhaps the single most important component of any model of diesel engine combustion. The complexity of the actual situation, which involves a heterogeneous, confined unsteady jet subjected to cross flow defies rigorous mathematical description at present. Consequently, simplifying assumptions and empirical relationships must be included to allow the rate of fuel-air mixing and droplet vaporization to be quantified. The analysis developed for inclusion in the overall model has the following objectives:

- To describe the gross fuel-air distribution within the fuel jet;
- To track the trajectory of fuel elements of known "age";
- To define the state of a fuel-air parcel at the onset of ignition, i.e., the fuel-air vapor ratio, the liquid vapor fuel ratio and the dropsize distribution.

The gross oversimplification is made in the analysis of the fuel spray dispersion that the fuel jet can be considered as a steady unconfined wall jet of air and vaporizing fuel droplets, shown schematically in Figure 4-2. The similar transverse velocity profiles are based upon constant injection conditions throughout the injection period. The steady state properties of the jet are determined in Eulerian coordinates. Each element of fuel is labeled upon injection, both with respect to its age (i.e., crank angle at injection) and its radial location within the jet. Both the location and the conditions of each fuel-air parcel are determined in Lagrangian coordinates by integrating the Lagrangian Eulerian (time space) relationship. The rate of droplet vaporization is determined by the properties of the surrounding air which will vary, both in space and time. This approach, which may be termed a "pseudo-steady" spray model, neglects:

- the effect of piston motion upon the spray geometry;
- relative motion between the droplets and the air;

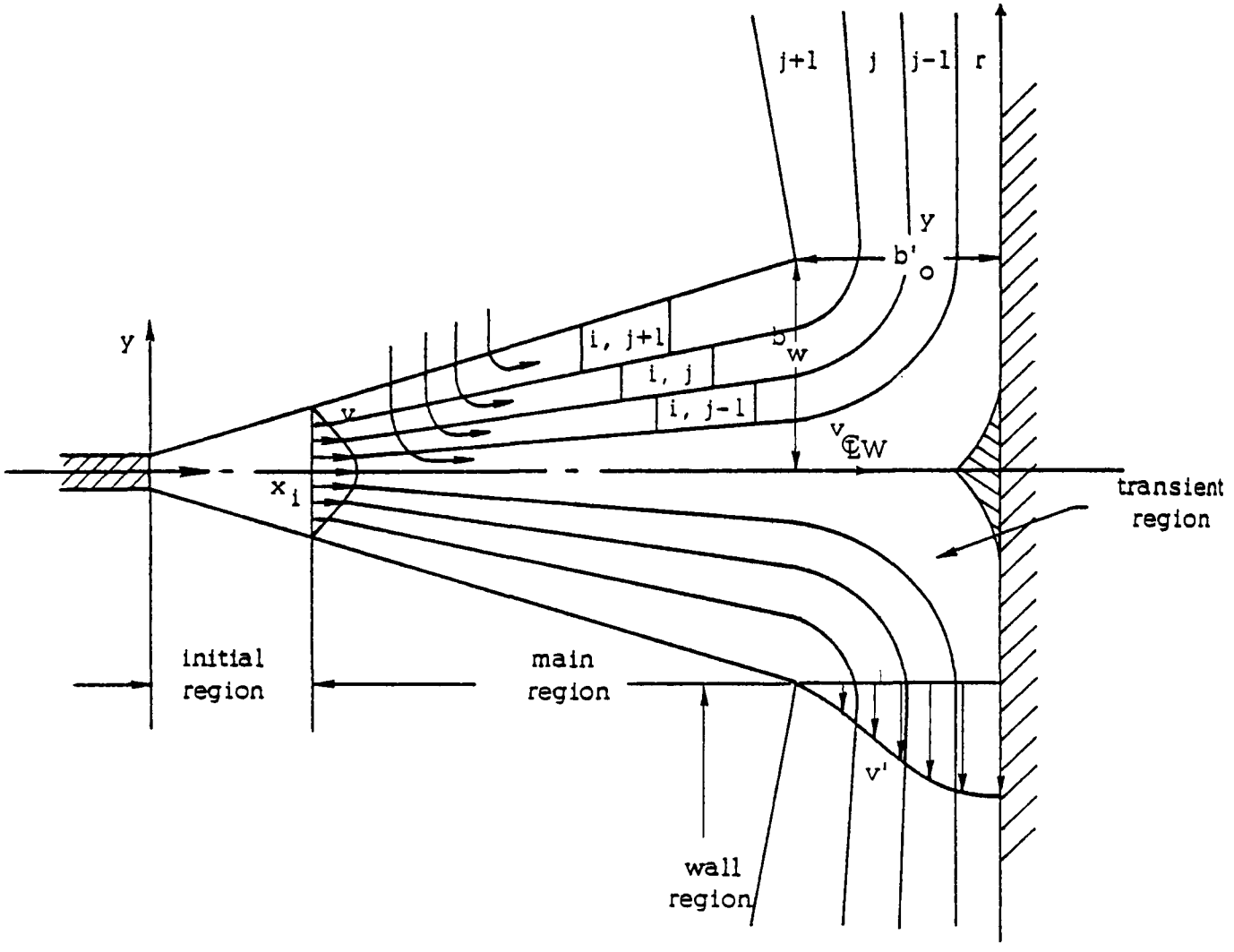

Note: I is equivalent to [(i-1) X (No. of shells) + j]

Figure 4-2 Schematic of Fuel Spray

- the transition zone from a free to a wall jet;
- the fuel volume;
- the curvature of the piston bowl;
- preferential fuel vapor transfer, all vapor remains associated with the parent fuel parcel;
- the influence of confinement both by the piston and cylinder walls and the adjacent fuel jets.

However, the following phenomena are included in the analysis:

- droplet heat-up and vaporization;
- jet entrainment due to impingement upon the wall;
- the influence of swirl on the jet entrainment rate.

The relationships governing the behavior of an unconfined jet impinging upon a plane wall in a quiescent atmosphere can be drived from fundamental turbulent jet theory (see Abramovich[18]) and the detailed formulations have been included in Appendix A. The influence of air swirl induced by the masked inlet valve on the fuel-air mixing rate is approximated by

$$\frac{m_a}{(m_a)_o} = 1.0 + C_{sef}\,(v_s/v_{fjo}) \qquad (4\text{-}42)$$

where C_{sef} is an adjustable constant obtained by matching experimental data.

Wise and Agoston[19] proposed a correction to the normal vaporization rate to account for liquid droplets in crossflow. A similar expression has been used to account for the influence of the swirling air motion on

droplet vaporization. The ratio of the vaporization rate, $\dot{m}_v$, to the vaporization rate without swirl $(\dot{m}_v)_o$ is given by:

$$\frac{\dot{m}_v}{(\dot{m}_v)_o} = 1.0 + C_{evap} Re^{1/2} Pr^{1/2} \tag{4-43}$$

where the Reynolds number is based upon both the droplet diameter and the swirl velocity and it is assumed that Pr = 1. The empirical constants C_{evap} is set at 0.276.

The vaporization rate without swirl is given by

$$(\dot{m}_v)_o = 4\pi\rho D r_l \ln \left|1 + \frac{1}{L} C_p (T_\infty - T_l)\right| \tag{4-44}$$

Under high pressure high temperature conditions the heat of vaporization is a function of droplet temperature T_l:

$$L = L_{298} \left(\frac{T_{crit} - T_l}{T_{crit} - 298}\right)^{0.38}$$

where L_{298} and T_{crit} are the latent heat at 298°K and the critical temperature of the fuel respectively. The droplet temperature is assumed to have a uniform value equal to the stable wet-bulb temperature based upon the conditions of the surroundings at the beginning of the fuel injection. Methods for evaluating the stable wet-bulb temperature of a vaporizing droplet are discussed in the recent work of Rosner and Chang[20]. A mean heat-up time τ_{hu} is used to account for the time taken for the droplet to attain the stable wet bulb temperature.

4.4 Ignition Delay

The objective of the ignition delay model is to provide a relationship whereby the time of ignition of each fuel/air parcel can be evaluated. The ignition delay time is calculated using the expression from work of Shipinski[21].

$$\tau_{ig} = A_{ig} (N_{ce})^{B_{ig}} (\bar{P})^{C_{ig}} \exp (E_{ig}/R\bar{T}) \qquad (4\text{-}45)$$

where τ_{ig}, the time of ignition in seconds, and the pressure and temperature are the average values calculated over the delay period, in atmospheres and ^{o}K respectively. The ignition delay model includes four empirical constants

$$A_{ig} = 1,224 \times 10^{-4}$$

$$B_{ig} = -0.69$$

$$C_{ig} = -0.386$$

$$E_{ig} = 9290 \text{ cal/mole}$$

representing the best fit to the experimental data.

4.5 Air Product Mixing

High speed photographic records were made during Phase I of the present program (Wilson et al[1]) which tended to suggest that after the initial vapor phase heat release, the contents of the cylinder approach well-stirred conditions on the macroscale. To accommodate these observations the model allows mass transfer to take place between "air" and "burning" zones in a random manner. After ignition of the vapor/air mixture in a fuel/air parcel the combustion product-droplet-air mixture continues to mix with the air zones, but not with other fuel/air parcels. Thus, the air zone is being continuously vitiated and vitiated air is being mixed with the vaporizing droplets. In the light of recent in-cylinder sampling investigations (see Appendix C) it appears that the concept of random mixing may not be representative of actual conditions. The mixing process used in the model does not retain any memory of the jet structure once ignition has occurred. However, although only preliminary results are available, sampling valve data suggest that mixing process may be dependent upon jet properties some time after ignition has taken place.

The air product mixing is modeled as a completely random process, i.e., the well-ordered jet is considered to have broken down and the mass

rate of dilution and vitiation is derived with the following provisions:

- only the "air" and burning zones are involved;
- turbulence is unsteady but homogeneous throughout the engine cylinder;
- the overall dilution rate decreases as the mass of available air decreases;
- overall dilution rate vanishes with the total mass of combustion products;
- the zonal dilution rate depends upon the zonal surface area in contact with "air" zone. This area is assumed to be proportional to the zonal volume

Thus, a rate of dilution can be expressed by

$$\frac{dm_D}{d\theta} = \frac{1}{\tau_{mix}} \frac{m_{aa} m_{bm}}{m_{aa} + m_{bm}} \qquad (4\text{-}46)$$

where m_{aa} is the mass of the "air" available for mixing, and is equal to the mass of unburnt "air" less the mass of "air" mixed with unburnt fuel vapor. An expression similar to Eqn (4-46) has been used by Bastress et al[2] where τ_{mix} was input as a arbitrary adjustable constant. Physically, τ_{mix} in Eqn (4-46) is the characteristic mixing time (measured in crank angles) and is related to the characteristic turbulent length scale ℓ and the turbulent diffusivity D by:

$$\tau_{mix} \propto \frac{\ell^2}{D}$$

the turbulent diffusivity is in turn related both to the scale of turbulence, ℓ, and the scale of turbulent velocity v_{turb} by:

$$D \propto \ell \cdot v_{turb}$$

Finally, ℓ and v_{turb} are scaled by the volume surface area ratio and mean flow velocity.

$$\ell \propto L = \frac{V}{A}$$

$$v_{turb} \propto \overline{U} = v_{char}$$

The characteristic charge velocity is defined by:

$$v_{char} = \left[\frac{m_a^o \left(v_p^2 + \overline{v}_s^2 \right) + m_{fj} v_{fjo}^2}{m_a^o + m_{fj}} \right]^{1/2}$$

where v_p is instantaneous piston velocity and $\overline{v}_s$ is the swirl velocity based upon swirl angular velocity and half bowl radius assuming solid body rotation. v_{fjo} is the fuel injecting velocity.

$$\tau_{mix} \propto \frac{L}{\overline{U}}$$

or

$$\tau_{mix} = \frac{RPM \times L}{C_{mix} \overline{U}} \qquad (4\text{-}47)$$

Here empirical constant C_{mix} is introduced. The zonal dilution rate for each burning zone is estimated by

$$\frac{dm_{D,I}}{d\theta} = \frac{\beta_{bm,I}}{\sum \beta_{bm,I}} \left(\frac{dm_D}{d\theta} \right) \qquad (4\text{-}48)$$

The vitiation rate from each burning zone is assumed to be directly proportional to the dilution rate and therefore can be evaluated by

$$\frac{dm_{v,I}}{d\theta} = C_{vidi} \frac{dm_{D,I}}{d\theta} \qquad (4\text{-}49)$$

4.6 Combustion

Combustion may take place within the cylinder in several modes. Fuel can exist in either the vapor state, or liquid droplets, the air can be mixed with the fuel prior to reaction or a flame can separate the reactants and diffusion of both reactants will, therefore, dictate the rate of heat release. The rate and timing of the heat release will control both engine performance and pollutant formation. In reality this complex process will involve droplets burning as clouds, combustion close to solid surfaces, fuel impingement on the piston bowl vaporization and subsequent combustion. However, the simplified approach included in this model only takes account of:

- Homogeneous premixed, fuel vapor mixed with the air prior to ignition
- Heterogeneous, fuel burns as single droplets surrounded by a diffusion flame in a fuel lean zone.
- Homogeneous diffusion, diffusion flames cannot be supported around droplets existing in fuel rich zones; immediately upon vaporization this fuel reacts with its surroundings giving equilibrium products for the composition and conditions of that zone.

4.6.1 Homogeneous (Premixed) Combustion

Equation 4-45 determines the point of ignition for the premixed fuel vapor-air produced in each parcel during the preparation to burn period. The temperature of the mixture after combustion of the fuel vapor is assumed to be the equilibrium temperature at the equivalence ratio, pressure and specific internal energy pertaining to that parcel. This assumption will only be valid when the residence time is greater than 10^{-4} seconds since certain radicals will not have equilibrated before that time. This time scale is slightly less than one degree C.A. for an engine operating at 1500 rpm.

4.6.2 Heterogeneous (Droplet) Combustion

When fuel droplets exist in an environment containing oxygen, reactions can occur in a narrow zone surrounding the droplet-the diffusion flame envelope. In recent years numerous theoretical and experimental studies have been carried out to establish the mechanism of combustion of single droplets in an infinite atmosphere (Williams[22,23]). Due to the complexity of the process, none of this work can be directly applied to heterogeneous combustion in diesel engines. The droplets do not exist in an infinite environment and interaction will take place between droplets. The atmosphere is not quiescent thus allowing the formation of wake flames or producing complete flame blow-off. Calculations indicate that droplet combustion does not take place as though single droplets existed in an unbounded environment since the volume necessary to accommodate such flames was found to be many times the engine displacement. The ultimate solution will involve some form of unsteady combustion coupled with effects due to relative motion between the droplet and its surroundings. As a very small first step, the classical droplet theories have been modified to provide flame confinement and to allow continuous vitiation of the atmosphere surrounding the droplets.

The basic assumption involved in the analytical solution for confined pseudo-steady state droplet combustion which has been included in the model are:

- combustion takes place under quasi-steady state conditions;
- the rate of chemical reaction involved in heat release are infinity fast
- the pressure throughout the system is uniform
- the system is spherically symmetric
- average values are used for the specific heat and thermal conductivity of the gas and liquid phases
- Lewis number is unity (i.e., $\rho D = \frac{\lambda}{c_p} = \text{constant}$)
- liquid temperatures are constant, the droplet temperature is given by the stable wet-bulb temperature of vaporization thus temperature transients in the liquid phase are neglected

- radiant heat transfer is negligible
- single component fuel composition
- body forces and internal motion within the droplet are negligible
- the droplets exist in a large but finite space which is continuously vitiated during the entire droplet lifetime.
- convective effects are neglected, the diffusion flame limit depends solely on ambient oxygen concentration.

The governing differential equations of mass, species and energy conservation are written as (Williams [23])

Continuity (4-50)

$$\frac{1}{r^2} \frac{d}{dr} (r^2 \rho v) = 0$$

Species

$$\rho v \frac{dY_i}{dr} = \frac{1}{r^2} \frac{d}{dr} \left(\rho D r^2 \frac{dY_i}{dr} \right) + \dot{w}_i \qquad (4-51)$$

Energy

$$\rho v \frac{dT}{dr} = \frac{1}{r^2} \frac{d}{dr} \left(\frac{\lambda}{c_p} r^2 \frac{dT}{dr} \right) - \frac{1}{c_p} \sum h_i^o \dot{w}_i \qquad (4-52)$$

The equation of state is

$$\rho T = \text{Constant} \qquad (4-53)$$

The boundary conditions at the droplet surface r_l, the flame surface r_f, and the assumed radius of influence r_∞ are presented below.

(i) at the droplet surface ($r = r_\ell$)

$$T = T_\ell \tag{4-54}$$

$$Y_{O2} = 0 \tag{4-55}$$

$$-\left[\rho D \frac{dY_i}{dr}\right]_+ = \left[\rho V (Y_{i+} - Y_{i-})\right] \tag{4-56}$$

$$\left[\lambda \frac{dT}{dr}\right]_+ = (\rho V L)_+ \tag{4-57}$$

Condition (4-56) is derived from species continuity at the liquid-gas interface. Condition (4-57) is deduced from an energy balance assuming a constant liquid phase temperature.

(ii) at the flame surface ($r = r_f$)

$$Y_{O2} = 0 \tag{4-58}$$

$$Y_f = 0 \tag{4-59}$$

$$-\frac{1}{j}\left(\rho D \frac{dY_{O2}}{dr}\right)_+ = \left(\rho D \frac{dY_f}{dr}\right)_- \tag{4-60}$$

$$-q \rho D \left(\frac{dY_f}{dr}\right)_- = -\left(\lambda \frac{dT}{dr}\right)_+ + \left(\lambda \frac{dT}{dr}\right)_- \tag{4-61}$$

Condition (5-60) states that the deliveries of fuel vapor and oxidant to the flame surface are in stoichiometric proportion. Condition (5-61) prescribes that the heat of combustion is equal to the sum of the heat transferred inward to the droplet and the heat transfer outward to its surroundings.

(iii) at a large distance from droplet ($r = r_\infty$)

$$T = T_\infty \tag{4-63}$$

$$Y_{O2} = Y_{O2,\infty} \tag{4-64}$$

$$Y_F = 0 \tag{4-65}$$

$$Y_{N2} = Y_{N2,\infty} \tag{4-66}$$

$$Y_{NO} = Y_{NO,\infty} \tag{4-67}$$

Analytical Solutions

Analytical integration of the governing differential will be described in this section.

If we let

$$Z_i = \frac{Y_i}{(\nu_i'' - \nu_i')W_i}$$

and

$$Z_T = \frac{C_p T}{(\nu_f'' - \nu_f')\, W_f\, q}$$

where q is the heat of combustion (in cal/gm) and ν's are the stoichiometric coefficients for a single stem chemical reaction

$$\sum_i \nu_i \chi_i \rightarrow \sum_i \nu_i'' \chi_i$$

Equations (4-51) and (4-52) become

$$\rho v \frac{dZ_i}{dr} = \frac{\rho D}{r^2} \frac{d}{dr}\left(r^2 \frac{dZ_T}{dr}\right) + \omega$$

$$\rho v \frac{dZ_T}{dr} = \frac{\rho D}{r^2} \frac{d}{dr}\left(r^2 \frac{dZ_T}{dr}\right) - \omega$$

where w is defined by $\dot{w}_i \equiv \omega(\nu_i'' - \nu_i')W_i$. If we further specify that

$$\beta \equiv Z_i - Z_j$$

or

$$\beta \equiv Z_i + Z_T$$

we have

$$\frac{\dot{M}}{r^2}\frac{d\beta}{dr} = \frac{1}{r^2}\frac{d}{dr}\left(r^2\frac{d\beta}{dr}\right)$$

where

$$\frac{\dot{M}}{r^2} \equiv \frac{\rho v}{\rho D}.$$

Integrating the above equation once, with respect to r, we have

$$\frac{d\beta}{dr} = \frac{C_1}{r^2}e^{-\dot{M}/r}$$

Further integration gives the general solution as

$$\beta = \frac{C_1}{\dot{M}}e^{-\dot{M}/r} + C_2 \qquad (4\text{-}68)$$

here C_1 and C_2 are the constants of integration, to be determined by imposing appropriate conditions in accordance with the assigned definition of β. The important relations deduced from the above general solution are explained briefly in the following.

Mass Burning Rate

The expression for mass burning rate, which is obtained by defining $\beta \equiv Z_T + Z_{O2}$ and utilizing the boundary conditions at the droplet surface and the far field, can be written as

$$\dot{m}_f = 4\pi\ \rho D r_1\ \left(\frac{r_\infty}{r_1} - r_\infty\right)\ \ell n\ (1 + B_2) \qquad (4\text{-}69)$$

Flame Radius

The location of flame surface can be identified by defining $\beta \equiv Z_f - Z_{O2}$ and making use of boundary conditions at r_1 and r_f, thus,

$$\frac{r_f}{r_1} = \left(\frac{r_\infty}{r_\infty - r_1}\right)^{\alpha} \Big/ \left[\left(\frac{r_\infty}{r_\infty - r_1}\right)^{\alpha} - 1\right] \tag{4-70}$$

where

$$B_2 = \frac{1}{L}\left[c_p\left(T_\infty - T_1\right) + \frac{q\, Y_{O2,\infty}}{j}\right]$$

$$B_4 = \frac{Y_{f1}}{1 - Y_{f1}}$$

$$\alpha = \frac{\ell n\,(1 + B_2)}{\ell n\,(1 + B_4)}$$

j = Stoichiometric Oxygen-fuel Mass Ratio

q = Heat of Combustion

Flame Temperature

In a similar manner, the temperature at the flame surface is obtained from

$$T_f = \frac{T_1 + T_\infty \dfrac{Y_{f1}}{Y_{O2,\infty}/j} + \dfrac{q\, Y_{f1}}{c_p}}{\left(1 + \dfrac{Y_{f1}}{Y_{O2,\infty}/j}\right)} \tag{4-71}$$

Additional information, such as major species and temperature distributions around a fuel droplet, are also required when it becomes necessary to evaluate the production of nitric oxide in these diffusion flames. These relations,

which can be obtained from methods similar to those described above, are listed as follows without further explanation.

Temperature Distribution

$$\begin{cases} T = T_f + \dfrac{(T_1 - T_f)\ (e^{-\dot{M}/r} - e^{\dot{M}/r_f})}{(e^{-\dot{M}/r_1} - e^{-\dot{M}/r_f})} & r < r_f \qquad (4\text{-}72) \\ T = T_\infty + \dfrac{(T_f - T_\infty)\ (e^{-\dot{M}/r} - e^{-\dot{M}/r_\infty})}{(e^{-\dot{M}/r_f} - e^{-\dot{M}/r_\infty})} & r > r_f \qquad (4\text{-}73) \end{cases}$$

Fuel Distribution

$$Y_f = \frac{Y_{f1}\,(e^{-\dot{M}/r} - e^{-\dot{M}/r_f})}{(e^{-\dot{M}/r_1} - e^{-\dot{M}/r_f})} \qquad r \le r_f \qquad (4\text{-}74)$$

and

$$Y_{f,1} = 1 - \left(\frac{1 + Y_{O2,\infty}/j}{1 + B_2}\right)$$

Oxygen Distribution

$$Y_{O2} = \frac{Y_{O2,\infty}\,(e^{-\dot{M}/r} - e^{-\dot{M}/r_f})}{(e^{-\dot{M}/r_\infty} - e^{-\dot{M}/r_f})} \qquad r > r_f \qquad (4\text{-}75)$$

Nitrogen Distribution

$$Y_{N2} = Y_{N2,\infty} + \frac{(Y_{N2,1} - Y_{N2,\infty})\ (e^{-\dot{M}/r} - e^{-\dot{M}/r_\infty})}{(e^{-\dot{M}/r_1} - e^{-\dot{M}/r_\infty})} \qquad (4\text{-}76)$$

$$r_1 \le r \le r_\infty$$

where nondimensional burning rate is defined by

$$\dot{M} = \frac{\dot{m}_f}{4\pi\rho D} \qquad (4\text{-}77)$$

and the nitrogen mass fraction at the droplet surface can be calculated by

$$Y_{N2,l} = \frac{1 - Y_{f,l}}{1 + X} \tag{4-78}$$

where

$$X = \frac{\left\{44\left[w + (w + \frac{x}{4})\left(\frac{X_{CO2}}{X_{O2}}\right)_{\infty}\right] + 18\left[\frac{x}{2} + (w + \frac{x}{4})\left(\frac{X_{H2O}}{X_{O2}}\right)_{\infty}\right]\right\}}{28\left[(w + \frac{x}{4})\left(\frac{X_{N2}}{X_{O2}}\right)_{\infty}\right]}$$

it is assumed that the only species present at the droplet surface are fuel vapor and the products of complete combustion, w represents the number of carbon atoms in a fuel molecule and x is the number of hydrogen atoms.

Determination of r_∞ in the Finite-Space Formulation

The solution for the bounded single droplet burning model requires the determination of a distance r_∞ for which the boundary conditions specified in equation 4-63 though 4-67 are applicable. This distance is evaluated by invoking the zonal oxygen concentration relation

$$\frac{4}{3}\pi r_{max}^3 \rho_\infty Y_{O2,\infty} \equiv \int_{r_f}^{r_{max}} \rho Y_{O2} (4\pi r^2 dr) \tag{4-79}$$

where r_{max} is a function of equivalent droplet center-to-center spacing. It is assumed that the volume of each zone is apportioned equally between all the droplets and r_{max} is evaluated by

$$r_{max} = \left(0.23873 \frac{V_{bm,I}}{N_d}\right)^{1/3}$$

where N_d is the total number of droplets in "I" th zone or more precisely:

$$r_{max} = 0.62 D_d$$

where D_d is droplet center-to-center spacing

Combining Eqn (4-69) and (4-71) and assuming an ideal gas Eqn (4-76) can be rewritten as:

$$r_{max}^3 = 3 \int_{r_f}^{r_{max}} \frac{\left(e^{-\dot{M}/r_f} - e^{-\dot{M}/r} \right) r^2 \, dr}{\left(e^{-\dot{M}/r_f} - e^{-\dot{M}/r}\right) + \frac{T_f}{T_\infty} \left(e^{-\dot{M}/r} - e^{-\dot{M}/r_\infty}\right)} \qquad (4\text{-}80)$$

In the above equation, T_f is readily determined from Eqn (4-70) and r_f is an implicit function of r_∞, thus Eqn (4-80) must be solved for r_∞ by graphic or trial and error methods.

A schematic of a droplet diffusion flame in a confined space is shown in Figure 4-3.

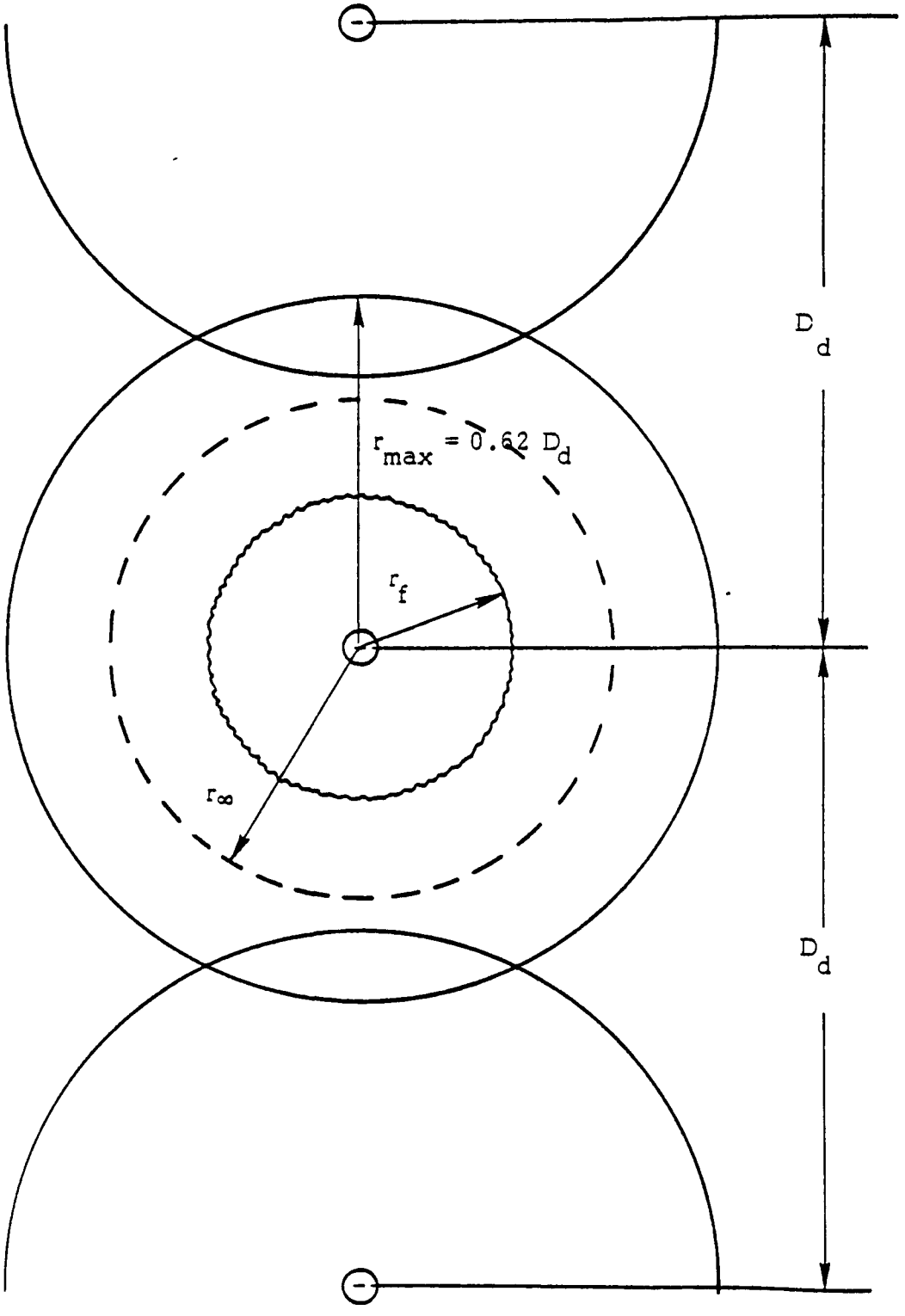

Figure 4-3 Schematic of Droplet Diffusion Flame in a Confined Space

4.7 Nitric Oxide Formation

The rate of the chemical reactions involved in the formation and destruction of nitric oxide are extremely temperature sensitive. Under conditions typical of normal diesel engine operation, characteristic residence times are small compared to the times necessary to achieve equilibrium. Consequently, the amount of nitric oxide formed will depend upon the time-temperature-pressure history of the reactants. If heat release took place in one homogeneous zone, temperatures would be too low to allow the formation of significant quantities of NO because of the extremely lean overall operating conditions. Thus, it becomes apparent that nitric oxide is formed in zones whose characteristic size is much less than the characteristic cylinder size and that local homogenity will exist on various scales within those zones.

Two zones of NO formation are identified in the model depending upon the scale of local homogenity:

- Reactants can be well mixed on a scale which is small compared to the total reacting volume and local gradients can be neglected. These well mixed zones will have a wide distribution of equivalence ratio. The rate of NO formation in regions of this type are calculated by the homogeneous NO equations.

- Reactants are separate and the reaction zone is characterized by steep gradients and molecular diffusion plays a strong role in NO formation in these regions. Reaction zones of this type can typically exist around a single droplet, a cluster of droplets or at the boundary of a fuel and air zone. In this model NO produced in diffusion flames is assumed to form around single fuel droplets and is calculated by the heterogeneous NO equations.

4.7.1 Homogeneous NO Formation

The calculation of the rate of homogeneous NO formation is based upon the Zeldovich mechanism[24] and assumes complete combustion of the reactants before NO formation begins and also that oxygen atoms are equilibrated with oxygen molecules. The governing kinetic equations are:

$$(1) \qquad O + N_2 \underset{K_{b1}}{\overset{K_{f1}}{\rightleftharpoons}} NO + N \tag{4-82}$$

$$(2) \qquad O_2 + N \underset{K_{b2}}{\overset{K_{f2}}{\rightleftharpoons}} NO + O \tag{4-83}$$

$$(3) \qquad [O]/[O_2]^{1/2} = K_{eq\,3} \tag{4-84}$$

The literature values of the forward and backward rate constants for these reactions are tabulated in Table 4-1 . The instantaneous NO production rate (gm/cm^3 - sec) in any zone can be determined by

$$(\dot{w}_I)_{Hom} = \left(\frac{30}{M_{bm,I}}\right) K_1 (m_{bm,I} - m_{df}) \left(\frac{p}{T_{bm,I}}\right)^{1/2} X_{O2}^{1/2} X_{N2} \left[\frac{1 - K_2 (X_{NO} X_{NO} / X_{N2} X_{O2})}{1 + K_3 (X_{NO}/X_{O2})}\right] (C_{nor}) \tag{4-85}$$

Where $M_{bm,I}$ is the averaged zonal molecular weight and

K_1 is equal to $0.22078\ K_{f1}K_{eq\ 3}$

K_2 is equal to $(K_{b1}K_{b2}/K_{f1}K_{f2})$

K_3 is equal to K_1/K_{f2}

Table 4-1 Literature Values of NO Rate Constants

Rate Constants	Values*	Units	Reference
K_{f1}	1.36×10^{14} exp (-75,400/RT)	cm^3/mole-sec	Baulch[25]
K_{b1}	3.12×10^{13} exp (-400/RT)	cm^3/mole-sec	Baulch[25]
K_{f2}	1.33×10^{10} T exp (-7,080/RT)	cm^3/mole-sec	Wray & Teare (26)
K_{b2}	3.2×10^{9} T exp (-39,100/RT)	cm^3/mole-sec	Wray & Teare (26)
$K_{eq\ 3}$	5.0 exp (-58,300/RT)	$\left(\frac{mole}{cm^3}\right)^{1/2}$	Caretto[27]

*R = 1.986 cal/mole-$^{\circ}$K

T = Temperature in $^{\circ}$K

The mass involved in the NO formation process in diffusion flames surrounding the burning droplets is evaluated by mass integration over flame zone:

$$m_{df} = \sum 4\pi \int_{r_1}^{r_\infty} \rho\, r^2\, dr \qquad (4\text{-}86)$$

which has been discounted from the homogeneous formation process shown in Equation (4-85). The summation in above equation is made over all droplets involved in this zone.

The nitrogen bound in the fuel which will be responsible for a very small amount of NO has not been considered in this analysis.

4.7.2 Heterogeneous NO Formation

The nature of the heat release process in a diesel engine dictates that the majority of fuel droplets will burn in vitiated air which also contains nitric oxide. At high NO concentrations the net rate of NO production is strongly dependent upon the concentration. Consequently, it is important that the concentration profile surrounding the burning droplet is known. The analytical solution described in Section 4.5.2 is used to define both the temperature and concentration field around the droplet and the NO kinetics discussed earlier are assumed to be valid, thus a local rate of NO formation can be defined. Consequently, only the following NO mass conservation equations must be solved, provided that it can be assumed the formation of NO has no influence on the flow field surrounding the droplet

$$\rho v \frac{dY_{NO}}{dr} = \frac{1}{r^2} \frac{d}{dr}\left(\rho D r^2 \frac{dY_{NO}}{dr}\right) + \dot{w}_{NO} \qquad (4\text{-}87)$$

The local NO production rate can be conveniently expressed in terms of species mass fraction by:

$$\dot{w}_{NO} = 5.095 \times 10^{-4} \left(K_{f1} K_{eq\,3}\right) \left(\frac{MP}{T}\right)^{3/2} Y_{N2}\, Y_{O2}^{1/2}$$

$$\left\{\frac{1 - 0.9955\left(\frac{K_{b1} K_{b2}}{K_{f1} K_{f2}}\right)\frac{Y_{NO}^2}{Y_{N2} Y_{O2}}}{1 + 1.142857\left(\frac{K_{b1}}{K_{f2}}\right)\frac{Y_{NC}}{Y_{O2}}}\right\} (C_{nor}) \qquad (4\text{-}88)$$

and the two-point boundary conditions are specified by

$$-\left(\rho D \frac{dY_{NO}}{dr}\right)_{+} = \left(\rho v Y_{NO}\right)_{+} = \rho v Y_{NO,l} \quad \text{at } r = r_l \tag{4-89}$$

$$Y_{NO} = Y_{NO,\infty} \quad \text{at } r = r_\infty \tag{4-90}$$

In the above equations, Y_{N2} and Y_{O2} and T are already known explicitly from the relationships described in Section 4.5.2. The solution to the above two point boundary value problem can be achieved by following a standard "trial and error" procedure

- guessing the initial condition, i.e., $Y_{NO,l}$ at the droplet surface
- integrating Equation (4-87) numerically throughout the entire flow field from r_l to r_∞ based on known Y_f, Y_{O2} and T distributions.
- matching $(Y_{NO,\infty})_{(calculated)}$ to $(Y_{NO,\infty})_{(specified)}$
- repeating the procedure until agreement is reached

The contribution of the NO formed in the droplet diffusion flame to the overall zonal production rate is calculated by integrating the NO production rate, $\dot{w}_{NO}$, over the diffusion flame zone, i.e.

$$\left(\dot{w}_{NO}\right)_{HET} = 4\pi r_l^3 \int_{r_l}^{r_\infty} \dot{w}_{NO} \left(\frac{r}{r_l}\right)^2 d\left(\frac{r}{r_l}\right) \tag{4-91}$$

4.8 Soot Formation and Oxidation

Little is known concerning the detailed mechanism of soot formation and the model of soot formation is based upon empirical relationships derived from experimental observations. It is believed that the following processes are involved in the formation of soot:

- dehydrogeneration: breakdown of hydrocarbon molecules to form molecules with a higher C/H ratio
- polymerization: formation of higher molecular weight molecules
- agglomeration: formation of solid particules

The most favorable conditions for soot production in diesel engines are those high temperature zones deficient in oxygen. These conditions are produced during the ignition delay period or during the early stages of combustion. An Arrhenias type equation for the rate of soot formation has been suggested by Khan and Greeves [4] which is based upon the local unburnt equivalence ratio, partial pressure, temperature and includes several empirically determined coefficients. The Khan and Greeves relationship is not directly applicable to this study due to the singularities in defining the zonal unburnt equivalence ratio (when it is based solely upon unreacted oxygen) for a fuel rich zone.

A modified rate equation based upon local equivalence ratio of the burned products their pressure and temperature has been used in this study is

$$\dot{w}_{sf} = A_{sf} \left(\frac{V_{bm,I}}{V} \right)^2 \left(\frac{\bar{T}}{T} \right) \phi^3 p \ \exp\left(-E_{sf}/RT\right) \tag{4-92}$$

The activation energy E_{sf} is taken to be 40 kcal/mole. P is pressure in atm. $\bar{T}$ is averaged temperature of cylinder contents and the pre-constant A_{sf} is fitted to exhaust soot data.

The mass rate of oxidation used is the expression proposed by Lee et al. [28]:

$$\dot{w}_{so} = A_{so} \left(\frac{m_s}{\rho_s d_s} \right) \left(\frac{Y_{O_2} P}{\sqrt{T}} \right) \exp - \left(E_{so}/RT\right) \tag{4-93}$$

Where P is in atm, and A_{so} has a value of 6.51×10^4. The averaged soot density ρ_s, and particulate diameter, d_s, are assumed to be 2.0 gm/cm^3 and 1μ respectively. The activation energy E_{so} is set equal to 39.3 Kcal/mole (also see Field et al[29]).

4.9 Nitric Oxide and Soot Formation Equations

The total zonal NO production rate is the algebric sum of the homogeneous and heterogeneous contribution:

$$(\dot{w}_{NO}) = (\dot{w}_{NO})_{HOM} + \sum(\dot{w}_{No})_{HET} \tag{4-94}$$

The summation in above equation is made over all droplets.

The species conservation equations for NO in the "air" and burning zones are written as:

"Air"

$$\dot{(Y_{NO})_a} = \frac{1}{m_a}\left\{\sum\left[(Y_{NO})_{bm,I} - (Y_{NO})_a\right]\dot{m}_{V,I} + (\dot{w}_{NO})_a\right\} \tag{4-95}$$

Burning Zone

$$\dot{(Y_{NO})}_{bm,I} = \frac{1}{m_{bm,I}}\left\{\left[(Y_{NO})_a - (Y_{NO})_{bm,I}\right](\dot{m}_{D,I} + \dot{m}_{apb,I})\right.$$

$$\left. - (Y_{NO})_{bm,I}(\dot{m}_{fdb,I} + \dot{m}_{fpb,I}) + (\dot{w}_{NO})_{bm,I}\right\} \tag{4-96}$$

The net rate of soot formation is

$$\dot{w}_s = \dot{w}_{sf} - \dot{w}_{so} \tag{4-97}$$

The species conservation equations for soot in the "air" and the burning zone are:

"Air"

$$\frac{\cdot}{(Y_s)_a} = \frac{1}{m_a} \left\{ \sum_I \left[(Y_s)_{bm,I} - (Y_s)_a \right] \dot{m}_{v,I} + (\dot{w}_s)_a \right\} \tag{4-98}$$

Burning Zones

$$\frac{\cdot}{(Y_s)_{bm,I}} = \frac{1}{m_{bm,I}} \left\{ \left[(Y_s)_a - (Y_s)_{bm,I} \right] (\dot{m}_{D,I} + \dot{m}_{apb,I}) \right. \tag{4-99}$$

$$\left. -(Y_S)_{bm,I} \ (\dot{m}_{fdb,I} + \dot{m}_{fpb,I}) + (\dot{w}_s)_{bm,I} \right\}$$

4.10 Equilibrium Compositions

The equilibrium species distributions (in mole fractions) of combustion products are computed by means of a computer program developed by the NASA Lewis Research Laboratory. For fuel-lean mixtures, eleven species including CO_2, CO, H_2O, H_2, NO, OH, N_2, O_2, H, N and O are considered and CH_4 is added for fuel-rich mixtures. The Argon content of the air is neglected.

For a given fuel, the species distribution are calculated as functions of three parameters: pressure, temperature and equivalence ratio. For computational efficiency, a set of species distribution tables, covering the pressure, temperature and equivalence ratio ranges of normal engine operation, are calculated and stored in magnetic tape. Consequently, a 3-D table look-up is the only operation needed whenever equilibrium composition, for specified pressure, temperature and equivalence ratio, is required.

4.11 Fuel Representation

The laboratory report on the diesel fuel used in this study gave the following properties:

Table 4-2

H/C (by mole, approx)	1.7
Gravity, ^{o}API	34.5
Total sulfur, wt %	0.3
Flash point, ^{o}F	170
Pour point, ^{o}F	20
Cloud point, ^{o}F	24
Cetane number	46.7
Viscosity, CS @ 100^{o}F	2.5
Aromatics, %	37.6
Distillation	
Initial boiling (^{o}F)	386
50% point (^{o}F)	514
End point (^{o}F)	658
Residue	1%
Total nitrogen, wt %	< 0.05

The model representation of this diesel fuel is a mixture of 50% (by volume) n-heptane (C_7H_{16}) and 50% toluene (C_7H_8). The sulfur and nitrogen content of the fuel are neglected. This fuel model is used in the parametric calculation of the equilibrium thermodynamic properties and species distribution of the combustion products.

The extended properties of the fuel mixture based upon the properties of the fuel model constituents are listed in the table.

Table 4-3

Molecular wt.	96.
Critical pressure (atm)	34.3
Critical temperature (^{o}K)	567.0
Density (at 298^{o}K)	0.851
Boiling point (1 atm)	377.6
Heat of Combustion (cal/gm)	10249.

4.12 The Method of Solution

The temperature of each gaseous zone is determined by integrating the energy equations (4-31a) through (4-31c). Since the liquid fuel temperature is frozen at the initial wet-bulb temperature, the energy equations (4-2) and (4-3) can be used to determine the energy transfer, for phase transition during both the fuel vaporization and the combustion periods. The internal energy is determined from the temperature, pressure and equivalence ratio. The initial temperature of a burning zone is calculated using the Newton-Ralphson method, based on the known internal energies of fuel and "air" before ignition, instantaneous heat losses and pressure.

The rate of heat transfer is described by Eqns (4-32) and (4-33). The mass transfer between zones is described by Eqns. (4-35), (4-42), (4-43), (4-48) and (4-49). The total mass of the individual zones is calculated by integrating Eqns (4-14) through (4-18). The instantaneous cylinder pressure is then determined from over-all equations of state. The over-all energy balance equation (4-27) and mass balance equation (4-29) are used to check the accuracy of the computational procedures at the end of each numerical integration step.

The pollutant zonal mass fractions are obtained by integrating the species conservation Eqns. (4-95) and (4-96) for NO concentration and by integrating

Eqns (4-98) and (4-99) for soot.

The governing differential equations in the analytical model of diesel engine combustion are all first order differential equations and can be represented symbolically as:

$$\frac{dY_i}{d\theta} = f(Y_i, \theta) \tag{4-100}$$

The symbolic variables Y_i are functions of crank angle θ. Numerically this first order system could be integrated by various finite difference techniques. For accuracy and computational efficiency, the modified iterative, second order Runge-Kutta method has been employed. The recurrence formula for the finite difference equivalence of eqn (4-100) can be written as:

$$Y_i^{n+1}(\theta + \Delta\theta) = Y_i(\theta) + \frac{\Delta\theta}{2}\left\{ f(Y_i, \theta) + f[Y_i^{n}(\theta + \Delta\theta), \theta + \Delta\theta] \right\} \tag{4-101}$$

where n is the index of integration and the initial (n=0) approximations are evaluated by

$$Y_i^{\circ}(\theta + \Delta\theta) = Y_i(\theta) + \Delta\theta \cdot f(Y_i^{\circ}, \theta) \tag{4-102}$$

At each integration step the iteration is continued until a stable pressure and mass averaged temperature is obtained.

4.13 Indicated Engine Performance and Engine Emission

The engine performance parameters, including indicated mean effective pressure, indicated horsepower and indicated specific fuel consumption are calculated by the following relationship:

Indicated Mean Effective Pressure (IMEP)

$$IMEP = \frac{2}{\pi D_e^{\,2} R} \left\{ \left[\int_{-180}^{\theta_{vc}} p \frac{dv}{d\theta} \, d\theta + \int_{\theta_{vc}}^{0} p \frac{dv}{d\theta} \, d\theta \right] \right.$$
$$\left. \left[+ \int_{0}^{\theta_{vo}} p \frac{dv}{d\theta} \, d\theta + \int_{\theta_{vo}}^{180} p \frac{dv}{d\theta} \, d\theta \right] \right\} \qquad (4\text{-}103)$$

where θ_{vc} and θ_{vo} are the intake valve closing angle and exhaust valve opening angle respectively. The sum of the first term and last term on right hand side of Eqn (4-103) is small and can be ignored when comparing engines of similar manifold pressures and valve timings.

Indicated Horsepower (IHP)

The total horsepower developed in the engine is calculated by:

$$IHP = \frac{(IMEP)\ (V_{dis})\ (RPM)}{396000 \times N_s} \quad (hp) \qquad (4\text{-}104)$$

Indicated Specific Fuel Consumption (ISFC)

The indicated specific fuel consumption given by:

$$ISFC = \frac{(60)\ (m_{fi})\ (RPM)}{N_s\ (IHP)} \quad (gm/hp\text{-}hr) \qquad (4\text{-}105)$$

is a comparative parameter that is indicative of the efficiency of an engine in converting chemical energy into work and $N_s = 2$ for four stroke engine, $N_s = 1$ for two stroke engine.

5.0 THE EMPIRICAL NATURE OF THE MODEL

One of the major objectives of this program was to develop a model describing the formation of pollutants in a compression ignition engine which contained the minimum number of arbitrarily assigned empirical constants. The previous section indicated that limitations in the fundamental knowledge of many of the physical processes described in the model necessitated that several empirical constants be included. Although the physical significance of the empirical constants included in the Ultrasystems' model has been discussed in the previous section, it is necessary to summarize the empirical constants used in the model and to ascertain the sensitivity of predicted engine performance to the value of those constants.

5.1 The Nature of the Empirical Constants

The empirical constants included in the model have been divided into two groups and the basis for this division is:

- the level of uncertainty associated with their numerical value;
- their importance with respect to the prediction of engine performance;
- the availability of experimental data to allow re-evaluation.

The first group of constants are considered to have nonadjustable values for the purpose of this study and are listed in Table 5-1. Although it is recognized that several of the constants listed in Table 5-1 cannot be considered as well established (e.g., E_s activation energy for soot formation), some bounds must be placed on the number of "adjustable" constants. Consequently, those constants included in Table 5-1 were selected because:

- they had values which were generally recognized and had been established from acceptable experimental evidence (e.g., C_a, C_b, C_{max}, δ, E_{ig}, B_{ig}, C_{ig} and C_{evap});
- they had been used previously and no new data was available to necessitate re-evaluation (e.g., ρD, A_{so}, E_s, C_{fj} and C_{wj});
- they were considered to have a minor influence on the calculation of engine performance (e.g., C_{fjo}).

Table 5-1 Nonadjustable Empirical Constants

Constant	Description	Literature Value	References	Remark
C_a	Pre-constant in Annand type of convective heat loss expression Eqn (4-32)	0.17	McAulay et al[15]	Literature value used
C_b	Power for Reynolds number dependent in Annand type of convective heat less expression, Eqn (4-32)	0.7	Sitkei[30] McAulay et al[15]	Literature value used
ρD	Product of density and mass diffusion coefficient used as a constant in droplet diffusion flame model	3.0×10^{-4} g-cm/sec	Bracco[31]	Literature value used
C_{evap}	Convective conrection on droplet vaporization, Eqn (4-43)	0.276	Wise[19] Ranz et al[32] Frossling[33]	Literature value used
C_{max}	See Eqn (4-37)	37.5	Lee[17]	Value obtained via curve fit to Lee's data
δ	See Eqn (4-36)	0.85	Lee[17]	Value obtained via curve fit to Lee's data
C_{fjo}	Initial free jet spread coefficient, Eqn (A-1)	0.135	Newman[34]	Literature value used
C_{fj}	Free jet main region, spread coefficient, Eqn (A-4)	0.175	Newman[34]	Literature value used
C_{wj}	Wall jet spread coefficient Eqn (A-14)	0.204	Gauntner et al[35]	Derived from Gauntner's results
E_{ig}	Activation energy for ignition reaction, Eqn (4-45)	9290. cal/ g-mole	Shipinski et al[21]	Literature value used
B_{ig}	Centane number dependence for ignition delay, Eqn (4-45)	-0.69	Shipinski et al[21]	Literature value used
C_{ig}	Pressure dependence for ignition delay, Eqn (4-45)	-0.386	Shipinski et al[21]	Literature value used
E_s	Activation energy for soot formation reaction, Eqn (4-92)	40 kcal/ g-mole	Khan & Greeves[4]	Literature value used
A_{so}	Pre-constant for soot oxidation reaction, Eqn (4-93)	6.5×10^4	Lee et al[28] Field et al[29]	Literature value used

Those empirical constants which have been termed adjustable are those which:

- have a high level of uncertainty associated with them, and are considered to have a significant effect upon the prediction of pollutant formation and engine performance.
- are peculiar to the present model.

The value of these constants will depend, to some degree, upon the characteristics of the engine being simulated. However, their value can be ascertained within limits from single cylinder experiments and exploratory model calculations. Seven constants have been placed in the second group which includes:

C_{sef} — C_{sef} (Equation 4-42) allows the rate of air entrainment by the jet to be modified to take account of cross flow effects. This parameter has a significant influence on the early stages of combustion, which is mainly premixed, and is therefore, responsible for the rapid pressure rise immediately following ignition.

C_{mix} — The parameter C_{mix} accounts for the "random mixing" process that is assumed to occur between burned zones, which will contain varying amounts of liquid and gaseous fuel, and the "air" zone. Thus, C_{mix} will have a strong influence on the processes occurring during the later stages of heat release. Variations in C_{mix} primarily affect the predicted cylinder pressure after ignition, and the value of C_{mix} is chosen primarily to give a fit to the measured pressure curve and secondarily, to match observed exhaust NO levels.

A_{ig} — A_{ig} allows the ignition delay to be predicted correctly. Values for A_{ig} can be found in the literature, but these cannot be considered universal since the ignition delay depends upon several operational parameters such as nozzle type, chamber configuration, etc. Therefore, it is considered desirable to tune A_{ig} for a particular engine configuration.

A_{sf} — The model does not attempt to include the detailed kinetics of soot formation, and it is considered that there is a large degree of uncertainty attached to the parameter A_{sf} which is obtained by matching the predicted and measured soot concentration levels.

C_{vidi} The parameter C_{vidi} has been included to provide some vitiation of the air prior to mixing with the burning zones during the air/product mixing processes. The value of C_{vidi} influences both the droplet burning rate and the early stages of NO formation. The suggested value is somewhat arbitrary. However, its influence on the prediction of performance and pollutant formation is concluded to be minimal.

τ_{hu} The droplet heat up time is a function of droplet size, convective transfer and the surrounding temperature. Detailed modeling of transient heat transfer effects within each individual droplet is considered to be outside the scope of this study and must be justified before consideration is given to its inclusion. A uniform value, which is approximately equal to the physical ignition delay (0.2 ms), has been chosen for all droplet sizes. It has been assumed that vaporization of liquid fuel does not occur during the heat up time.

C_{nor} It has been well established that it is not possible to decouple the kinetics of NO formation from those of hydrocarbon combustion. Super-equilibrium radical concentrations are known to occur in reacting regions and elementary reactions other than those described by Equations 4-83 through 4-84 take part in NO formation. Consequently, it is reasonable to expect that any NO prediction which is based solely upon the Zeldovich model would be an underprediction in those zones where combustion is taking place. A value of $C_{nor} = 5.37$ has been used previously by Kahn and Greeves[4] to allow exhaust NO levels to be calculated using the Zeldovich mechanism.

Table 5-2 lists the seven empirical constants which are considered to be adjustable, together with their suggested values and the method used to determine this value.

Table 5-2. Adjustable Empirical Constants

Constants	Equations	Suggested Value	Remarks
C_{sef}	4-42	4.3	Correlate to pressure-crank angle data in initial stage (premixed) combustion
C_{mix}	4-47	7.8E-3	Correlate to pressure-crank angle data in the final stage of combustion
C_{nor}	4-85 4-88	5.37	Match the measured exhaust NO value. Same value has been used by Khan and Greeves[4]
A_{ig}	4-45	1.47E-4	Match the measured ignition delay data
A_{sf}	4-92	3.52	Match the measured exhaust soot concentration
C_{vidi}	4-49	0.1	--
τ_{hu}	--	0.2 ms	Droplet heat up time, assumed to be equal to typical physical delay time

5.2 Exploratory Computations

Engine performance data and exhaust pollution levels obtained from a series of single cylinder experiments were used to evaluate the values of the constants listed in Table 5-2. The direct injection single cylinder engine had the following characteristics:

Displacement	2340 cm^3
Bore	13.97 cm
Stroke	15.24 cm
Connecting rod	30.48 cm
Piston bowl/bore	0.59
Fuel nozzle type	Roosa pencil injector
Nominal orifice size	0.0254 cm
Cone angle	160°

The values of the adjustable constants used in later calculations were determined by fitting the predictions to measurements obtained when the engine was operated under the following conditions (baseline case):

Speed	1500 rpm
Load	equivalence ratio 0.6
Compression ratio	17:1
Swirl	Medium
Fuel injection timing	20° BTDC
Injection duration	17° CA
Air pressure	30 in. Hg. absolute
Mean Wall temperature	500° K

Initially the model was tuned using the baseline case to give an acceptable fit of the measured and calculated cylinder pressure as a function of crank angle. The computed pressure curve for these engine conditions is presented in Figure 5-1, together with the measured pressure curve. In order to establish confidence in both the model and the values chosen for the empirical constants, further computations were made with injection times of -25° and -12°. These computations were made without subsequent adjustment of any of the constants. The resulting calculations can be compared with measurement in Figure 5-2 and it can be seen that there is excellent agreement instantaneous cylinder averaged NO concentrations for all three injection timings. Included on Figure 5-3 are the measured exhaust NO_x values for these conditions. The calculated averaged instantaneous soot concentration (in gm/gm-of-fuel) for all three cases are shown in Figure 5-4 and the calculated engine performance parameters are listed in Table 5-3.

Table 5-3

Calculated Engine Performance Parameters

θ_{inj}	-12	-20	-28
Indicated Mean Effective Pressure (psi)	83.3	82.2	74.25
Indicated Horsepower (hp)	22.5	22.1	20.05
Indicated Specific Fuel Consumption (lb/hp-hr)	0.441	0.446	0.494

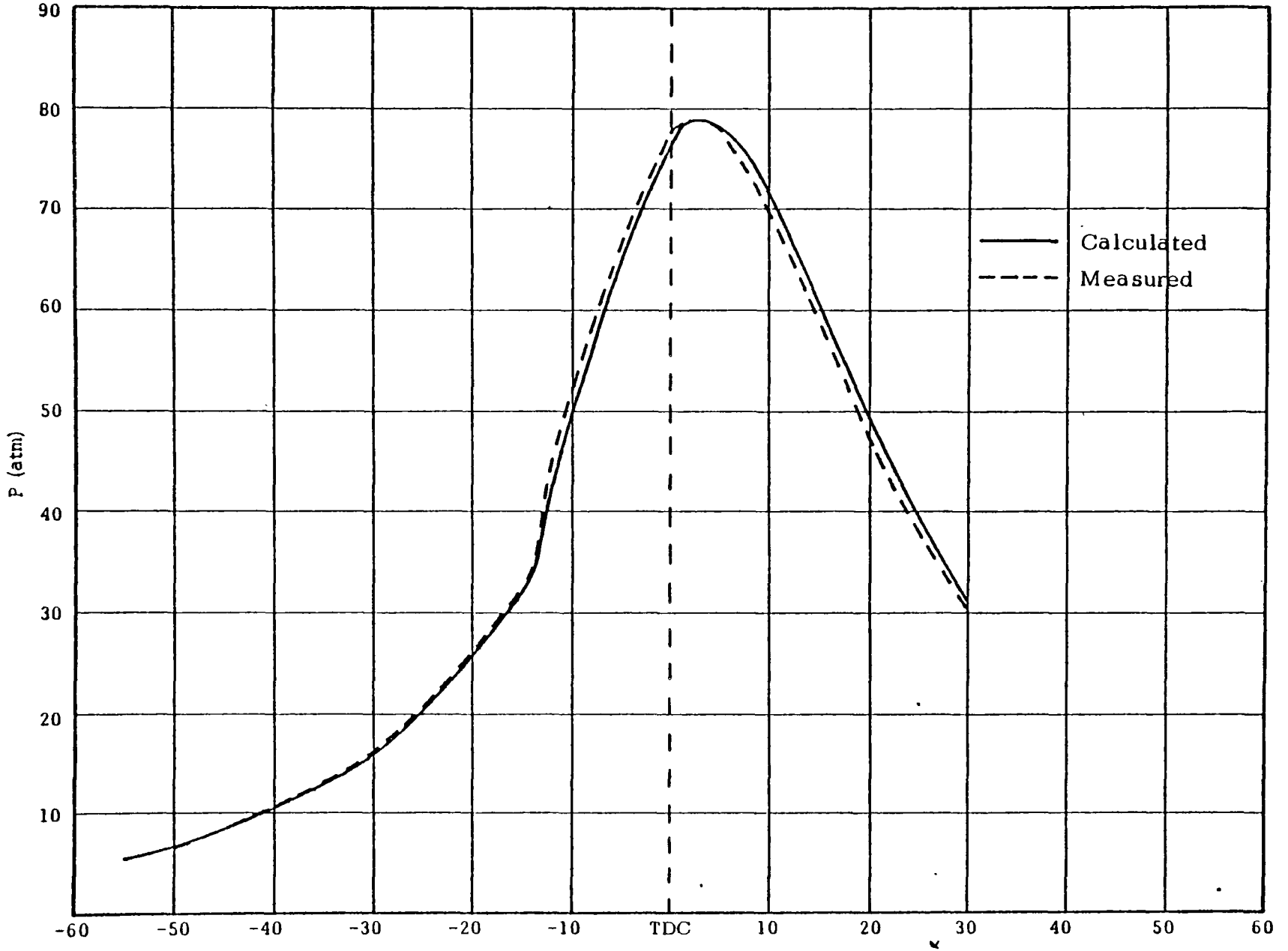

Figure 5-1 Calculated and Measured Pressure-Crank Angle History for Baseline Case (ϕ = 0.6 Speed = 1500 rpm θ_{int} = 20° and Medium Swirl)

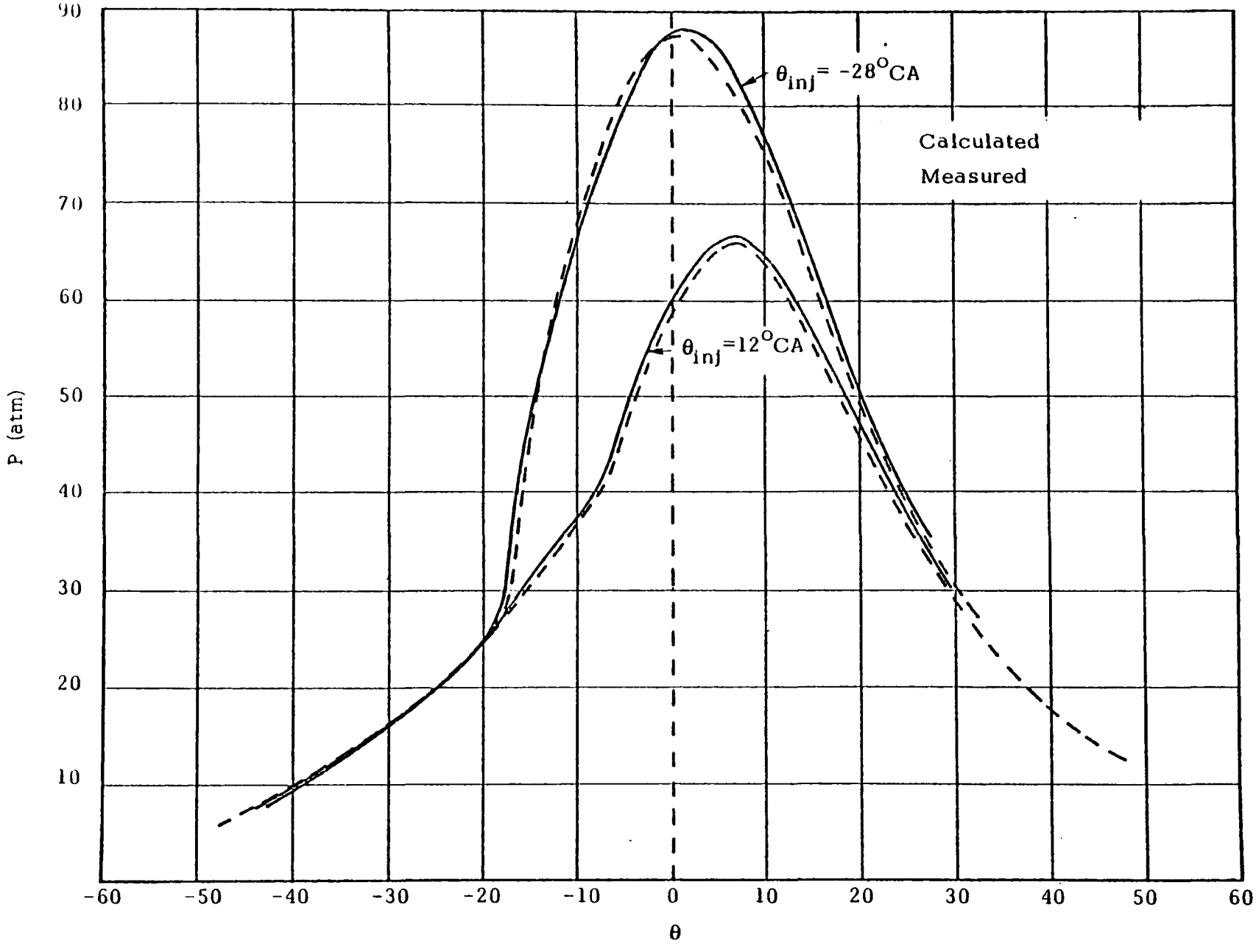

Figure 5-2 Calculated and Measured Pressure Crank Angle Histories of Cases (θ_{inj} = -28° and -12°, ϕ=0.6, speed = 1500 ppm)

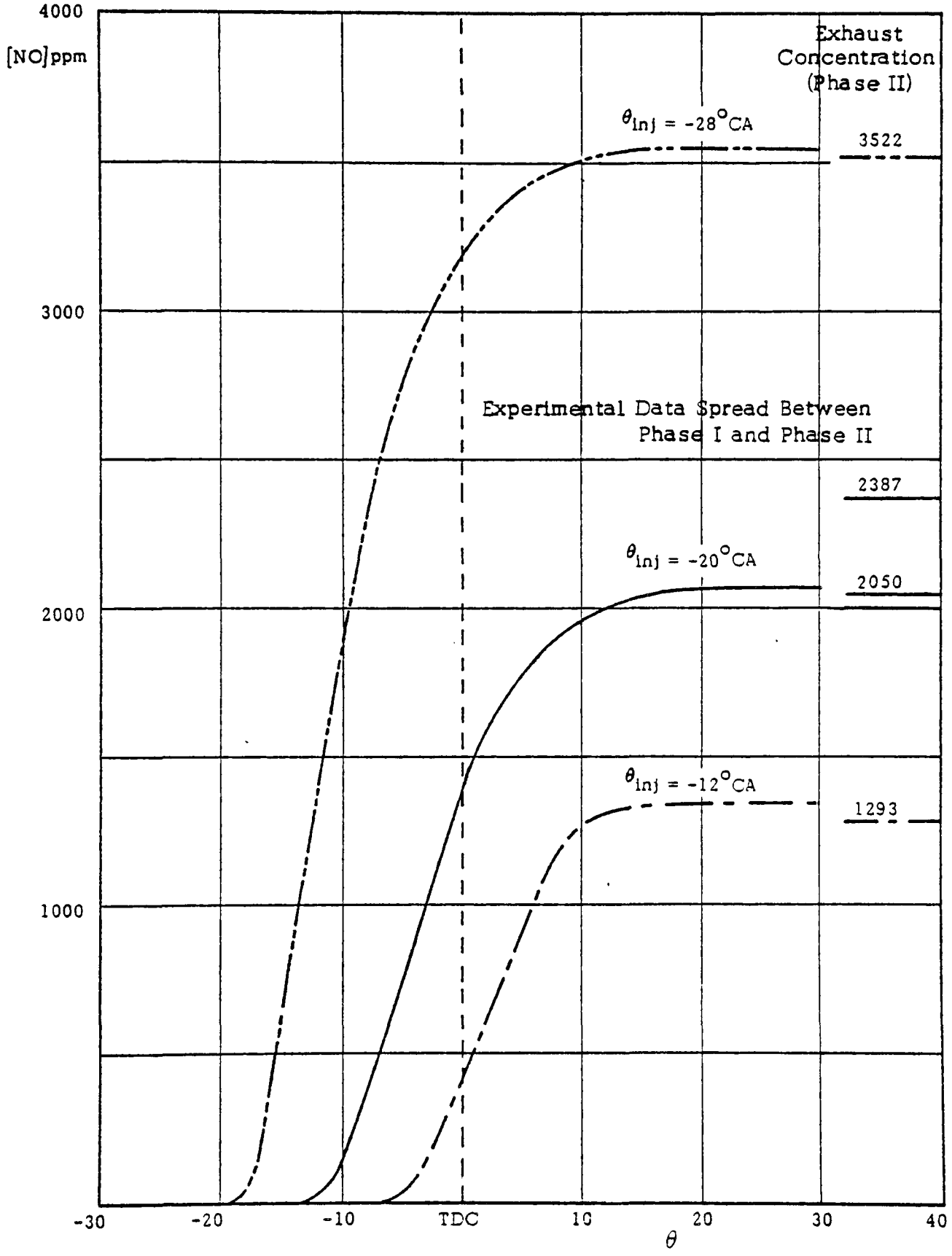

Figure 5-3 Comparison of Calculated Instantaneous NO with Measured Exhaust Levels for Various Injection Timing

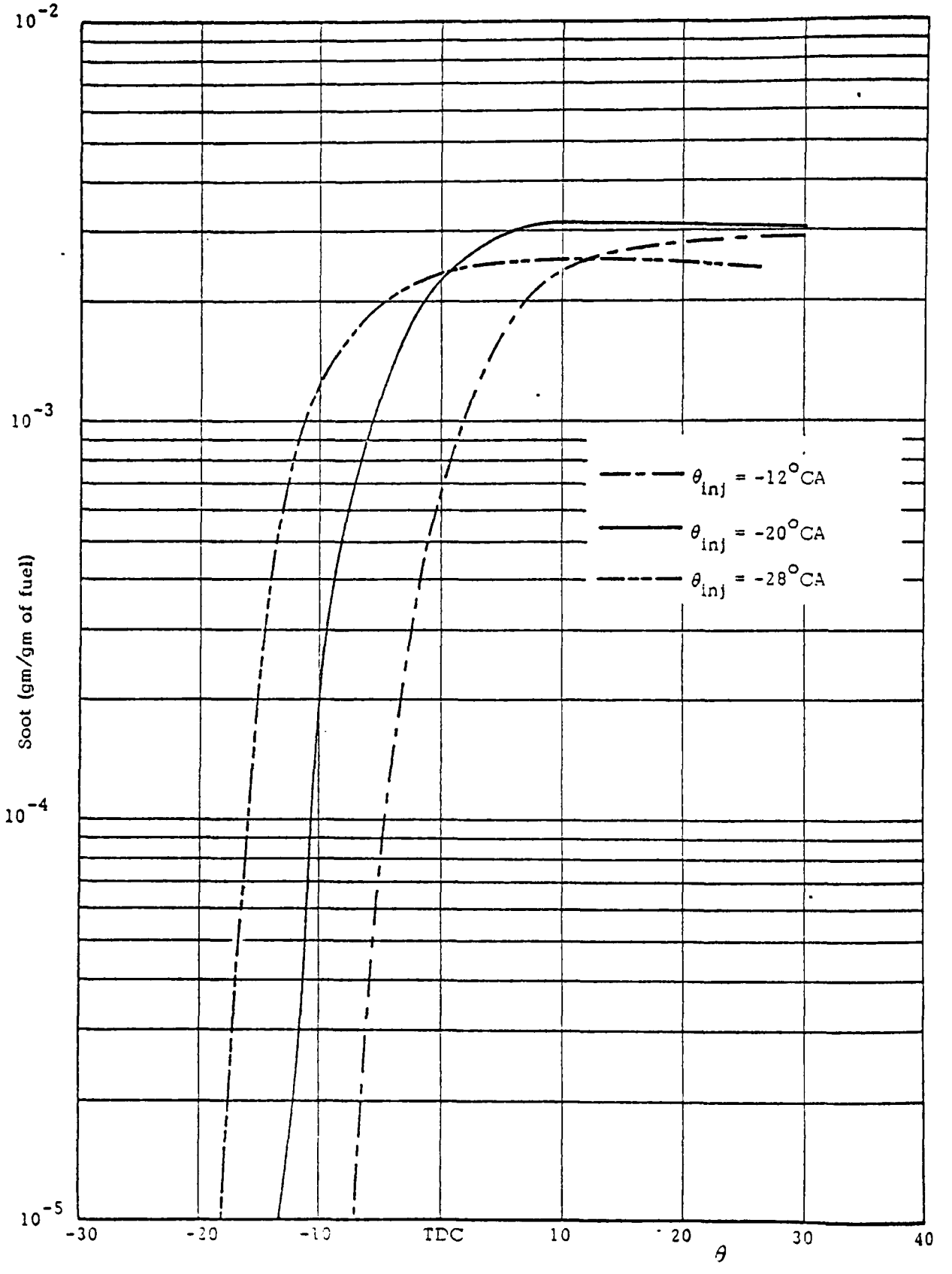

Figure 5-4 Calculated Instantaneous Value of Soot (in gm/gm of total fuel injection)

The engine performance is, of course, strongly linked to the rate of fuel-air mixing and the state of the fuel, i.e., liquid or vapor. Figure 5-5 presents the distribution of fuel between these states from the onset of injection (-20°) to almost complete combustion ($+60^{\circ}$). Fuel can exist as:

- unburned liquid fuel, i.e., that liquid fuel which is heating up but not vaporizing or which is vaporizing;
- unburned fuel in the vapor state which is composed mainly of fuel vaporized before the onset of ignition;
- burning liquid fuel, i.e., those droplets contained in burning zones.

Figure 5-5 shows that initially the mass of unburned liquid fuel is equal to the mass of fuel injected. During this period the droplets are being heated, but are not vaporizing. Before ignition the mass of fuel vapor increases, but it is rapidly burned out once ignition is initiated (at $\theta = -13^{\circ}$). From this time on the mass of unburned liquid fuel also decreases. The plateau in the liquid fuel curve represents the constant droplet heat-up time. After all the premixed vapor has burned, the conditions are such that fuel can only exist as a droplet in a burning zones or as unburned liquid fuel.

Elements of fuel are tagged by two indexes upon injection, reflecting their crank angle at birth, and their location with respect to the fuel spray axis. After ignition only a single index is used, reflecting age since the location is irrelevant in the random mixing process. The history of two such zones is given in Figure 5-6. The calculation of equivalence ratio ϕ does not include fuel in the liquid state, only vapor and products are considered. Thus, as fuel either evaporates or burns, the equivalence ratio increases and then decreases by dilution. The temperature of the lean zone increases from the onset of ignition because fuel is able to burn; however, the temperature of the rich zone hardly varies because of the heat requirements associated with vaporization. In the extremely rich zone virtually no NO is produced because temperatures are too low by the time oxygen becomes available, and the NO that is found in this zone is due mainly to dilution. This highlights one of the weaknesses of the model which does not allow for NO formation by Fenimore type mechanisms[11].

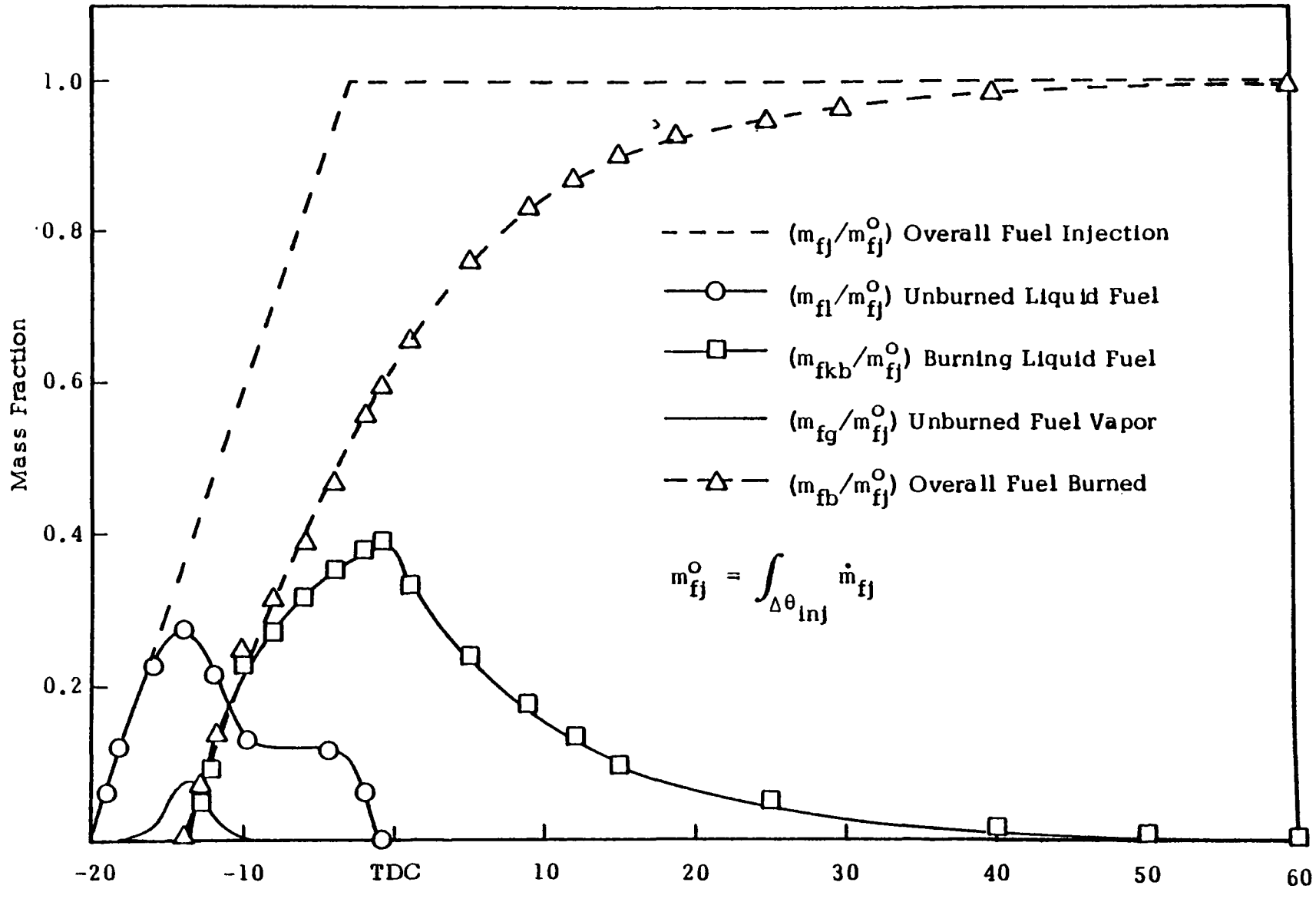

Figure 5-5. Distribution of Fuel in Different States (Baseline Operation)

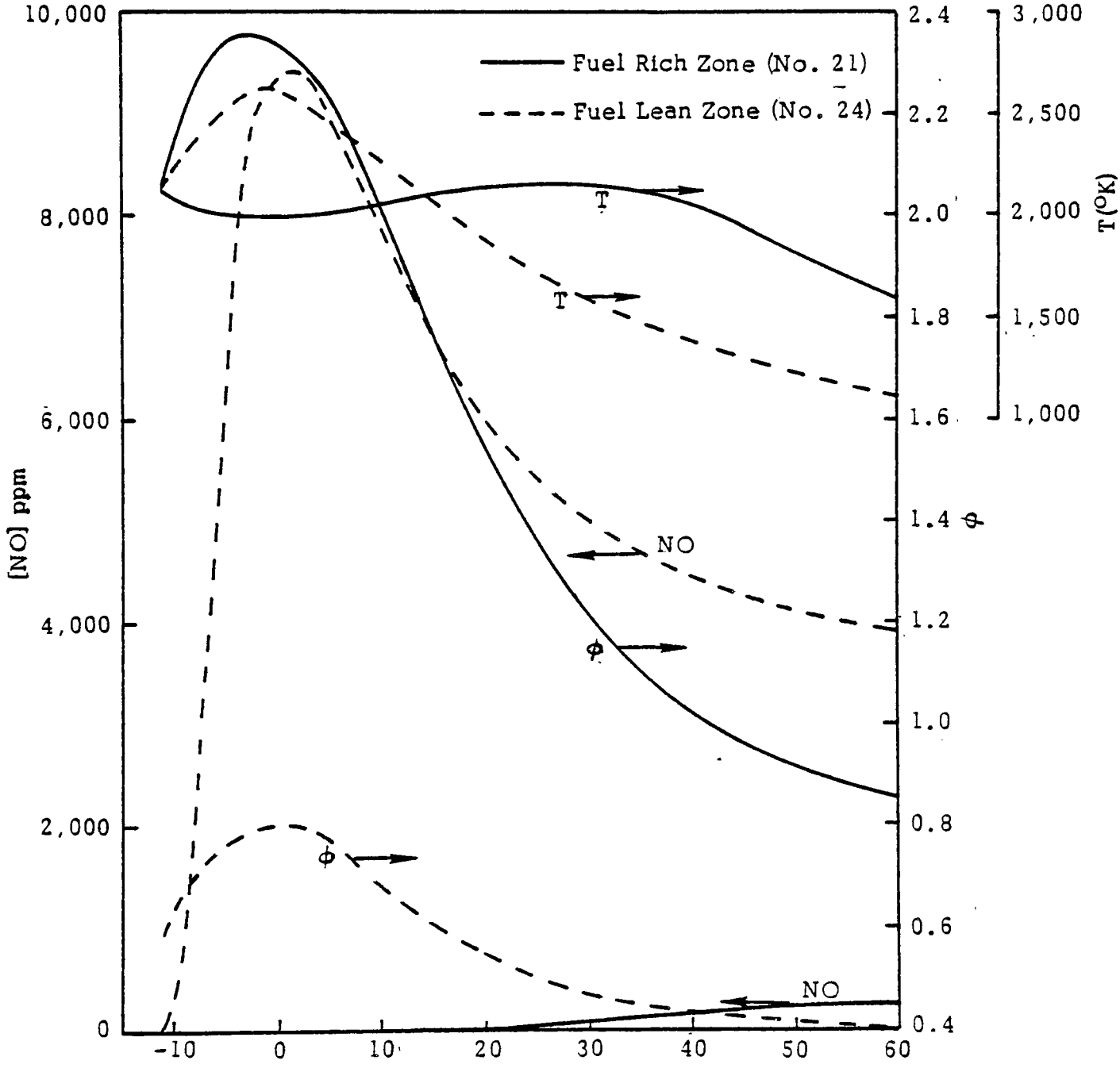

Figure 5-6. Instantaneous Zonal Temperatures, Equilvalence Ratios and NO Mole Fraction for a Typical Fuel Rich and a Typical Fuel Lean Zone

However, it can be seen that there is a very rapid rate of production of NO in the fuel lean zone. Figure 5-7 presents similar comparisons for the instantaneous zonal mass of liquid fuel and soot for the same two zones. In contrast to the NO production, soot is hardly formed in the lean zone, emphasizing that which is well known, i.e., conditions which reduce NO formation tend to enhance soot formation.

5.3 Sensitivity Analysis

A sensitivity analysis has been carried out to assess the influence of the adjustable constants on the calculated emission levels. The range covered in this analysis for each constant is given in Table 5-4 and the results of the computations are presented graphically in Figures 5-8 and 5-9 for nitric oxide and soot, respectively. Both the calculated emissions and the empirical constants have been normalized by the baseline values.

Table 5-4. Values of Empirical Constants for Sensitivity Analysis

Case	Variable	Baseline	1	2
1	C_{sef}	4.3	2.15	8.6
2	C_{mix}	7.8E-3	3.9E-3	1.56E-2
3	C_{nor}	5.37	1.0	8.0
4	C_{vidi}	0.1	0.0	0.2
5	τ_{hu}	2.0×10^{-4}	1.0×10^{-4}	3.0×10^{-4}

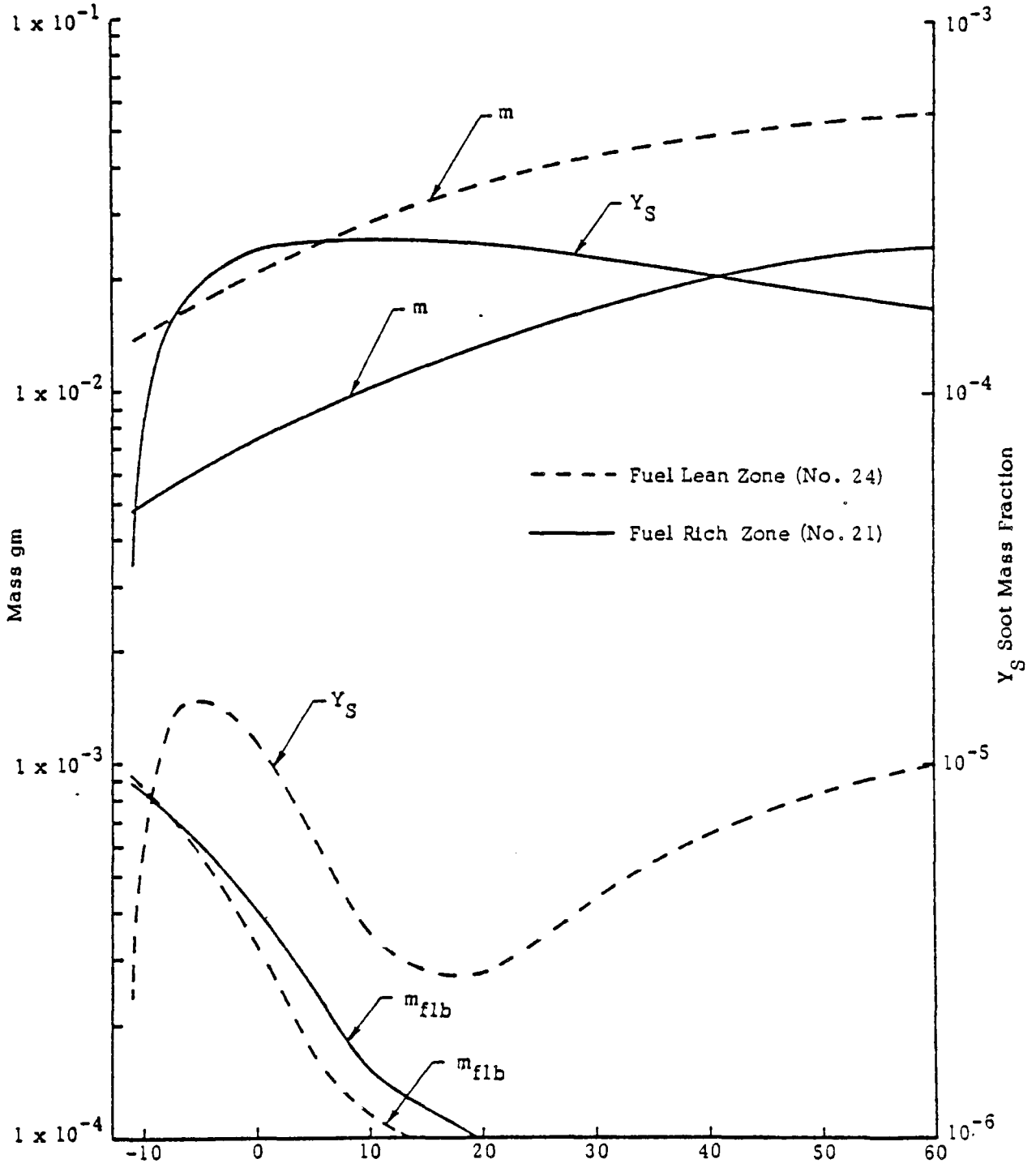

Figure 5-7. Instantaneous Zonal Masses, Masses of Burning Fuel and Soot Concentrations for Typical Fuel Rich and Fuel Lean Zones

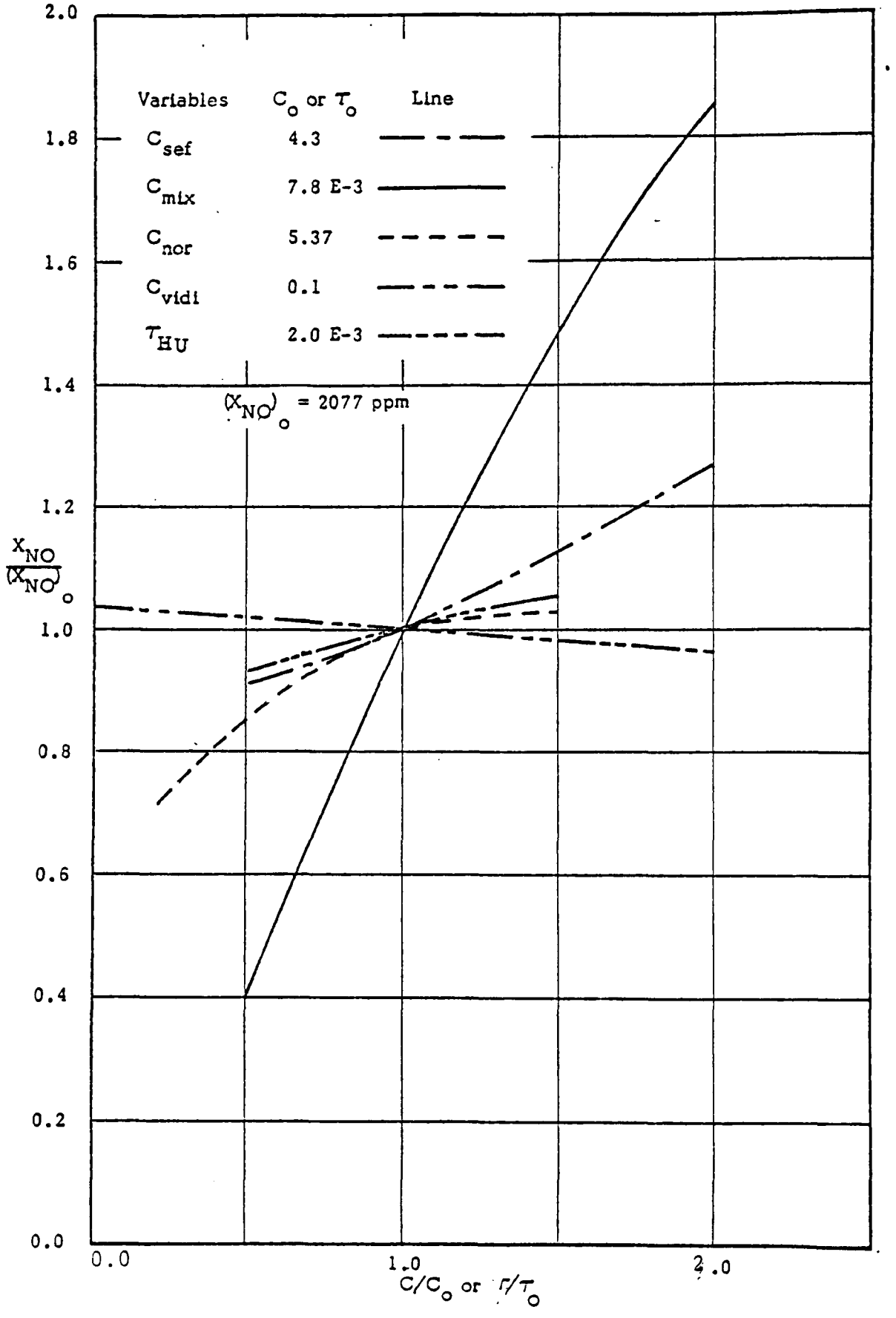

Figure 5-8 Effect of Empirical Constants on NC Prediction

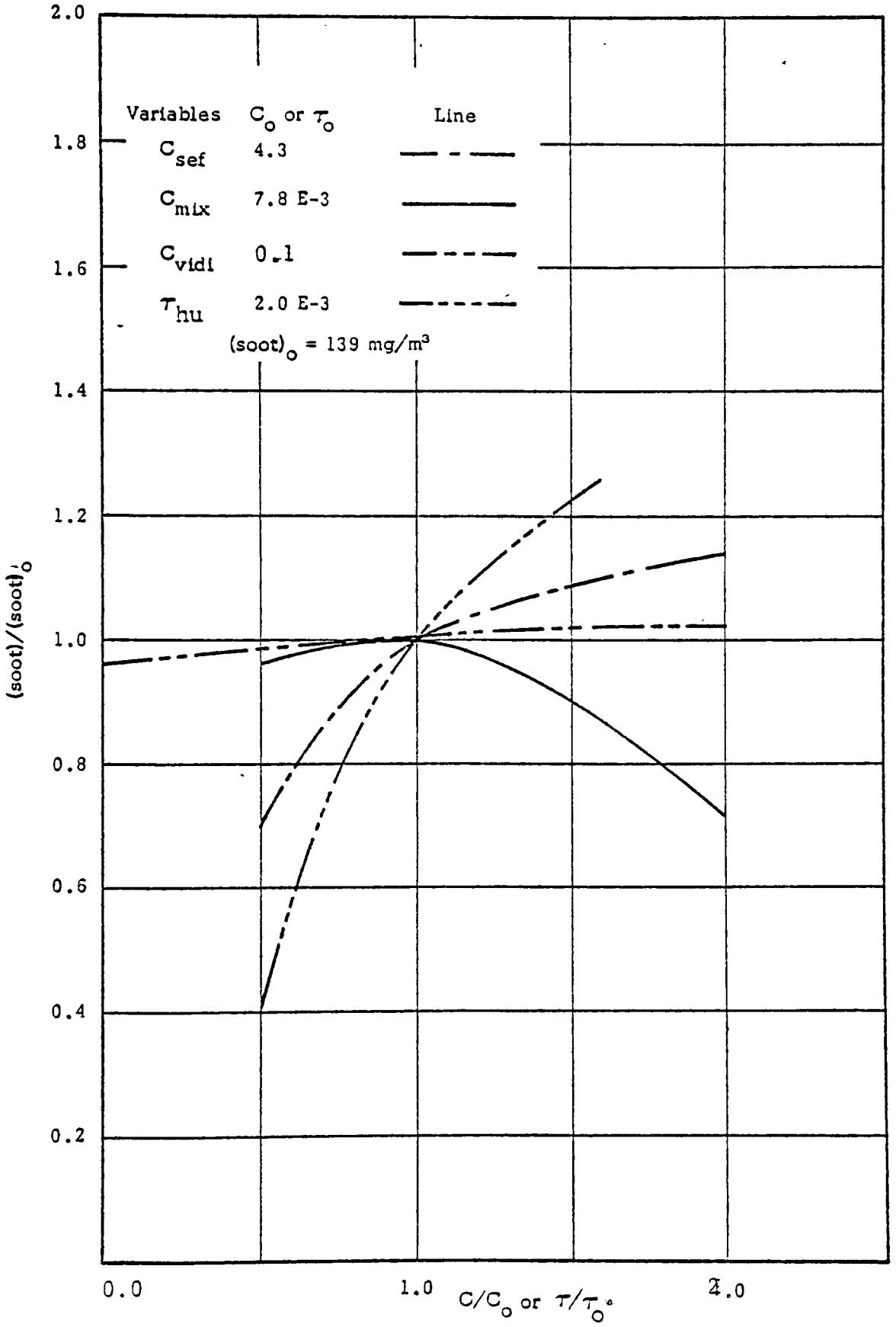

Figure 5-9 Effect of Empirical Constants on Soot Prediction

It was apparent from the calculations concerning NO formation in lean versus rich zones that the major "valve" on calculated NO is the equivalence ratio of each zone. Thus, it is not surprising that the constants which influence mixing, strongly affect the NO calculations. It is, however, surprising that the strongest influence is provided by C_{mix} which is associated with the mass transfer processes which occur after ignition, rather than C_{sef} which controls entrainment by the fuel jet. This can be attributed to the fact that the calculated peak temperatures for lean mixtures occur close to TDC and the mass transfer rates between the air zone and burning zones are higher, thus producing more lean burning zones.

τ_{hu} has a stronger influence on soot emissions than on NO. Also, the relative influence of C_{sef} and C_{mix} on soot production is different from that on NO. Increased mixing after ignition tends to decrease soot emissions.

Table 5-5 lists predicted peak pressures and the crank angle at which it occurs for the range of constant variables once more illustrating the significance of the mixing parameters.

Table 5-5. Effect of Empirical Constants on the Prediction of Peak Pressure (Baseline is P_{max} = 78.83 atm at 3° CA)

Variables	Percent Changes in Value	Predicted P_{max}	Peak Pressure Timing °CA
C_{sef}	+100	82.42	+3 TDC
	- 50	76.49	+3 TDC
C_{mix}	+100	88.49	+4 TDC
	- 50	72.55	+1 TDC
C_{vidi}	+100	79.44	+3 TDC
	-100	78.22	+3 TDC
τ_{hu}	+ 50	80.64	+4 TDC
	- 50	76.75	+3 TDC

5.4 Droplet Diffusion Flames as a Source of Nitric Oxide

The model of pollutant formation in diesel engines grew from a belief that spherical droplet diffusion flames characterized the total class of high temperature diffusion flames which were responsible for pollutant formation. No claim was made that such a belief would improve heat release predictions nor that it actually described the burning process. However, it did dictate the development of the model. Since a spherical diffusion flame was assumed the influence of droplet interaction, and the relative velocity between the droplets and their surroundings was ignored. In the early stages, droplets are confined by the jet and even without violent mixing it is difficult to believe that single droplets existing in an infinite environment will actually simulate the process. It is more real to consider that the droplets exist as a cloud and act as a source of fuel which is transported to the boundary of the cloud. More serious is the tacit assumption of a quiescent atmosphere, droplet velocity lag would produce wake flames which are dissimilar in structure to spherical diffusion flames or even produce blow-off. Fuel vapor can be stripped from the parent droplet, it may partially mix with oxident before combustion, and is therefore, unlikely to remain associated with the parent droplets.

Calculations have been made in an attempt to ascertain the contribution to the total NO production of the two modes of NO formation included in the model. This was done by separately suppressing the homogeneous and heterogeneous NO formation mechanisms. The calculated instantaneous NO concentration history for the baseline case for these computations and the normal predictions are shown in Figure 5-10. The NO formation from the droplet diffusion flame appears to be only significant during the early stages of NO formation. It can be seen that contributions of NO from the homogeneous and heterogeneous phases are not additive and NO formed in homogeneous zones appears to suppress NO formation in the heterogeneous phase.

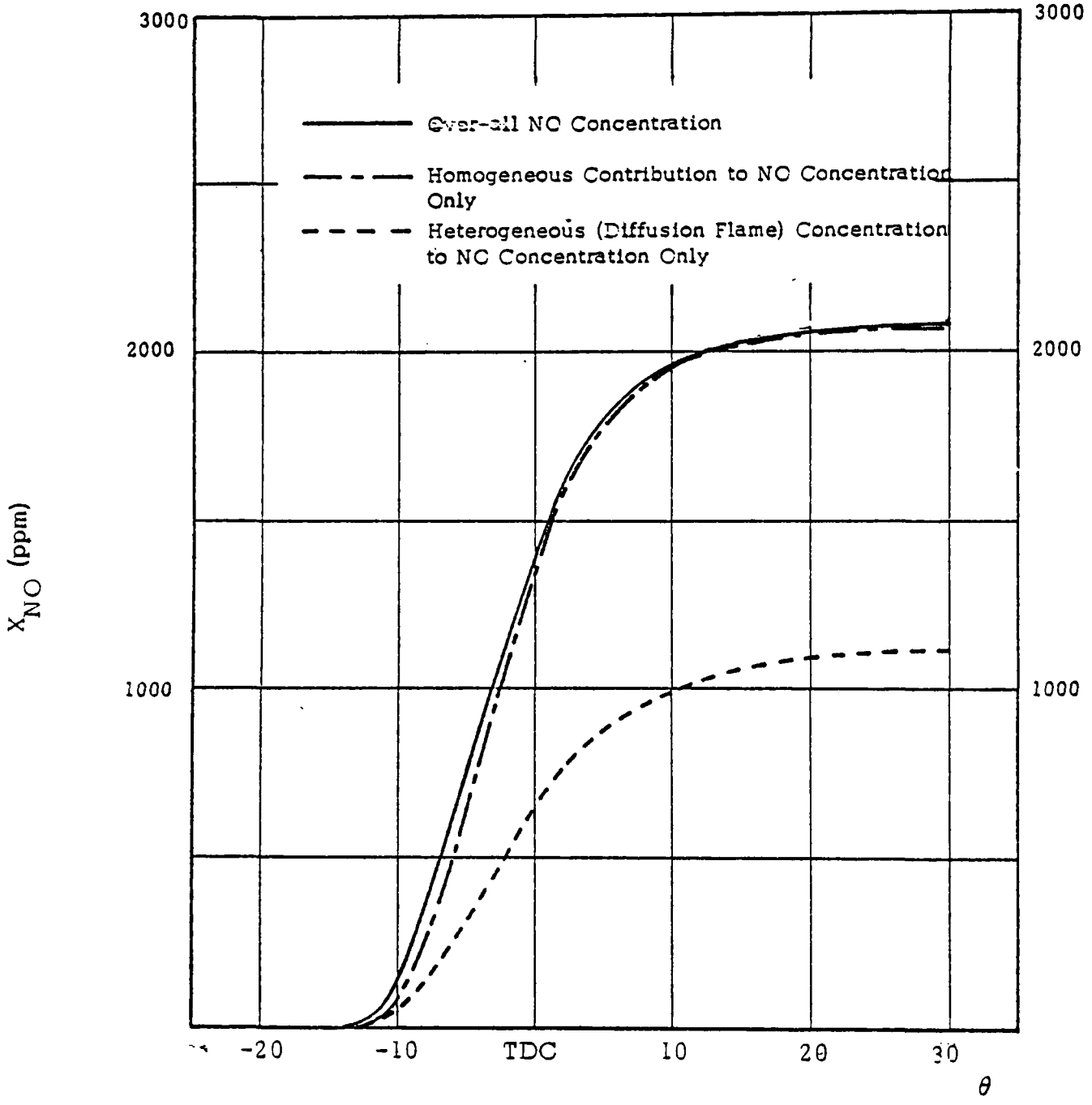

Figure 5-10 Instantaneous Diffusion Flame and Homogeneous Contributions to NO Concentration (Baseline)

The relatively minor influence of the heterogeneous phase on the total production of NO as shown by the model can be explained by:

- The majority of the droplets are burned in fuel rich zones where diffusion flames cannot be established because of the lack of oxygen. Less than 20 percent of the droplets have sufficient oxygen (assumed to be 2 percent in these calculations) to allow the formation of diffusion flames.
- Most of the droplets react in atmospheres containing NO which may actually result in the destruction of NO, if not, it will certainly reduce the rate of production.

Figures 5-11 and 5-12 present the results of calculation demonstrating the influence of the droplet environment on the production of NO. The calculations were carried out with a droplet radius r_l of 15μ and a constant ambient pressure and temperature of 50 atm and 2000°K respectively, and the major ambient species were assumed to be in equilibrium. The effect of ambient NO concentration (for $\phi_\infty = 0.4$) is shown in Figure 5-11, the NO formation rate decreases linearly with increasing ambient NO concentration, and when the environment contains NO concentrations in excess of the equilibrium value the rate becomes negative. Figure 5-12 shows the influence of ambient oxygen concentration for both zero ambient NO and equilibrium ambient NO. The NO formation rate increases rapidly with increasing ambient oxygen concentration.

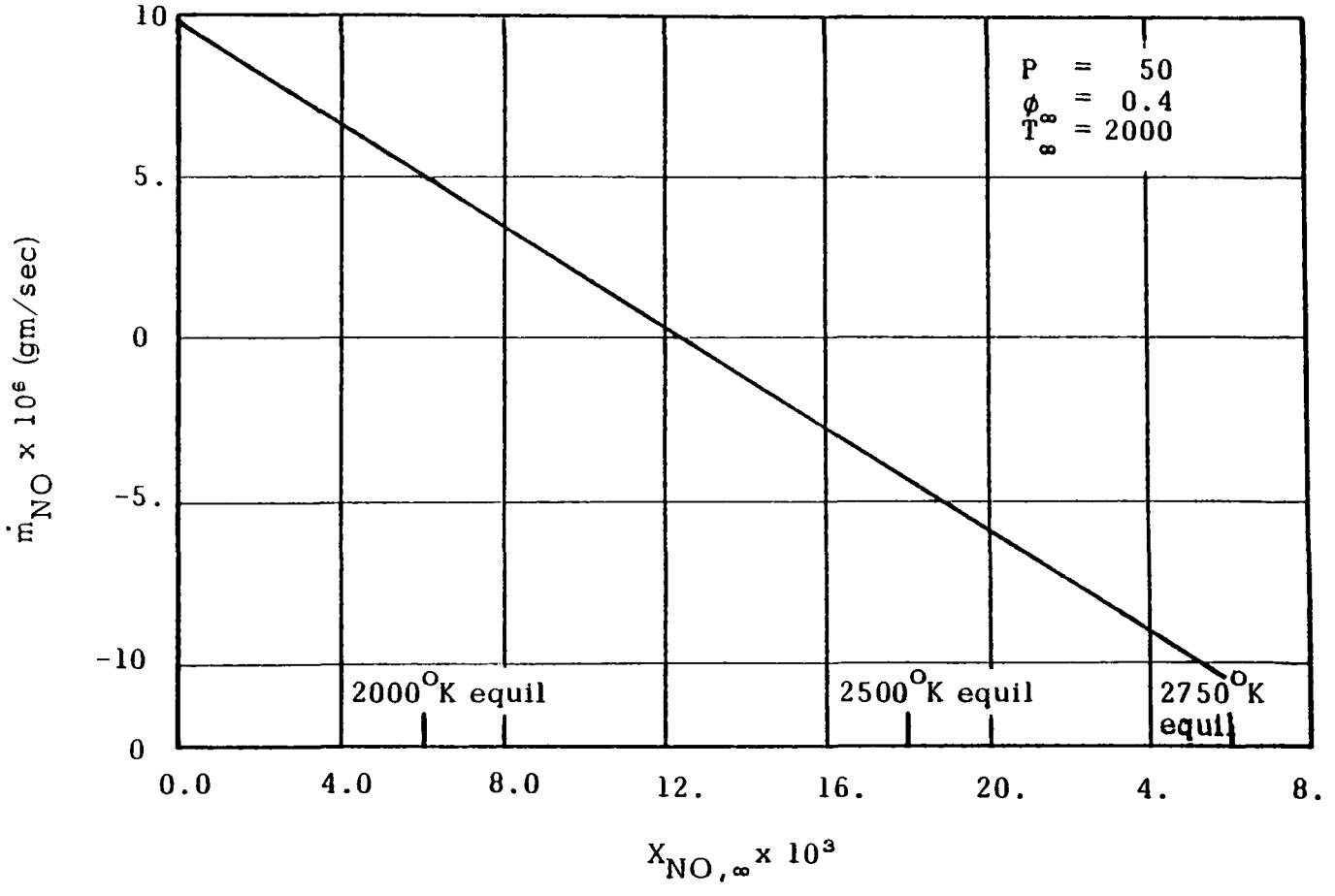

Figure 5-11 Effect of Ambient NO Concentration Formation Around a Burning Droplet

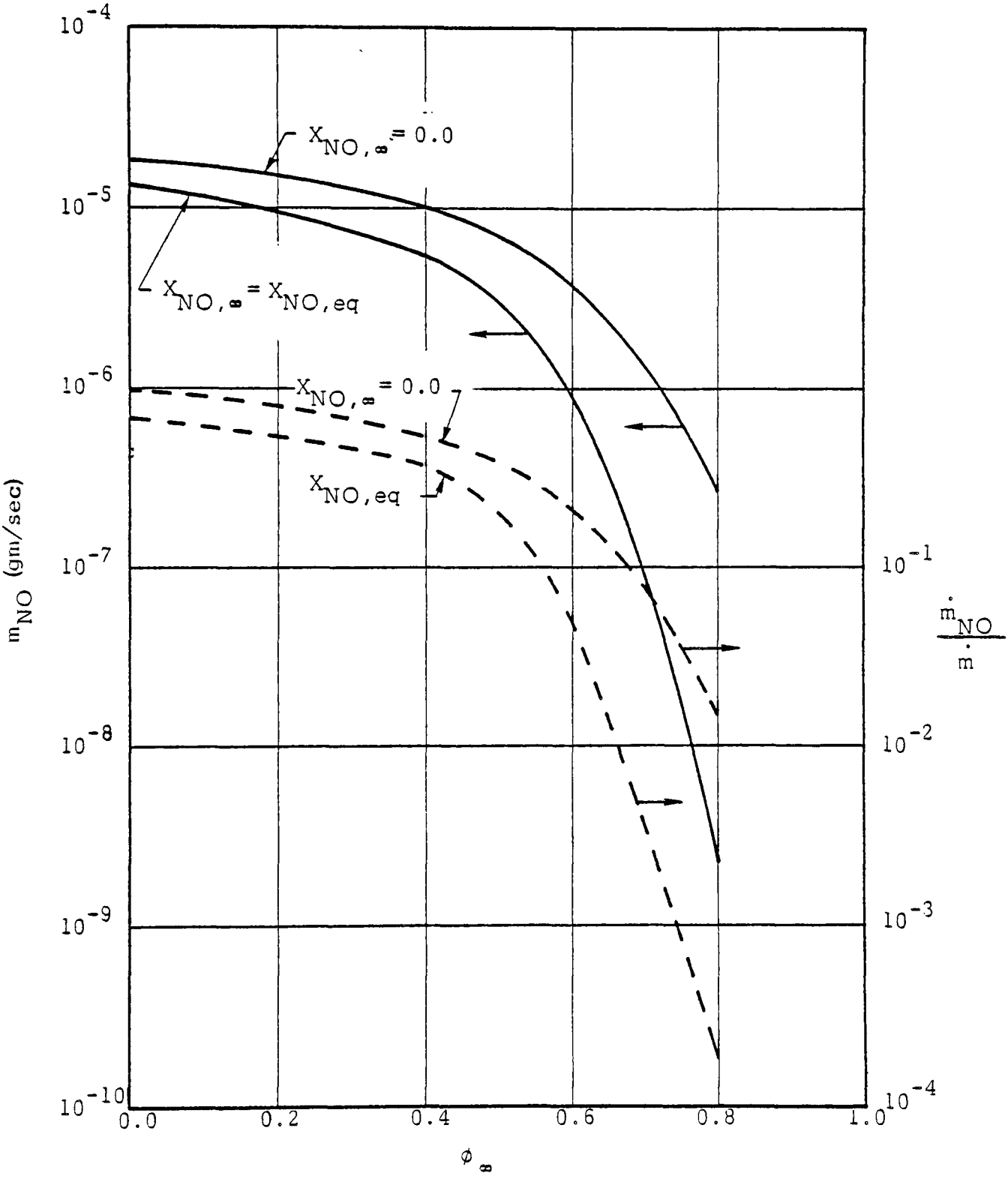

Figure 5-12 Effect of Ambient Oxygen Concentration on Rate of NO Formation Around a Burning Droplet

6.0 COMPARISONS BETWEEN ENGINE EMISSION LEVELS AND MODEL PREDICTIONS

The tuned model predictions have been compared to the engine performance data reported by Wilson et al[1]. The characteristics of the single cylinder experimental diesel engine were described in Section 5.2 as were the engine conditions used for the baseline data. The response of the model to the following parameters has been investigated:

- Engine operational parameters - timing, load and speed and compression ratio;
- Charge intake parameters - air swirl, turbocharging and exhaust gas recycle;
- Fuel injection parameters - diameter and number of orifices.

Calculations of both soot and NO formation are carried only as far as 30° after top dead center since initial calculations indicated formation and distribution rates were negligible beyond this point because of the low zonal temperatures. Calculated NO levels are given in ppm and soot in mg/m^3.

6.1 Effect of Engine Operating Parameters

Effect of Timing

The effect of fuel injection timing on exhaust NO level is well known. Timing retardation significantly reduces the emission of NO due to:

- reduction of ignition delay;
- heat release in the expansion stroke where bulk temperatures and pressure are declining
- reduction of the total residence time.

These effects are more pronounced at high load, that is, when the duration of fuel injection is longer. The comparisons of calculated and measured exhaust NO concentration are shown in Figure 6-1. For $\phi = 0.6$, a delay 8° CA injection reduces the NO by 35 percent, conversely a 70 percent increase in NO is observed by 8° CA timing advancement over baseline case. The effect of timing on the level of soot in the exhaust is shown in Figure 6-1. Higher

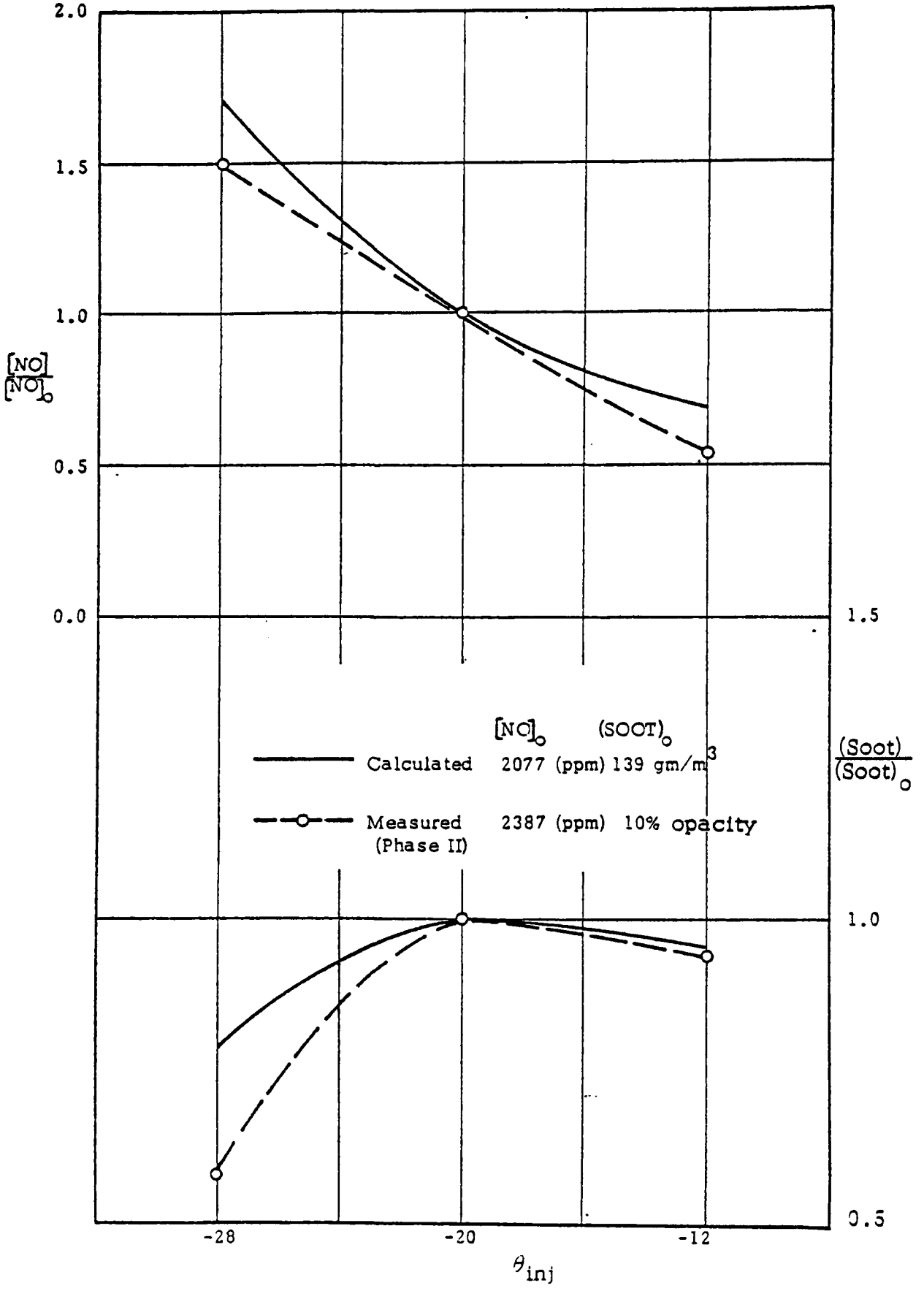

Figure 6-1 Effect of Timing

exhaust smoke is detected when the timing is retarded. Approximately 12 percent reduction in peak pressure is observed for every 8^{o} CA injection timing delay.

Effect of Load

The effect of overall equivalence ratio, ϕ, on NO and soot emission is shown in Figure 6-2. It has generally been observed that both NO and soot emissions decrease with load. The calculations were made with a constant injection rate and the load was varied by reducing the injection duration. The explanation for the increased soot emission at the lowest load ($\phi = 0.3$) is uncertain, and this is contrary to all the other experimental observations, but it could reflect a decrease in the rate of soot oxidation because of the lower temperatures.

Effect of Speed

Calculations were made for two engine speeds while the overall equivalence ratios and injection rates were maintained constant, thus the duration of fuel injection was increased from 17^{o} to 23^{o} corresponding to an engine speed increase of 1500 rpm to 2100 rpm. The comparison between the calculated and measured data is shown in Figure 6-3. The effect of residence time in a high temperature and pressure environment which is inversely proportional to the engine speed, is the dominating factor. The other effects of higher speed in the real engine such as higher injection pressure, higher valve overlap are not reflected by the calculations, however, compared to the residence time effect these are of minimum significance.

Effect of Compression Ratio

Decreasing the compression ratio will cause a decrease in both the cylinder temperature and pressure, both of which will tend to reduce the rate of NO formation. However, there are other important influential factors such as the effects of heat transfer and ignition delay.

The overall effects of the compression ratio on emission level are shown in Figure 6-4. The model predicts the trends; however, the comparisons of absolute magnitudes are very poor. The exaggerated influence of compression

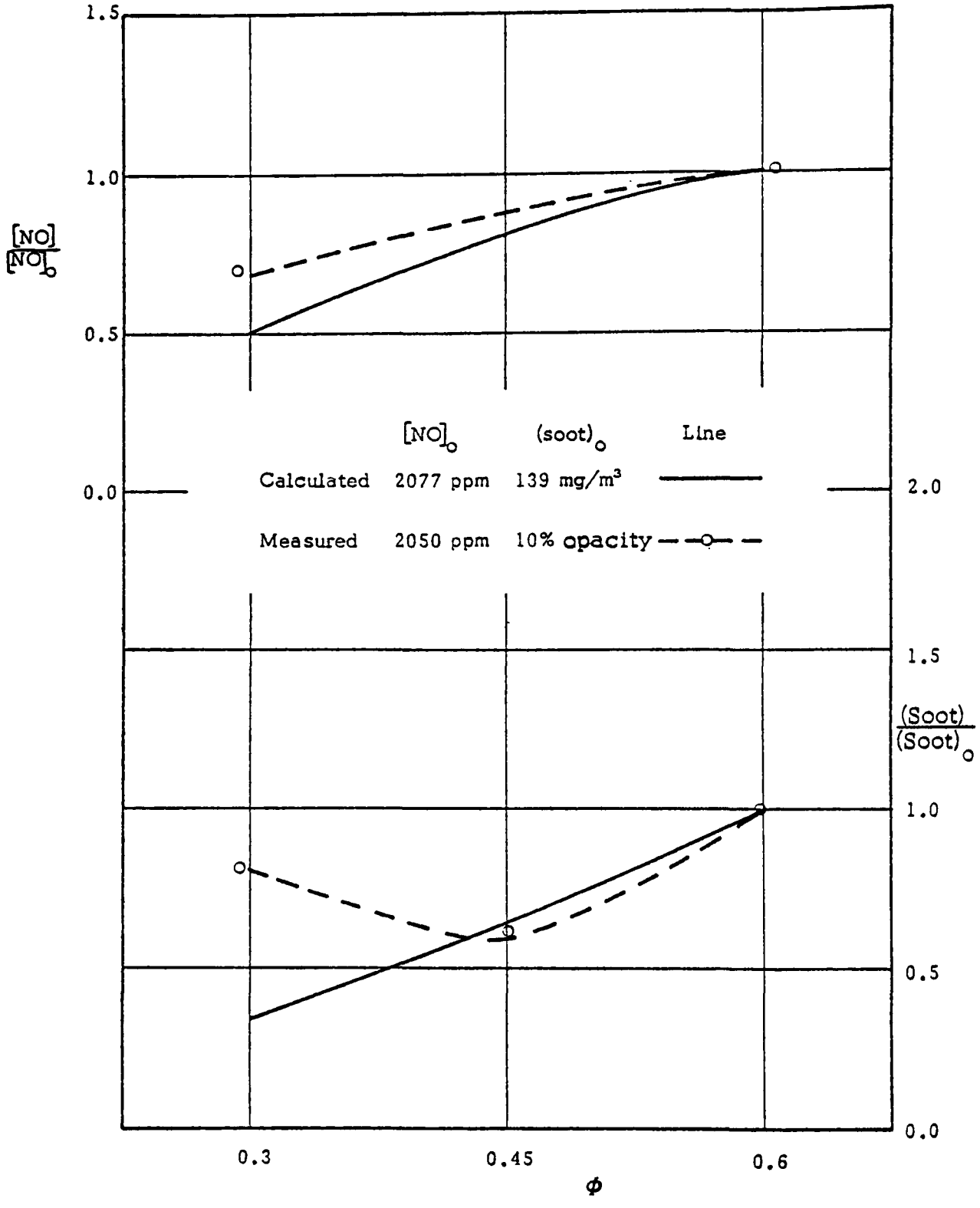

Figure 6-2 Effects of Load

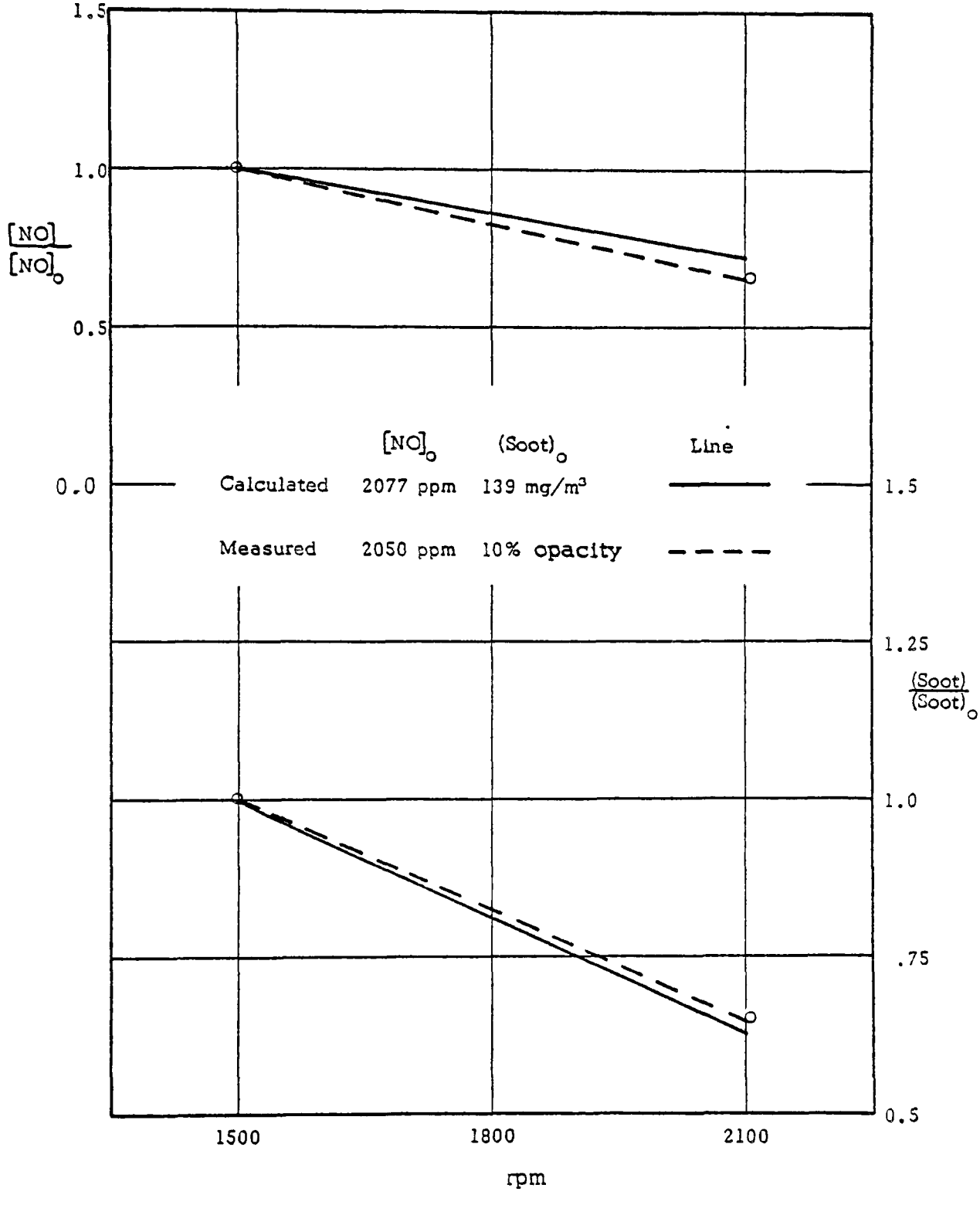

Figure 6-3 Effect of Engine Speed

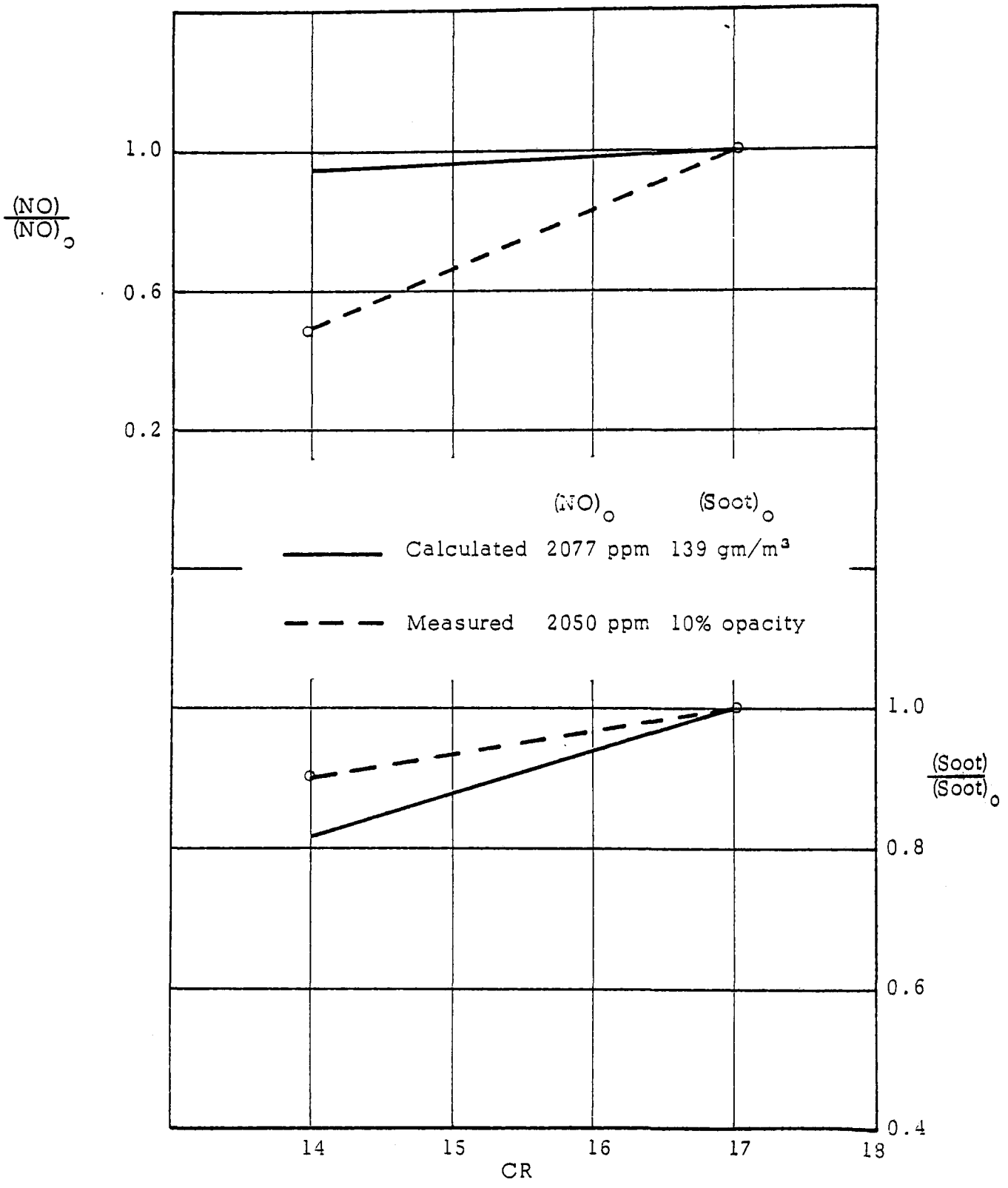

Figure 6-4 Effect of Compression Ratio

ratio can be attributed, in part, to C_{nor} which had been fitted for a higher compression ratio.

6.2 Effect of Charge Intake Parameters

Effect of Exhaust Gas Recirculation (EGR)

The effect of EGR was computed assuming a constant mass flow of intake charge (i.e., mass of fresh air intake plus mass of recirculated exhaust gas) and maintaining both the overall fuel/air ratio (i.e., proportionally reducing the fresh air intake and the mass of fuel) and the fuel injection rate constant. Figure 6-5 shows that excellent agreement is obtained between predicted and calculated NO emission from the measured values. However, there is complete disagreement with the measured soot values which probably reflects the model's lack of real understanding of the density of soot formation and does not take adequate account of the influence of temperature.

Effect of Air Swirl

The influence of the level of air swirl on NO formation can be seen in Figure 6-6, the NO concentration increases with increasing swirl. This effect is caused by the improved fuel-air mixing which leads to earlier heat release, thus the higher local temperatures and the increased oxygen availability promote NO formation. The experimental data from Phase I and that obtained during experiments with the sampling valve are scattered. Data reported by CAV[4] is also plotted for comparison and to give an indication of the normal trend.

The comparison of measured and calculated exhaust soot level is poor, particularly at higher swirl levels. This error is probably caused by an over-estimate of the influence of temperature on soot formation which is used in the present study. Thus, the higher dilution due to the higher swirl does not significantly lower soot emission in the calculated results.

Effect of Turbocharging

The effects of turbocharging on NO are plotted in Figure 6-7 and are compared with the experimental data obtained during Phase I. Poor agreement is shown between the predictions and measurements at low levels of super-charging. Computations at higher manifold pressure and higher loads were

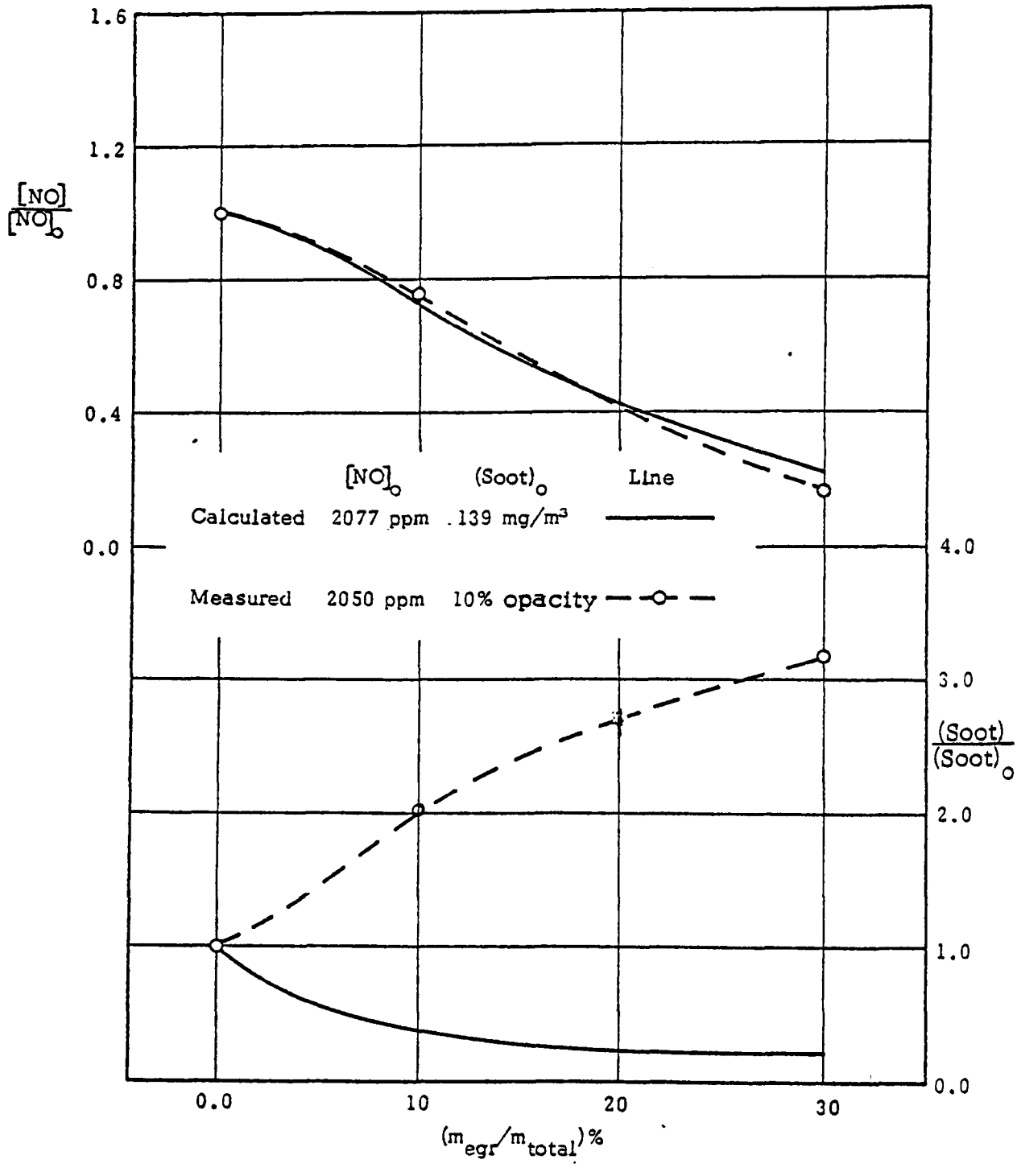

Figure 6-5 Effect of Exhaust Gas Recirculation

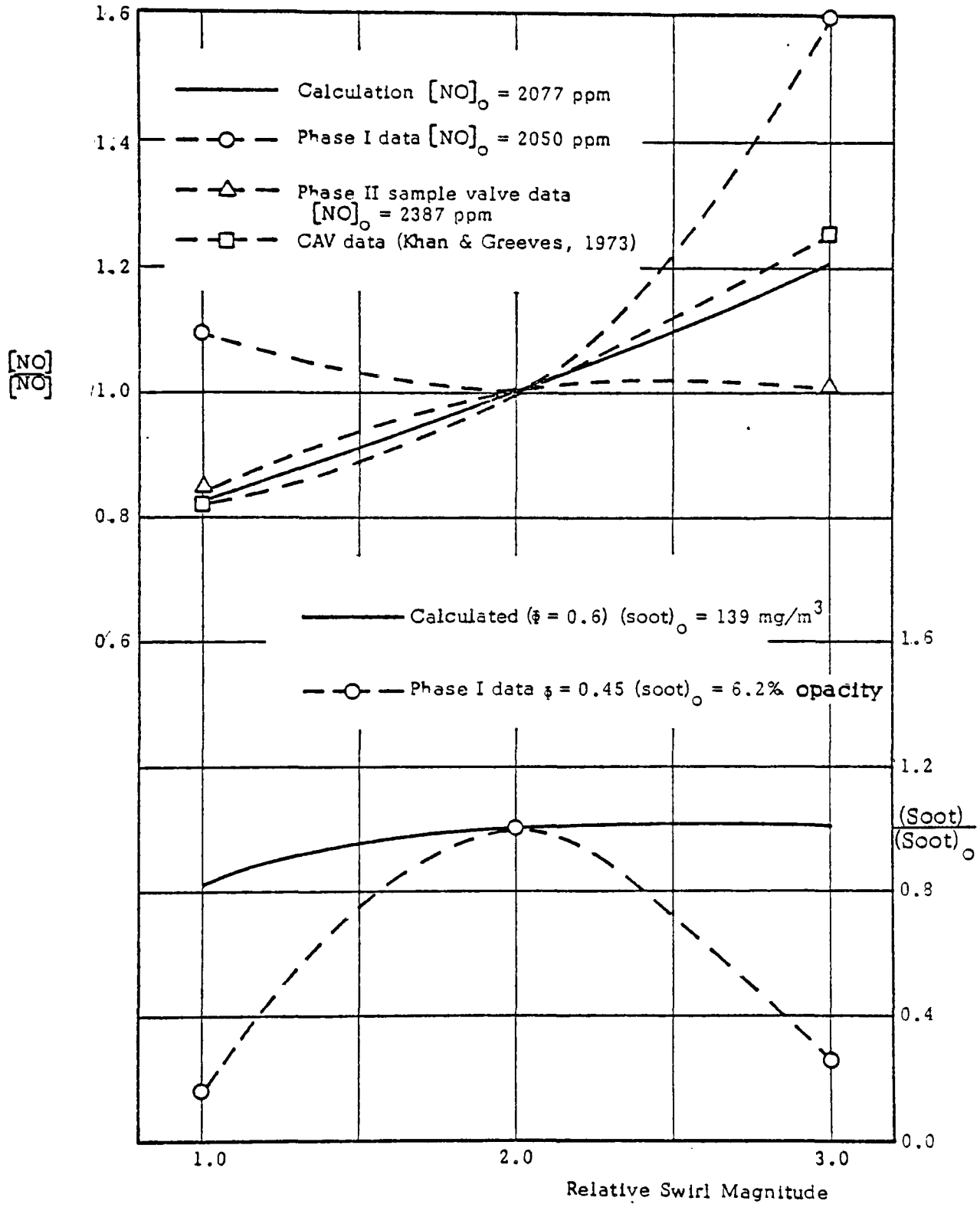

Figure 6-6 Effect of Swirl

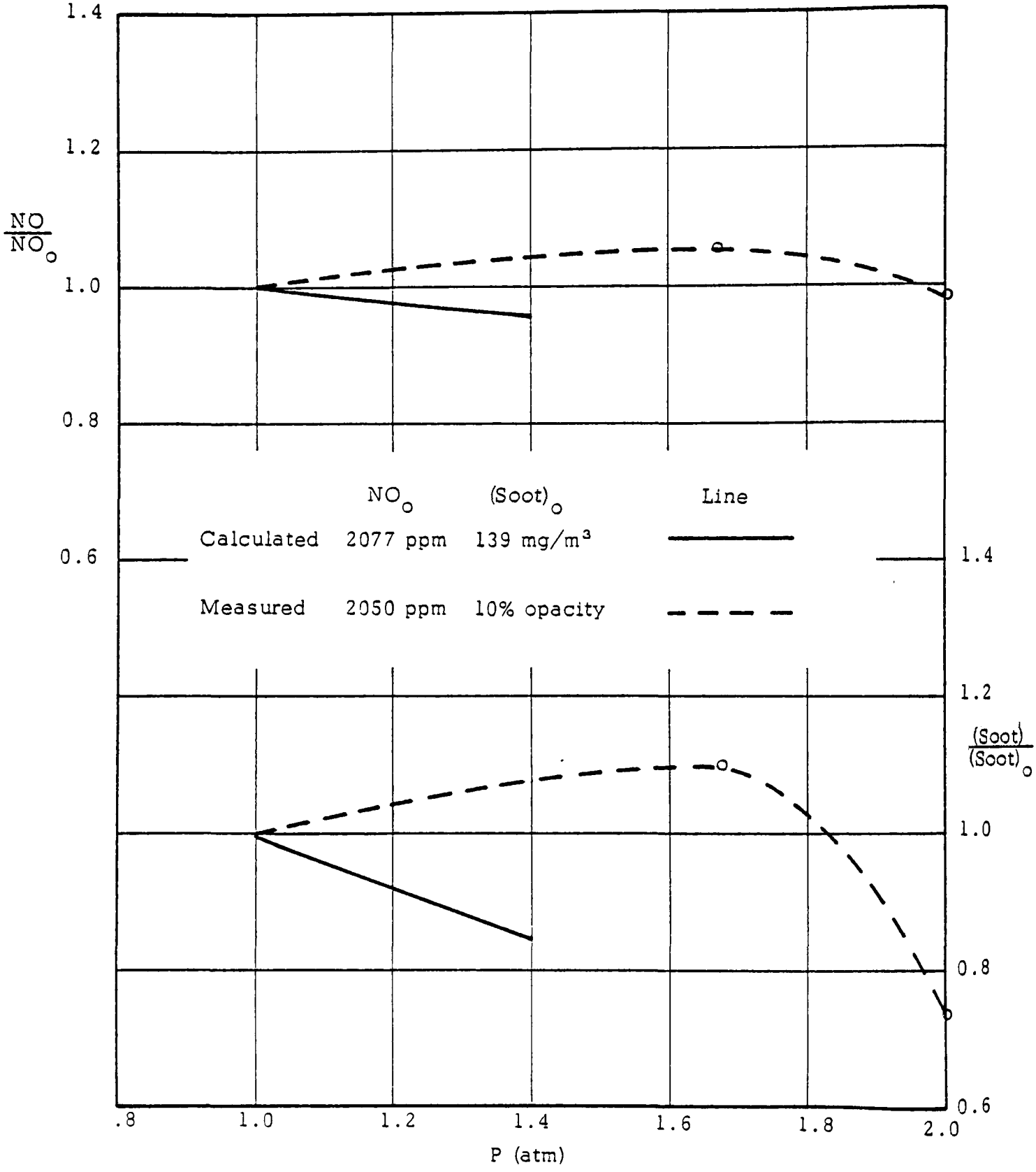

Figure 6-7 Effect of Turbocharge

limited by equilibrium species tables and thermodynamic property expressions; however, in future work this could easily be remedied.

6.3 Effect of Fuel Injection Parameters

Injector Orifice Diameter

The diameter of the fuel injection orifice affects both the fuel dispersion rate and the drop size distribution. Calculated exhaust pollutants for various fuel orifice diameters are plotted in Figure 6-8, along with the experimental data. The computations are based on constant total orifice area and a constant total fuel mass. The emission of an engine with larger and therefore fewer orifices showed substantial reductions in NO. The phenomena is mainly caused by a smaller total surface-to-volume ratio of vaporizing and burning fuel droplets in association with an increased mean droplet diameter which, in turn, reduces rates of vaporization, mixing and thus energy release rates.

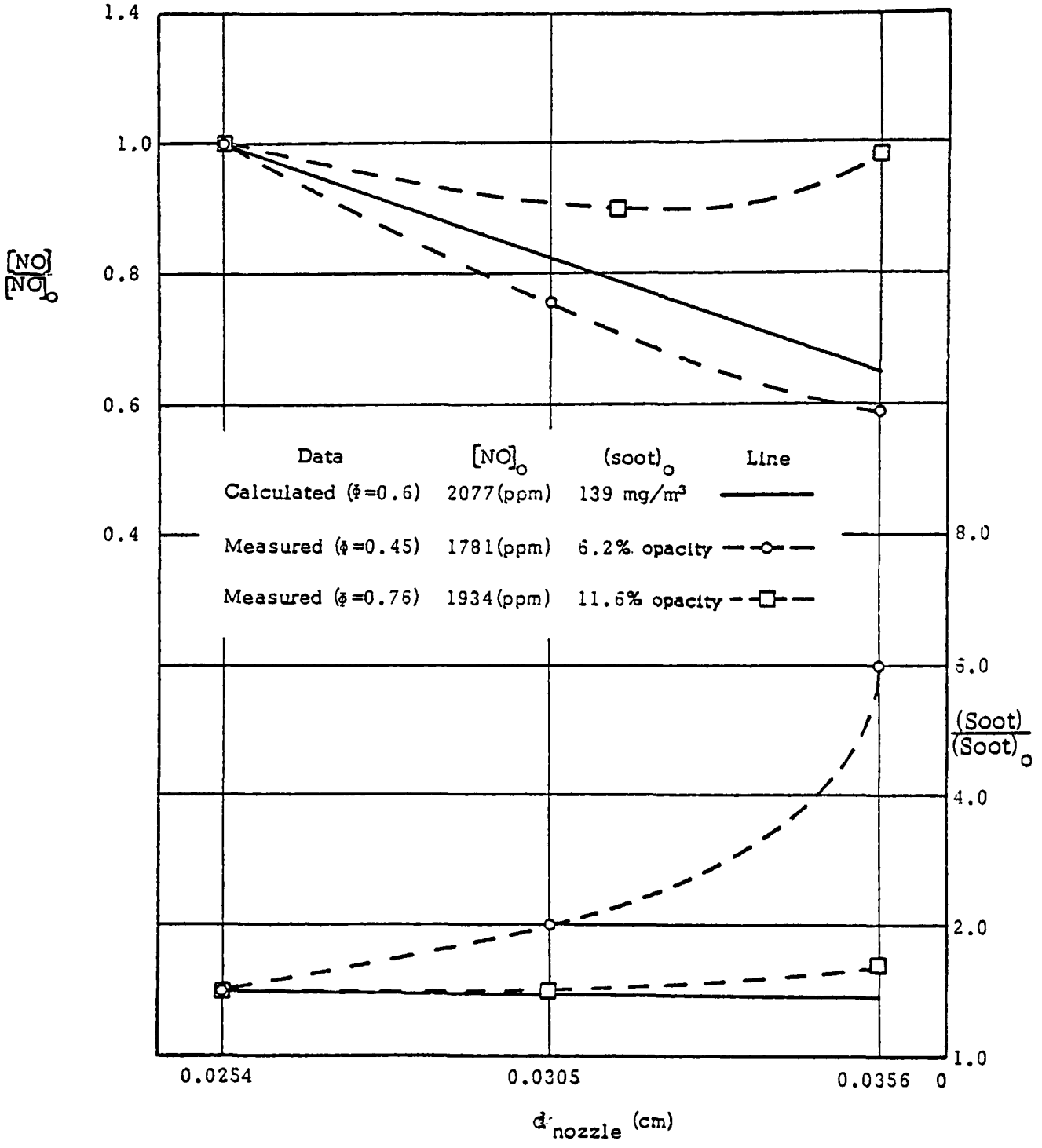

Figure 6-8 Effect of Orifice Diameter

7.0 LIMITATIONS OF THE MODEL AND RECOMMENDATIONS FOR FUTURE WORK

While it is unlikely that a diesel engine will be designed solely on the basis of a mathematical model, such a model can provide insight which will allow more rapid development of engines. The preceding sections have described the development of an analytical model which simulates the mechanisms of heat release and pollutant formation occurring within a direct injection diesel engine. Several simplifying assumptions have been made during the development process to allow the complex phenomena, which occur in practice, to be treated mathematically. Thus, the ultimate goal, that of building a model based entirely upon physical and chemical laws and free from empiricism has not been achieved. What has been accomplished is the construction of a modular model which will predict, after tuning, most of the pollutant emission characteristics of a single cylinder diesel engine. Its modular nature will enable the rapid update of any of the model's components as improved fundamental and experimental information becomes available.

Recognizing that gaps in fundamental knowledge make the inclusion of several empirical constants mandatory, the success of the model must be judged from predictions after adjustment of these constants for a particular class of engine. To date, the model has only been compared to single cylinder engine data. On the basis of these comparisons it can be concluded that the overall predictive capability of the model with respect to pressure history and exhaust NO levels is good while its ability to predict exhaust soot emissions can only be considered as fair. The model's predictive performance has been summarized qualitatively in Table 7-1.

Table 7-1. Summary of Model Predictive Capability

Variables	Exhaust NO	Exhaust Soot
Fuel Injection Timing	good	good
Load	good	fair
Engine Speed	good	good
Compression Ratio	poor	fair
Exhaust Gas Recirculation	good	poor
Swirl	good	poor
Turbocharge	poor	fair
Nozzle No. and Diameter	good	fair

Initial concepts concerning the formation of pollutants in compression ignition engines directed the model towards the consideration of droplet combustion. It was believed that spherical diffusion flames formed around droplets were typical of the "diffusion flame" nature of the combustion process. Experience with the model tends to refute this hypothesis. Undoubtedly, diffusion flames exist within the heat release zone, however their scale is apparently very different from those modeled by a spherical diffusion flame surrounding a single droplet. In order to include this type of heat release zone, a pseudo steady state confined droplet model has been formulated. Model calculations indicate that droplet contribution to the total production of NO is only significant in the early stages of heat release, and has a negligible influence on the final exhaust value. The results of these calculations can be attributed to:

- A large fraction (approximately 80 percent) of the droplets are contained within rich zones which cannot support spherical diffusion flames.
- The droplet lifetime is restricted to the time period close to top dead center where the available volume is small and therefore, the volume available for each separate spherical flame is small, thus minimizing the total flame surface area.
- The droplet environment contains NO produced during premixed combustion which will reduce the net rate of NO formation.

Exercise of the model has highlighted several deficiencies and omissions which can be easily modified in the near term; these include:

- Modifications to extend the equilibrium species tables to higher pressures and richer mixtures.
- Limits can be imposed upon the equilibrium assumption to enable carbon monoxide and hydrocarbon levels to be predicted.
- The model contains a very simple ignition criteria and it should be modified to take account of the equivalence ratio and temperature history of the fuel parcel.
- Mixing between burning zones should be included.

Four general areas of ignorance have been identified which require considerable effort to allow improvements to be made to the model; these include a transient fuel spray model, non-uniform fuel injection rate, an improved fuel spray dispersion model, and an improved energy release model. Both physical and numerical experiments will be necessary to allow improvements to be made in these components.

Transient Fuel Spray

The present model considers that the fuel spray behaves as though it were a steady state jet. No attempt has been made either to model the leading or the trailing edge of the jet. More experimental information is required before a realistic approach can be included in the model which will describe these transient phenomena.

Fuel Air Mixing

In view of the conclusions concerning fuel droplets, it is suggested that numerical and physical experiments be conducted to establish the importance of droplets. The phenomena of ignition may well be strongly linked to droplet properties. However, it appears that the major portion of the jet could be treated as a gaseous fuel. This would simplify certain aspects of the model and allow a more rigorous treatment of the fuel/air mixing process to take account of the following.

- air swirl;
- jets in cross flow; and
- jet interaction and three dimensional effects

An essential prerequisite for an improvement in the fuel/air mixing model is more detail of the mixing processes occurring in the cylinder under fired conditions. This is particularly true of conditions after ignition. A major unanswered question concerns the lifetime of the well-ordered jet structure.

Non-Uniform Fuel Injection Schedule

The fuel injection schedule is assumed to be constant. As a first simple step towards taking account of a non-uniform injection schedule the model could be modified to calculate the entrainment into a series of steady jets with different injection rates.

Heat Release Model

Improvement in the heat release model will be necessary if a more real approach to pollutant formation is required. This could occur if engines with low pollutant potential were being considered or fuels containing significant quantities of bound nitrogen were to be utilized. Under these conditions it will be necessary to treat the hydrocarbon oxidation process in more detail than the present equilibrium assumption.

In view of the fact that the model has only been tested against one set of experimental data, a necessary first set in deciding where the model needs the most refinement is it's application to other engine geometries and multicylinder engines.

8.0 NOMENCLATURE

A	Area (cm^2) or pre-exponential factors.
b	Jet half width (cm)
C	Constants
C_p	Constant pressure specific heat (cal/gm-°K)
C_v	Constant volume specific heat (cal/gm-°K)
D	Diffusion coefficient (cm^2/sec)
D_e	Engine bore (cm)
d	Droplet diameter (cm)
d_{max}	Maximum droplet diameter (cm)
E	Activation engine in Arrhenius rate expression
erf	Error function
f, F/A	Fuel/air ratio by mass
G	Mass fraction of a drop size group
h	Enthalpy (cal/gm)
I	Integral function
J	Heat equivalent of work
j	Stoichiometric oxygen - fuel mass ratio
K	Reaction rate constants, or absorption coefficient in measure of density of radiating particle per unit path length
L	Latent heat or characteristic length
m	Mass (gm)
$\dot{m}$	Mass flow rate (gm/CA)
M	Molecular weight
$\dot{M}$	Nondimensional droplet burning rate
N_{ce}	Cetane Number
P	Pressure (atm)
$\dot{P}$	Pressure derivative (atm/CA)
$\dot{Q}_c$	Rate of convective heat transfer (Cal/CA)
$\dot{Q}_R$	Overall ratio of radiative heat transfer (Cal/CA)
$\dot{q}$	Zonal rate of heat transfer (Cal/CA)
q	Heat of Combustion (Cal/gm)
R	Gas constant
R_L	Connecting rod length (cm)

NOMENCLATURE (Cont'd)

R_w	Crank radius or half stroke length (cm)
R_e	Reynolds number
r	Radial coordinate (cm)
T	Temperature (°K)
t	Time (sec)
u	Internal energy (cal/gm)
V, V_c	Volume and clearance volume (cm^3)
v	Velocity (cm/sec)
$\dot{W}$	Production rate (gm/cm^3-sec)
$(\dot{W})$	Production rate(gm/sec)
w	Number of carbon atoms in a fuel molecule
X, [ ]	Mole fraction
x	Axial or downstream coordinate (cm), or number of hydrogen atoms in a fuel molecule
Y	Mass fraction
y	Radial or cross-stream coordinate (cm)

Greek Symbols

σ	Stephen Baltzman constant
α	Absorptance or $\alpha = 1/(1+f)$
β	Volume ratio
γ	Fraction factor of convecture heat transfer
θ	Crank angle
Φ	Equivalence ratio defined as $\Phi = (F/A)/(F/A)_{stoich.}$
ρ	Density (gm/cm^3)
ξ	Nondimensional radial coordinate, y/b
κ	Thermal conductivity (cal/cm-sec-°K)
μ	Absolute viscosity (gm/cm-sec)
δ	Parameter for drop size distribution
τ	Characteristic time
η	Defined by $\eta = f/(1+f)$

Subscripts and Superscripts

a	Air (instantaneous)
a,a	Air available for air/product mixing process
apb	Air in premixed burning process
b	Burning process, or backward reaction
bm	Combustion products (instantaneous)
c	Convecture heat transfer or clearance
char	Characteristic properties
crit	Critical conditions
CO2	Carbon Dioxide
D	Dilution process (cumulated)
e1,e2	Vaporization process
eq	Equilibrium
fv	Fuel vaporized (cumulated)
fg	Fuel vapor (Instantaneous)
fld	Liquid fuel ignited (cumulated)
flb	Liquid fuel in burning process (instantaneous)
fdb	Liquid fuel burned in diffusion flame process (cumulated)
fpb	Fuel vapor burned in premixed process (cumulated)
fl	Liquid fuel in vaporizing process (instantaneous)
fj	Fuel injection process (cumulated), or free jet
f	Fuel, or forward reaction
H2O	Water
HET	Heterogeneous process
HOM	Homogeneous process
hu	Heat-up process
i	Zonal identification, i = a, fg, (bm,I)
ig	Ignition
inj	Fuel injection
I	I'th burning zone
j	Shell index
l	Liquid phase or droplet surface
max	Maximum
mix	Mixing process

NOMENCLATURE (Cont'd)

N2	Nitrogen
NO	Nitric Oxide
O2	Oxygen
o	Initial condition
os	Stoichiometry
r	Radiation
s	Soot; Swirl
sf	Soot formation process
so	Soot oxidation process
turb	Turbulence
v	Vitiation process (cumulated)
w	Wall
wj	Wall jet
$\mathfrak{C}$	Centerline
$(\dot{\cdot})$	Rate in crank angle (i.e. $d/d\theta$)
$(\bar{\ })$	Averaged value
$^{\infty}$	Ambient conditions

Note: Where other symbols are used, they are defined in the text.

9.0 REFERENCES

1 Wilson, R. P. Jr., Waldman, C.H. and Muzio, L.J., "Foundation for Modeling NO_x and Smoke Formation in Diesel Flames", Final Report for Phase I, EPA-460/3-74-002a, January, 1974

2 Bastress, E.K. et al, "Model of Combustion and Nitrogen Oxide Formation in Direct and Indirect Injection Compression-Ignition Engines" SAE No. 719053, 1971

3 Khan, I.M., Greeves, G. and Probert, D.M., "Prediction of Soot and Nitric Oxide Concentrations in Diesel Engine Exhaust," Inst. Mech. Engr., Paper C142/71, 1971

4 Khan, I.M. and Greeves, G., "A Method of Calculating Emissions of Soot and Nitric Oxide from Diesel Engines," SAE Paper No. 730169, January, 1973

5 Shahed, S.M., Chiu, W.S. and Yumla, V.S., "A Preliminary Model for the Formation of Nitric Oxide in Direct Injection Diesel Engines and Its Application in Parametric Studies," SAE Paper 730083, 1973

6 Shahed, S.M., Chiu, W.S. and Lyn, W.T. "A Mathematical Model of Diesel Combustion", Institution of Mechanical Engineers (1975).

7 Lyn, W. T., "Study of Burning Rate and Nature of Combustion in Diesel Engines," IX Symposium (International) on Combustion, 1963

8 Lyn, W. J., and Valdmanis, E., "The Effects of Physical Factors on Igntion Delay" SAE Paper 680102, 1968

9 Lyn, W. T. and Valdmanis, E., "The Effect of Physical Factors on Ignition Delay," Proceedings of Inst. of Mech. Engrs., Vol. 181, 2A, No. 1, 1966

10 Bowman, C. T., The Fourteenth Symposium (International) on Combustion, p. 729, The Combustion Institute, 1973

11 Fenimore, C. P., "Formation of Nitric Oxide in Premixed Hydrocarbon Flames", Thirteenth Symposium on Combustion, The Combustion Institute, p. 373, 1971

12 Myerson, A. L., Fifteenth Symposium (International) on Combustion, p. 1085, The Combustion Institute, 1975

13 Gordon, S. and McBride, B.J., "Computer Program for Calculation of Complex Chemical Equilibrium Compositions, Rocket Performance, Incident and Reflected Shocks, and Chapman-Jouguet Detonation", NASA, SP-273, NASA Lewis Research Center, 1971

14 Annand, W.J.D., "Heat Transfer in Cylinders of Reciprocating Internal Combustion Engines", Institution of Mech. Engrs. 1962

15 McAulay, K.J., et al, "Development and Evaluation of Simulation of Compression-Ignition Engine", SAE Paper No. 650451, 1965

16 Borman, G., "Mathematical Simulation of Internal Combustion Engine," Ph,D Thesis, University of Wisconsin, 1964

17 Lee, D. W., "The Effect of Nozzle Design and Operating Conditions on the Atomization and Distribution of Fuel Sprays", NASA Rept., 425,1932

18 Abramovich, G.N., "The Theory of Turbulent Jets", M.I.T. Press, 1963

19 Wise, H. and Agoston, G.A., "Burning of Liquid Droplet", Literature of Combustion of Petroleum, American Chemical Society, Washington, D.C., p. 116-135, 1958

20 Rosner, D.E. and Chang, W.S., "Transient Evaporation and Combustion of Fuel Droplet Near Its Critical Temperature". Combustion Science and Technology, Vol. 7, p. 145-158, 1973

21 Shipinski, J., Myers, P.S. nd Uyehara, D.A., "A Spray-Droplet Model for Diesel Combustion", Proc. Instn. Mech. Engrs., Vol. 184, PE 3J, p. 28-35, 1969

22 Williams, A., "Combustion of Droplets of Liquid Fuels: A Review", Combustion and Flame, Vol. 21, p. 1-31, 1973

23 Williams, F.A., "Combustion Theory", Addsion-Wesley Publishing Co., 1965

24 Zeldovich, J., "The Oxidation of Nitrogen in Combustion and Explosion", Acta Physicochimica USSR 21, 557, 1946

25 Baulch, D.L., Drysdale, D.D., and Lloyd, A.C., "High-Temperature Reaction Rate Data No. 1", Dept. of Physical Chemistry, The University; Leeds, England, May 1968

26 Wray, K.L. and Teare, J.D., "Shock Tube Study of Kinetics of Nitric Oxide at High Temperatures", J. Chemical Phys. 36, 2582, 1962

27 Caretto, L.S., Sawyer, R.F. and Starkman, E.S., "The Formation of Nitric Oxide in Combustion Processes", University of California Rpt. TS-68-1, 1968

28 Lee, K.B., Thring, M.W., and Beer, J.M., "On the Rate of Combustion of Soot in a Laminar Soot Flame," Combustion and Flame 6 p. 137-145, 1962

29 Field, M.A. et al, "Combustion of Pulverized Coal" BCURA, Cheney & Son Ltd., Banbury, England, 1967

30 Sitkei, G. and Ramanaiah, G. V., "A Rational Approach for Calculations of Heat Transfer in Diesel Engines", SAE Paper No. 720027, 1972

31 Bracco, F.V., "Nitric Oxide Formation in Droplet Diffusion Flames", 14th International Symposium on Combustion, p. 831-842, 1972

32 Ranz, W.D., Marshall, W.R., Chem. Eng. Prog. Vol. 48, p. 141-173, 1952

33 Frossling, N., Gerlands Beitr. Geophysics, Vol. 52, p. 170, 1938

34 Newman, J.A. and Brzustowski, T.A., "Behavior of a Liquid Jer Near the Thermodynamic Critical Region", AIAA, Vol. 9, No. 8, 1971

35 Gauntner, J.W., Livingood, J.N.B. and Hrycak, "Survey of Literature on Flow Characteristics of Single Turbulent Jet Impinging on a Flat Plate", NASA TN D-5652, Lewis Research Center, 1970

APPENDIX A

Simplified Representation of Fuel Spray

The basic fuel spray model assumes a two-phase round jet in a quiescent ambient atmosphere which impinges on a flat wall in a finite distance. A schematic representation of the jet is shown in Figure 4.2 . The jet is characterized by four distinct flow regions:

- The initial region: extends from the orifice exit plane to the apex of constant velocity core x_i
- The main region: includes that part of the jet from the end of the potential core to the wall. This region is characterized by the decay of centerline velocity and self-preserving transverse profiles
- The transient region: the region where the jet is deflected and trasnformed from a free jet to a wall jet
- The wall region: includes that portion of the jet where it spreads three-dimensionally and axisymmatically with respect to axis of injection.

(i) Initial Region

The growth law in this region is calculated by

$$\frac{db}{dx} = 0.135 \left(1 + \frac{\rho_a}{\rho_f \mathbb{C}_o}\right) \qquad \text{(A-1)}$$

where constant $C_i = 0.135$ was used by Newman and Brzustowski[34].

(ii) Main Region

Self-preserving velocity and fuel concentration profiles (Abramovich[18]), are assumed.

$$\frac{v}{v_{\mathbb{C}}} = (1 - \xi^{1.5})^2$$

$$\frac{\left(\rho_f / \rho_a\right)}{\left(\rho_f / \rho_a\right)_{\mathfrak{L}}} = \left(1 - \xi^{1.5}\right) \tag{A-3}$$

where $\xi = \frac{y}{b}$ and the constant growth law is assumed:

$$\frac{db}{dx} = C_{fj} = \text{constant} \tag{A-4}$$

where $C_{fj} = 0.175$ corresponds approximately to 10 degree half spray angle. Utilizing the law of conservation of momentum, the decay of centerline velocity in main region can be derived as:

$$V_{\mathfrak{L}} = \frac{1}{2}\left\{\frac{-J_f I_{f5}}{\rho_a b^2 I_{f4} I_{f3}} + \sqrt{\left(\frac{J_f I_{f5}}{\rho_a b^2 I_{f4} I_{f3}}\right)^2 - 4\left(\frac{J_m}{\rho_a b^2 I_{f4}}\right)}\right\} \tag{A-5}$$

Similarility from the law of conservation of fuel mass, the decay of fuel concentration in the main region can be obtained as:

$$\left(\frac{\rho_f}{\rho_a}\right)_{\mathfrak{L}} = \frac{J_f}{\rho_a v_{\mathfrak{L}} b^2 I_{f3}} \tag{A-6}$$

The values of the integrations

$$I_{fn} = 2\pi \int_0^1 \left(1 - \xi^{1.5}\right)^n \xi \, d\xi \tag{A-7}$$

are listed in Table (A-1) for various n.

J_f and J_m appearing in the above equations are the flux fuel mass and the flux of momentum, respectively.

The locus of the mass element in "j" shell is expressed by

$$(j - 1/2)\Delta I_f = 2\pi b^2 \int^{\xi_j} \rho_f v \xi \, d\xi \qquad (A-8)$$

(iii) Transient Region

The initial conditions of the wall jet are obtained from conversation of mass and mechanical energy during the transition. The initial width and velocity of 3-D wall jet are expressed as:

$$b_o' = \frac{I_{f2}}{I_2}\left[\frac{b_w v_{\ell w}}{(V'_\ell)_o}\right] \qquad (A-9)$$

$$\left(v'_\ell\right)_o = \left\{\frac{I_2\,[\rho_a I_{f6} + \rho_{f\ell w} I_{f7}]}{I_{f2}\,[\rho_a I_6 + (\rho_{f\ell}')_o I_{f7}]}\right\}^{\frac{1}{2}} v_{\ell w} \qquad (A-10)$$

The initial fuel density of the wall jet at the location nearest to the wall is obtained from conservation of fuel mass:

$$\left(\rho'_{f\ell}\right)_o = \frac{I_f I_2}{b_w^2 v_{\ell w} I_{f2} I_3} \qquad (A-11)$$

Where subscript "o" represents the values at r = b and the numerical values of the integrations

$$I_n = 2\pi \int_o^1 (1 - \xi^{1.5})^n \, d\xi$$

are evaluated and listed in Table (A-1). It should be noted that the energy dissipation and entrainment during the transition from the jet to the wall jet are not considered.

(iv) Wall Region

Self-preserving velocity and fuel concentration profiles are assumed i.e.

$$\frac{v'}{v'_{\xi}} = (1 - \xi^{1.5})^2 \tag{A-12}$$

$$\frac{(\rho_f/\rho_a)'}{(\rho_f/\rho_a)'_{\xi}} = (1 - \xi^{1.5}) \tag{A-13}$$

The boundary layer in the vicinity of the wall is not considered here. The growth law of the wall jet is:

$$\frac{db'}{dr} = C_{wj} = \text{constant} \tag{A-14}$$

where $C_{wj} = 0.204$ is taken from the work by Gauntner, et al [35].

The fuel concentration nearest to the wall, derived from mass conservation relationship is

$$\left(\frac{\rho_f}{\rho_a}\right)'_{\xi} = \frac{I_f}{\rho_a v'_{\xi} (r + bw)\, b' I_3} \tag{A-15}$$

The velocity decay, derived from conservation of momentum flux, is

$$v'_{\ell} = \frac{-\frac{I_5}{I_3} J_f + \sqrt{\left(\frac{I_5}{I_3} J_f\right)^2 + 4 (r + b_w) b' \rho_a I_4 J'_m}}{2 (r + b_w) b' \rho_a I_4} \qquad \text{(A-16)}$$

where initial jet momentum flux is

$$J_m' = b_w b_o' (v'_{\ell})_o^2 [\rho_a I_4 + (\rho'_{f\ell})_o I_5] \qquad \text{(A-17)}$$

Similar to Eqn (A-9) the Trajectories of fuel elements in the wall region are computed from

$$\frac{1}{5.5} \xi_j^{5.5} - \frac{3}{4} \xi_j^4 + \frac{3}{2.5} \xi_j^{2.5} - \xi_j = \frac{-(j - \frac{1}{2}) \Delta J_f}{2 \pi \rho'_{f\ell} v'_{\ell} (r + b_w) b'} \qquad \text{(A-18)}$$

Table A-1 Numerical Values of I_n & I_{fn}

n	I_n	I_{fn}
1	3.7699	1.3446
2	2.8274	0.8105
3	2.3122	0.5592
4	1.9854	0.4209
5	1.7487	0.3311
6	1.5738	0.2709
7	1.4730	0.2276

APPENDIX B

Coefficients for Equations (4-25) and (4-26)

These polynomial coefficients are obtained from least-square curve fitting of computed results from NASA Equilibrium Program[13], particularly for H/C equals 1.7. For fuel having different H/C, these coefficients have to be reevaluated.

Table B-1. $\phi \leq 1.0$

i	a_i	b_i	d_i	r_i
1	-5.5492E+01	7.3465E+02	1.3700E+01	6.8789E-02
2	7.8374E-02	3.7817E-02	-1.1-17E+00	4.3293E-03
3	1.6734E-04	-1.0774E-04	-5.7155E-01	-9.8361E-01
4	-1.1376E-07	6.1112E-08	-2.6780E+01	6.6435E+00
5	4.0737E-11	-1.4435E-11	7.2448E+00	1.1172E-01
6	-5.4383E-15	9.9489E-16	1.3090E+00	2.3055E+00
7			5.0189E-01	-2.5753E+01
8			-5.2147E-01	-4.0113E-01
9			5.3444E-02	
10			-2.6396E+00	
11			1.6069E+00	

Table B-2. $3.5 > \phi > 1.0$

i	a_i	b_i	d_i	r_i
1	-8.5550E+02	-1.1796E+02	9.7714E+00	4.3246E-02
2	2.5318E-01	6.5986E-01	4.3547E+00	1.2509E-02
3	-1.6176E-05	-1.1693E-03	-7.2560E-02	2.3144E-01
4	-1.0564E-07	7.1490E-07	-9.6828E+00	-3.8400E-01
5	7.2508E-11	-1.8777E-10	-1.5763E+01	-3.3850E-03
6	1.2100E-14	1.7905E-14	2.3124E-01	-4.0000E+00
7			-6.4446E+00	2.9256E-01
8			7.2392E+00	-1.7973E-02
9			5.2083E-03	
10			2.2071E+01	
11			-2.5775E+01	

APPENDIX C

CHARACTERIZATION OF DIESEL COMBUSTION BY DIRECT IN-CYLINDER SAMPLING

C-1. INTRODUCTION

The model of diesel engine combustion described in the body of this report includes several arbitrarily adjusted constants and is based upon a healthy dose of conjecture. In an attempt to provide experimental evidence to support the model development, an effort has been made to characterize the cylinder contents during the period of heat release. Wilson et al[1] reported earlier unsuccessful efforts to utilize ultraviolet emission and absorption spectroscopy for this purpose. A sampling valve, which was designed by the Ricardo Company and provided to Ultrasystems by the General Motors Research Laboratories, has been used in an attempt to provide data to aid further model development.

In addition to the overall objectives stated above, one important feature of the project was to establish the validity of the results from in-cylinder direct sampling. The project could not be concluded in the present study, but answers to the following questions were sought:

- What kind of spatial and temporal resolutions are possible?
- On what scale is it possible to characterize gradients and unmixedness in the system?
- To what degree is the sample analyzed, representative of the system being measured?

C-2. *EXPERIMENTAL EQUIPMENT*

The characteristics of the single cylinder diesel engine used in these experiments have been given elsewhere[1]. The sampling valve was designed around a powerful electromagnet and armature originally intended to operate a Societe Francaise d'Etudes et de Development de l, Injection (S.O.F.R.E.D.I.) diesel fuel injector. A detailed description of the development,

construction and operation has been given by Nightingale[2]. Details of the sampling valve tip used in this investigation are given in Figure C-1. Valve lift and open times are dependent upon spring strength, which acts to close the valve, and the magnitude and duration of the current pulse passing through the electromagnet. Since cylinder pressure acts to open the valve, adjustments must be made to provide constant sampling conditions for different loads and crank angles. The actual valve opening time represents a compromise between that necessary to provide sufficient sample for analysis and a desire to maintain a high temporal resolution. Figure C-2 provides a schematic of the sampling system. In the final series of tests the triggering delay electronics for activating the electromagnet which allowed an accurate adjustment of the triggering crank angle were supplied by AiResearch.

Experience with the sample valve indicated that the titanium valve tip and seat could not maintain satisfactory operation under conditions of high load and insertion. In the initial series of tests an insertion of 1/4 in. was only possible at part load. Leakage occurred after a short period of time due to the forging action of the valve stem. This problem was overcome in the final test series by using Waspolloy (0.50 Nc; 0.19 CN, 0.14 CO, 0.04 MO and 0.03 Tc) for the valve seat and titanium carbide for the stem tip. These design modifications allowed operation under high engine load conditions with full insertion without leakage. Included in Figure C-1 is an alternate valve tip design which utilizes a sphere as the tip, rather than a conical section. The sphere is a press fit into the end of the stem and the seat is coined rather than machined thus allowing rapid inexpensive renewal of the valve component not subject to failure.

The sampling probe could be located in three different ports in the cylinder head. Rotation of the fuel injector then allowed samples to be obtained on these three radii at any distance from the fuel jet axis. Figure C-3 shows the radial location of the three sampling ports.

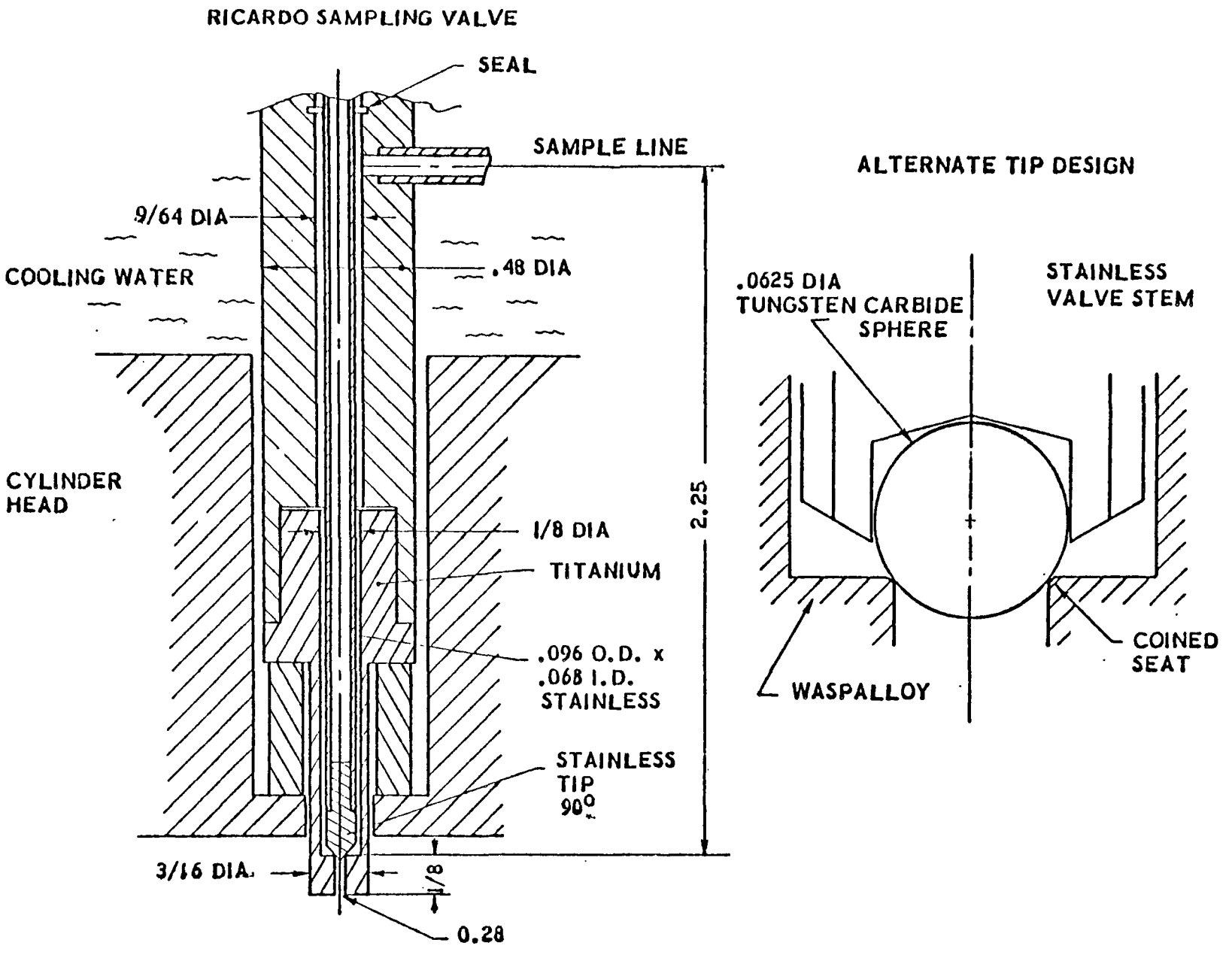

Figure C-1. Details of Sampling Valve Tip

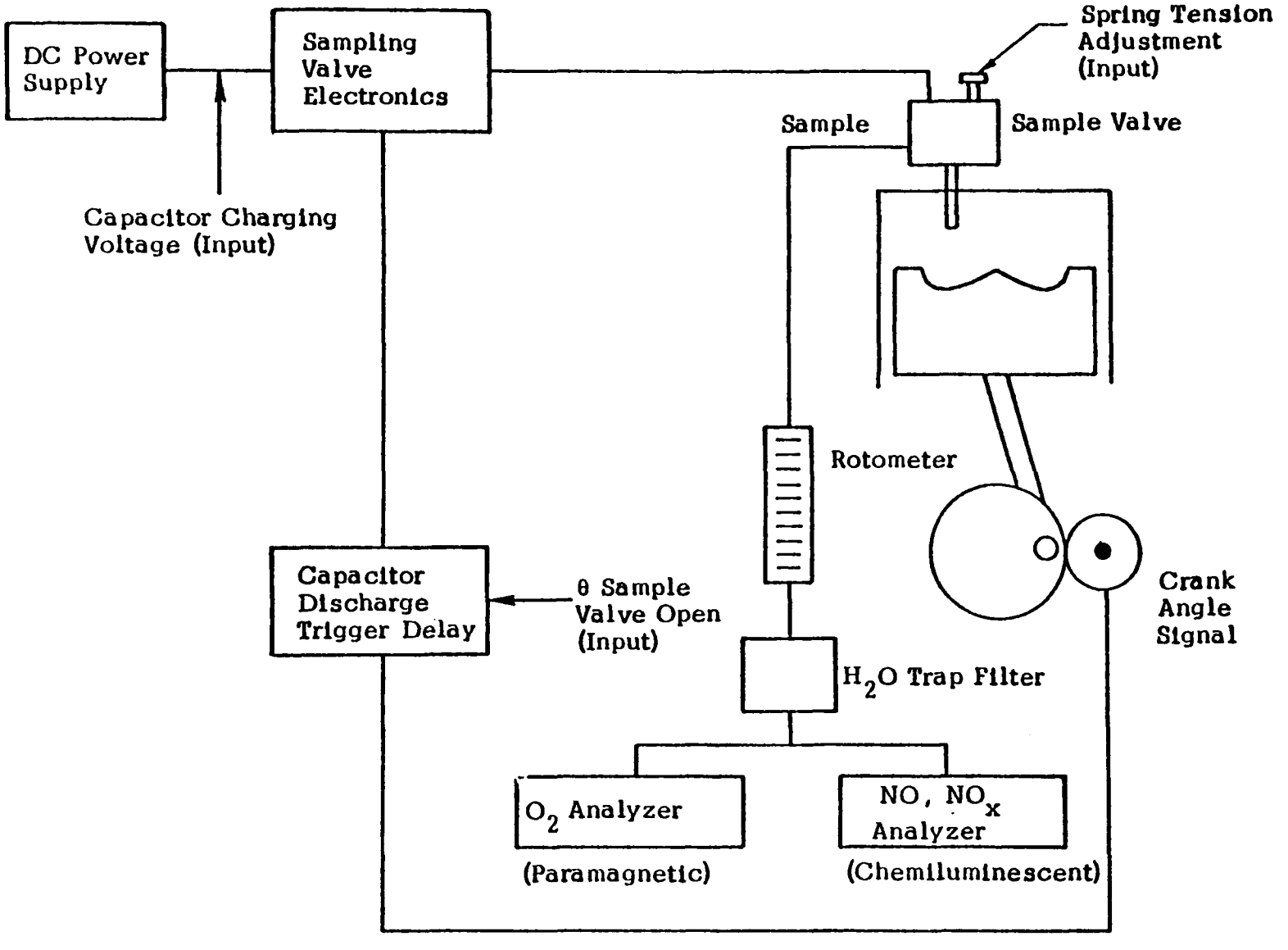

Figure C-2. Schedule of Sampling System

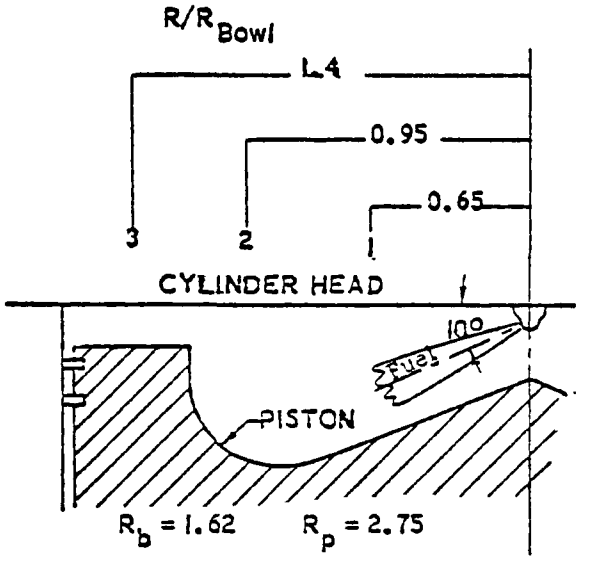

Figure C-3. Location of Sample Valve Ports

C-3. RESULTS

Four test series, all of which were not completed, have been carried out using the sampling valve:

Series 1 – All exhaust values were higher than the local values at 40° after TDC .

Series 2 – Problems with the sampling train were corrected, but engine failure occurred before the test matrix was completed.

Series 3 – Complete test matrix, but discrepancies apparent in results.

Series 4 – Partial test series with new valve tip and seat after the engine had been rebuilt.

An impression of the differences in the results obtained from the various test series can be gained from the curves of NO_x versus sampling valve opening time presented in Figure C-4. In Series 1 all the sample valve NO_x values dropped below the exhaust value. Although local values must not necessarily agree with the exhaust level at 40 ATDC it was thought that the sample valve values should show some distribution about the final level. Examination of the sample train indicated that NO was being converted to NO_2 in the sample line with subsequent loss of NO_2 in the condensate. Sample line lengths were reduced, a chemical drier was eliminated from the train and a water trap fitted close to the outlet of the sample valve. After these modifications, results typified by those shown in Figure C-4 for Series 2 were obtained. Unfortunately, before the second test series could be completed, an engine failure occured and after repair the pollutant emissions for the same nominal engine conditions were different.

In the third series of tests a complete test matrix was carried out and the curves presented in Figure C-4 give an impression of their characteristics in comparison with earlier results for the same engine condition. Table C-1 lists the test matrix which was carried out in the third series of tests, and a complete listing of experimental data is included in Appendix D.

Three problems are apparent upon examination of this data:

- Variation in exhaust levels for what are nominally the same engine conditions.
- Differences in the influence of swirl on exhaust emissions from test to test.
- Errors in the measurement of NO_x concentrations.

An impression of the reproducibility of the exhaust NO levels can be gained from the results presented in Table C-2. Even discounting the obvious rogue values, the results exhibit a considerable degree of scatter. This scatter may be associated with slight changes in engine parameters such as ignition timing. Whatever their cause, they indicate that the in-cylinder sampling results could have a greater level of uncertainty.

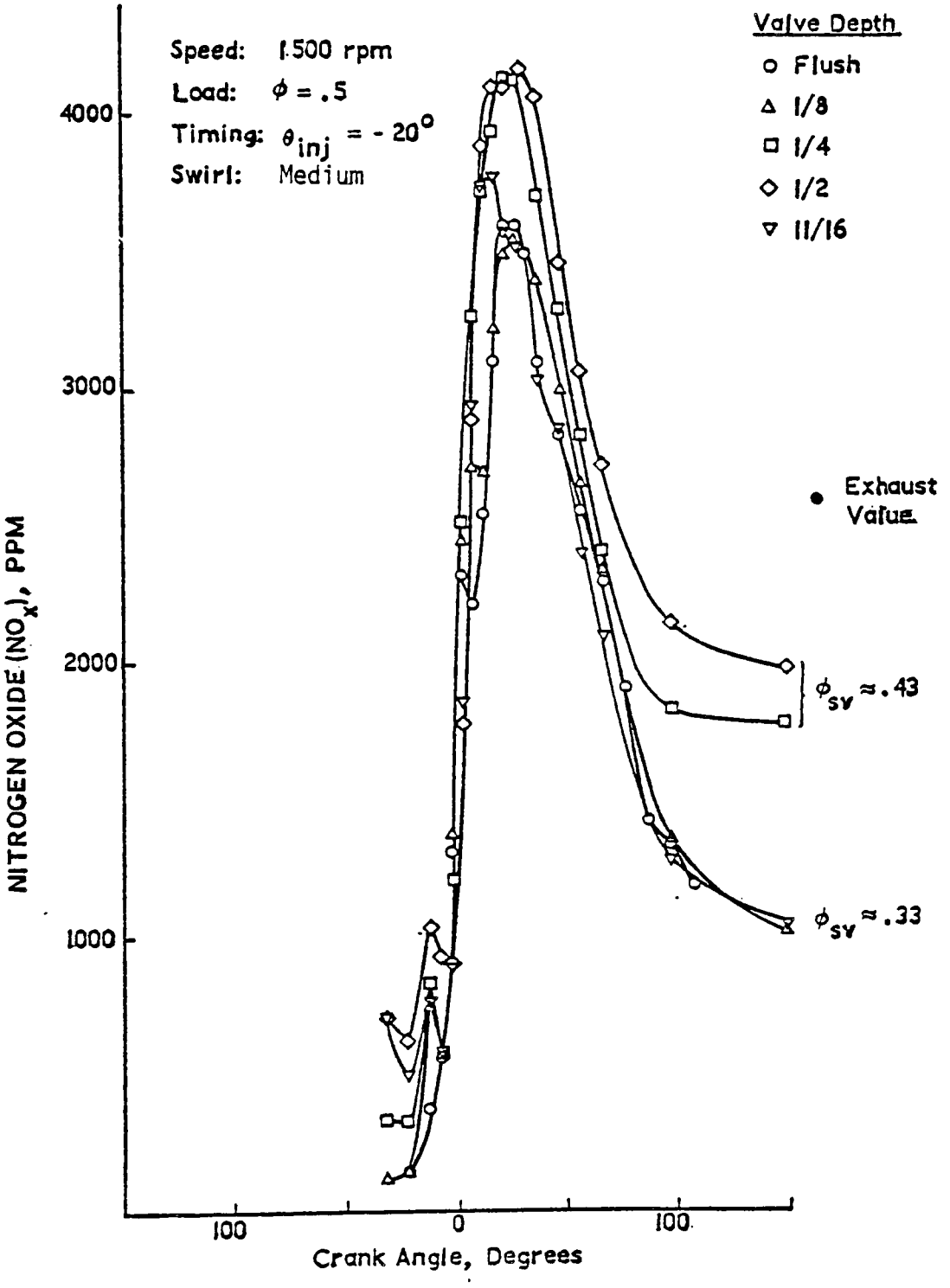

Figure C-4. Dependence of Sample Valve Measurement on Valve Insertion Depth

Table C-1. Experimental Condition for In-Cylinder Investigations

Series	R.P.M.	Load	No. of Orifices in Injector	Timing	Swirl	No. of Valve Locations	Remarks
A	1500	0.6	6	-20	Low Medium High	8 7 6	
B	1500	0.6	4	-20	Medium	6	
C	1500	0.6	6	-28	Medium	8	
D	1500	0.6	6	-12	Medium	8	
E	2100	0.6	6	-20	Medium	4	
F	1500	0.35	6	-20	Low Medium	2 2	* *
G	1500	0.35	6	-28	Medium	2	*
H	1500	0.35	6	-12	Medium	2	*
I	1500	0.3	6	-20	Low Medium	6 8	

*Series with sample valve inserted 0.25 in.

Table C-2. NO_x Exhaust Emission Levels Measured For Different Sample Valve Locations (Series 3)

θ_{inj}		
-20°	-28°	-12°
2431	3210	1254
2333	3100	940
2435	3245	1412
2382	3540	1395
2360	3600	1085
2669	3823	1230
2840	4440	1209
2300	3640	1300
2460		1300
Swirl	Medium	
Load ϕ	0.6	
RPM	1500	

As discussed earlier, between the second and third test series there was an unexplained jump in the baseline emission levels. What is perhaps more disquieting, is that there was also a change in the behavior of the engine. Data presented in Section 6 shows that the measured influence of swirl level on NO_x emissions was not reproduced from Phase I to Phase II. The emission levels tabulated in Table C-3 indicate that the "influence of swirl" also varied between the second and third sampling valve test series.

Table C-3. Comparison of the Influence of Exhaust Emission Levels for Series 2 and 3

1500 rpm $\varphi = 0.6$ -20 ATC

Series 3

Low Swirl		Medium Swirl		High Swirl	
NO_x	O_2	NO_x	O_2	NO_x	O_2
1805	8.8	2431	8.7	2534	8.4
1780	8.8	2435	8.6	2200	8.6
1555	8.8	2383	8.7	2200	8.6
1717	8.8	2396	8.8	2190	9.0
1670	8.6	2300	8.8	2100	8.6
1685	8.3	2460	8.7	2450	8.9
1830	9.0	2411	8.3		

Series 2

2230	8.8	1340	7.0	2800	8.4
2290	7.5	1430	7.8	2830	7.8
2470	8.1	1200	7.6	2670	8.8
		1460	8.0	2880	8.9

The dead volume in the sampling system was reduced as much as possible. However, the sample analyzed always contained a significant fraction of NO_2, and it is not known whether all of this is due to oxidation in the sample line or whether NO_2 is actually formed in the cylinder. Consequently, the concentration of interest is that of the total nitrogen oxides since the NO level will not be sufficient to characterize the pollutant content of the sample. NO_x levels were determined by passing the sample through a converter which normally converts the nitrogen dioxide to nitric oxide, thus allowing the total nitrogen oxides to be measured by the chemiluminescent analyzer. However, when the sample contains fuel gases such as hydrocarbons and carbon monoxide (the sample would probably also include hydrogen, but this was not measured) NO_x levels lower than NO levels can be recorded. Typical results are presented in Table C-4 where it can be seen that for samples withdrawn around TDC the NO_x levels are obviously in error. Thus, the results will misrepresent actual NO_x levels when fuel gases are present tending to give lower rates of NO_x increase since these are the samples normally containing fuel gases.

The modified valve design allowed measurements to be made during the fourth test series with much deeper valve insertion distances. Several of the results obtained with this design are presented in Figure C-1. Time restricted the extent of the test matrix which was limitted to one sample valve position (No. 2) with the fuel nozzle rotated such that the sample valve was located 30° downstream from the initial jet orientation. Probe insertion was varied between the flush condition and 11/16 inch penetration. Swirl and injection times were varied, while load and speed were held constant at $\phi = 0.5$ and 1500 rpm. Considerable care was taken to ensure that exhaust levels were reproducible and that actual sample valve data was repeatable.

In the fourth series of tests the sample valve was operated over a wider cycle range since it was expected that at sample times greater than $+100^{\circ}$ the sample valve concentration would approach the exhaust values. As shown in Figures C-4, 5, 6 and 7, this was not the case for this one sample valve

Table C-4. Examples of Erroneous NO_x Concentrations Due to Converter Errors

Sample Time	Measured NO_x ppm	Measured NO ppm	Calculated NO_2 ppm	Measured O_2 %
-32	291	166	125	19.5
-22	201	113	88	19.0
-12	126	322	-196	14.2
-7	1880	1600	280	11.0
-2	2722	2300	422	10.5
3	3580	2811	769	10.7
-22	152	140	12	19.8
-12	255	350	-95	9.8
-7	245	410	-165	8.5
-2	1085	960	125	12.0
3	2130	1820	310	13.2

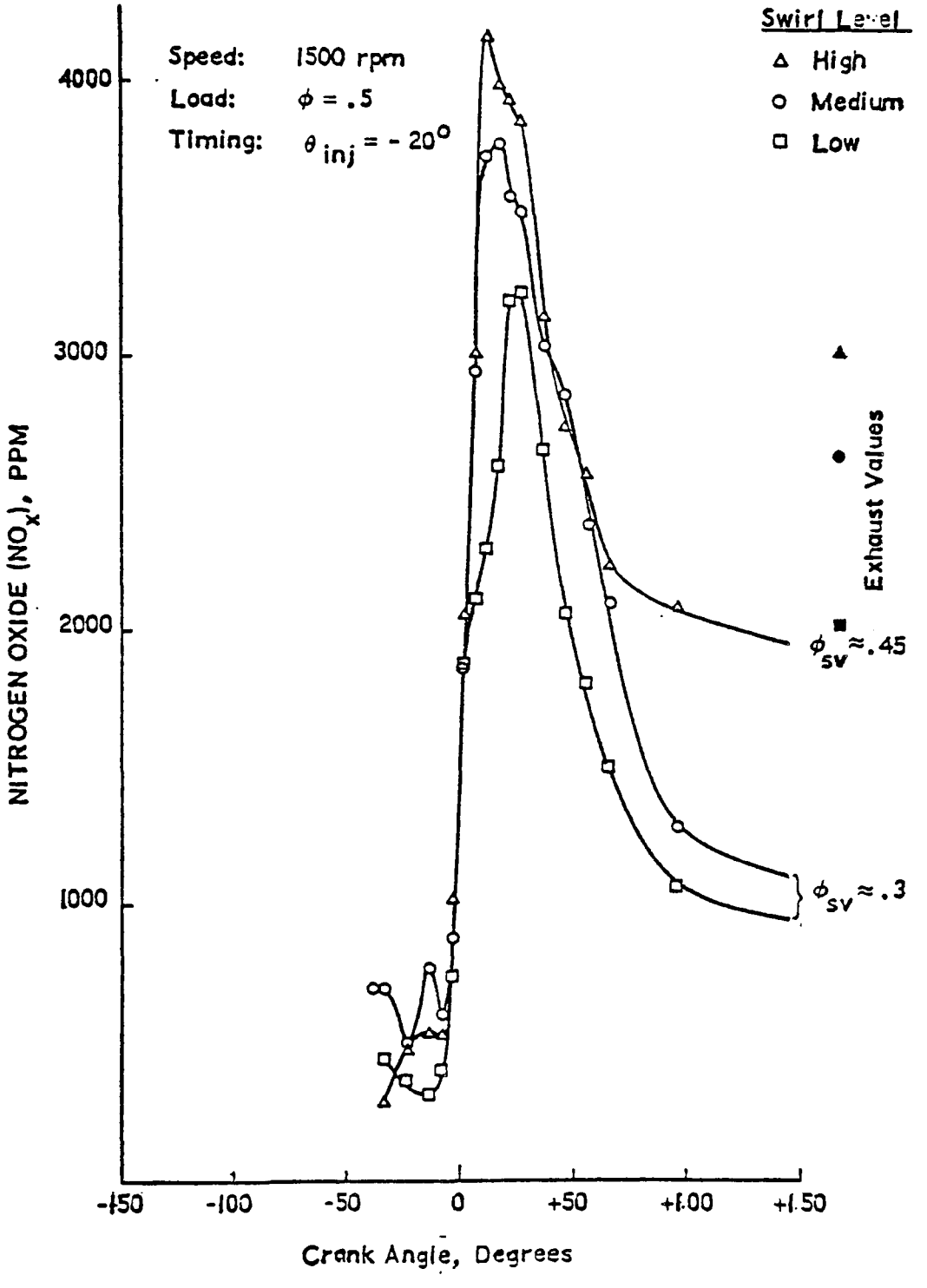

Figure C-5. Dependence of Sample Valve Measurement on Swirl Level - 11/16" Valve Insertion

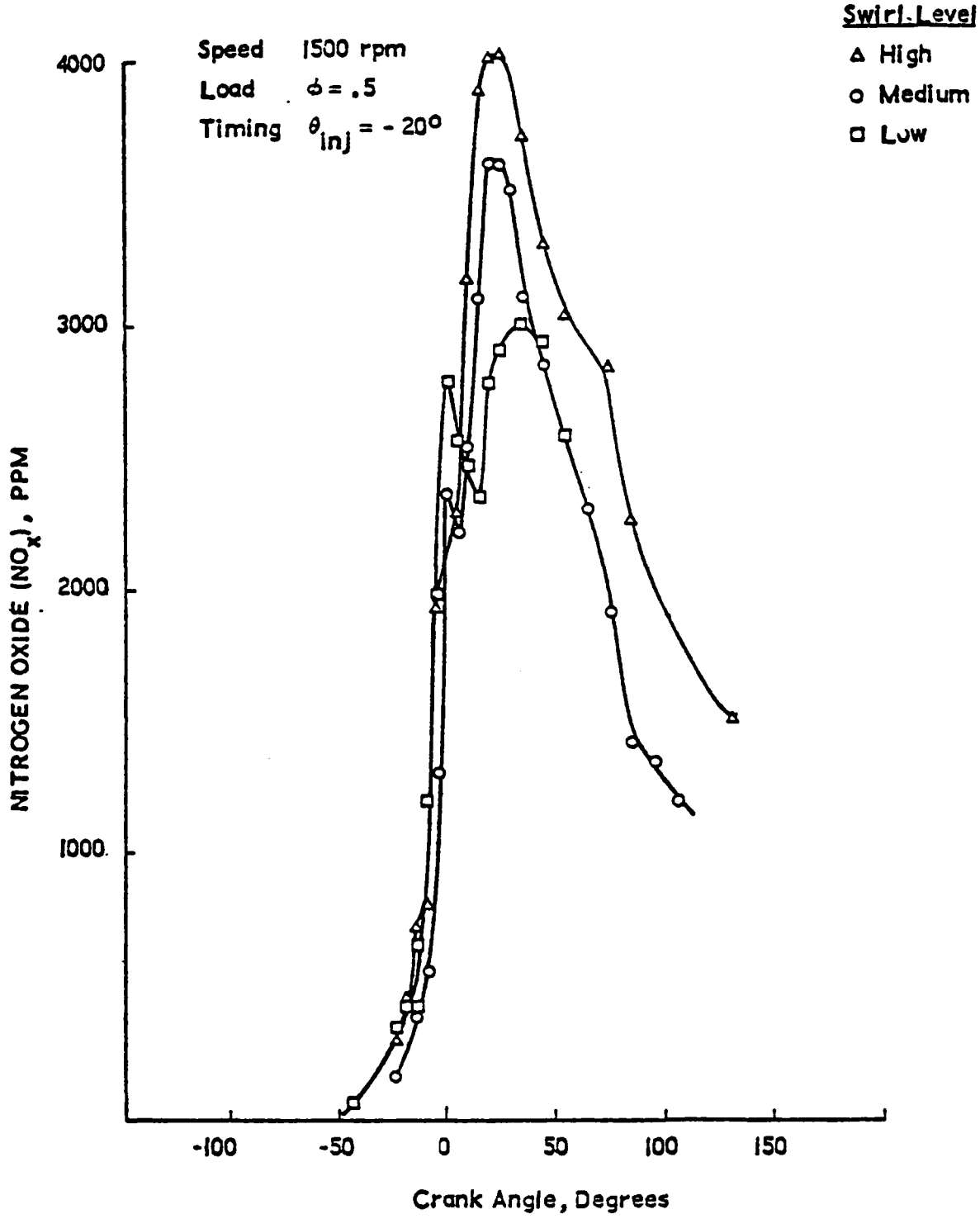

Figure C-6. Dependence of Sample Valve Measurements on Swirl Level - Flush Valve Position

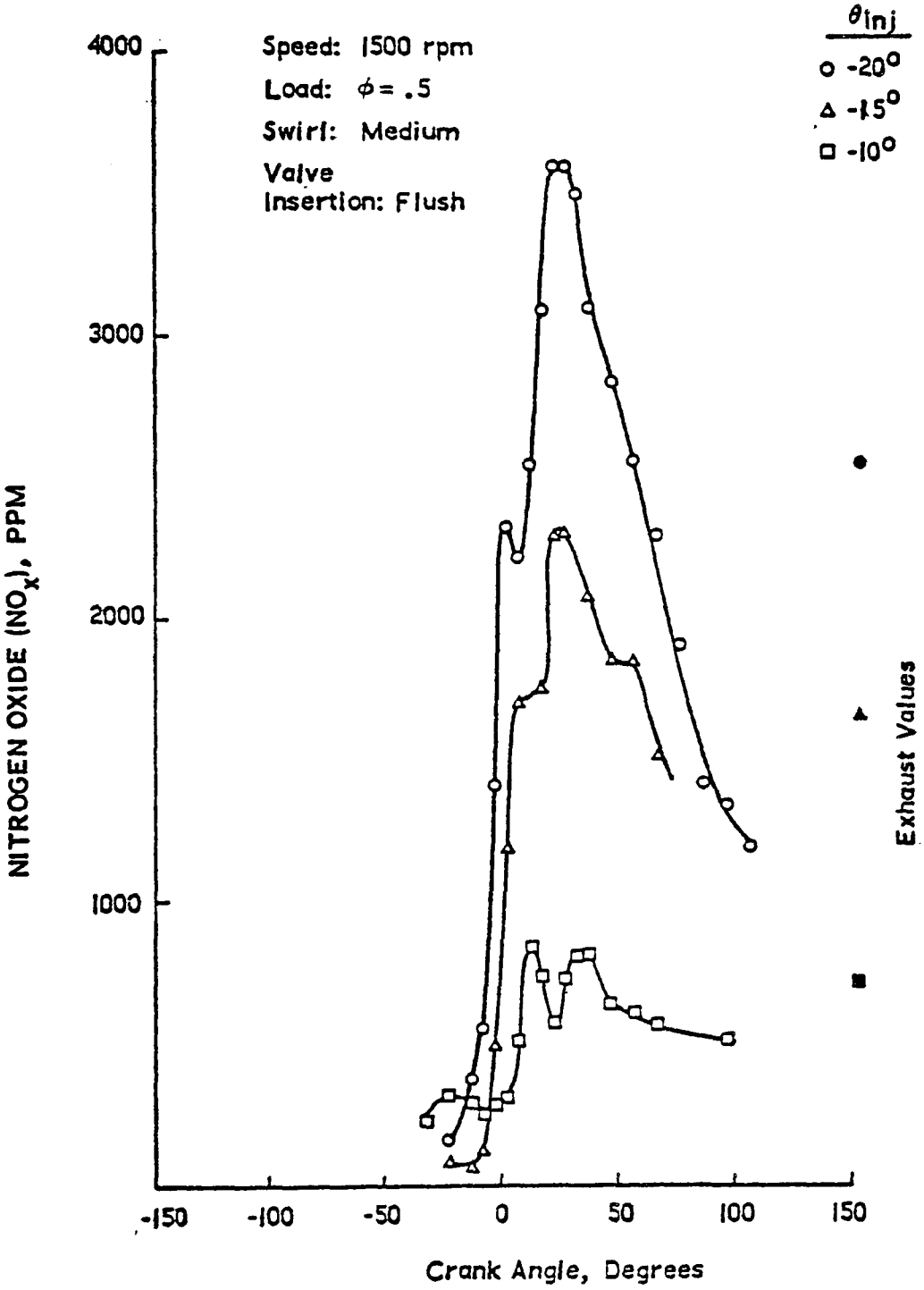

Figure C-7. Dependence of Sample Valve Measurement on Injection Timing

location the final sample yielded NO_x levels lower than the exhaust value. Some idea of the unmixedness existing in the cylinder can be gained from the results showing the influence of valve insertion depth shown in Figure C-4. Peak NO levels are considerably greater than the exhaust value. Also, the peak value does not increase monotonously with increasing insertion depth.

Increasing swirl increases exhaust NO levels which is reflected in the peak NO levels recorded by the sample for two insertion depths (see Figures C-5 and 6). It should be noted that peak levels tend to occur later in the cycle for lower swirl levels. The dip in the NO_x level close to TDC with the lowest swirl level when the valve was in the flush position appear to be real as the results could be repeated.

Variation of the injection timing produces a radical change in the character of the NO_x versus crank angle curves when the valve is flush with the cylinder head. The rise in NO_x is delayed in agreement with the delay in fuel injection.

C-4. DISCUSSION

Two issues must be addressed relating to the correspondence between the measured concentrations and those actually existing in the cylinder before discussing the implications of the results, these are:

1. Is the sample ingested into the valve representative of the concentration at the probe position and sampling time in the absence of the probe?
2. Does the sample undergo chemical transformation in the probe?

Complete answers to these questions are not available although it is possible to define possible effects and construct plausable arguments as to their magnitude. Regarding the first question posed above, the following effects can perturb the sample:

- influence of the inserted probe tip on local gasdynamics and combustion;

- ingestion of the quench layer adjacent to the probe tip;
- influence on the local gasdynamics of the sink strength during the sample period;
- size and duration of the sample as they affect spatial and temporal resolutions

Simple fluid mechanical arguments suggest that the quench layer and injector trapped mass do not represent a significant effect at the sample rates under consideration. This conclusion has been borne out by varying the sample rate and the duration of the valve opening time. The presence of the probe itself undoubtedly outweighs the sink and sample size effects. Fortunately the flow is predominantly across the probe and hence the largest perturbation to the flow lies in the wake, downstream of the probe. All of these items taken together probably mean that the sample should be considered as representative of a zone whose scale is that of several probe diameters. The long valve open time ($\approx$ 1 msec) is probably the single most severe effect with regard to both temporal and spatial resolutions due to high swirl velocities which can convect material from 30° upwind during this period.

With regard to chemical transformation within the probe, the following effects may be of concern:

- lack of adequate quenching within the probe;
- catalytic wall reactions;
- presence of carbon in the probe;
- presence of condensate in the sample line

Analysis of the first point requires the recognition that the probe's internal gasdynamics is an unsteady filling and emptying process. The stem fills over a period of 0.5-1.0 msec and empties over a period of 80 msec. During this process the sample at first expands very rapidly and then undergoes a reheating through shock compression and boundary layer stagnation. Although the required quench rates are severe, an analysis of this process indicates that the favorably lower pressures in the probe combined with the cool walls is adequate to terminate the nitrogen oxide production. This conclusion seems to be validated by the independence of measured NO_x with sample rates for rates greater than 300 SCCM. However, conditions may not be adequate to insure complete quenching of all reactions concerning carbon monoxide burnout.

The possible presence of carbon in the prove and its effect on NO reduction remains an open question. Sample lines must be kept short to reduce NO to NO_2 conversion; this effect must be significant with typically 10 percent conversion even with short sample lines.

In the results presented in Figures C-4 to C-7 the probe was located well out near the bowl edge and somewhat downstream of the jet impingement point. It seems reasonable to hypothesize that samples collected at this point will be lean and will, therefore, be representative of regions of high rates of NO formation. As time proceeds it can be assumed that gases in the vicinity of the sample valve will eventually show a decrease in NO concentration for several possible reasons:

- as time proceeds work extracted by the piston will cool the zones and reduce the NO production rate.
- as the temperature drops further mixing with available air will serve to dilute the NO concentration faster than production can compensate
- as time proceeds the sampling point will begin to experience zones containing "younger" fuel; that is, fuel which entered the system after ignition. Such zones are likely to have been initially richer in composition before reaching the sampling point because their fuel was not consumed in the intial stages of heat release. Hence such zones would never experience high NO levels even though at the time of sampling these may have reached a lean (but cool) condition.

Indeed all of the test conditions exhibited this rapid rise to high NO values followed by decay to quite low values.

In all cases the NO concentration at the time of exhaust valve opening was below the exhaust emission measurements by typically 1000 ppm. An obvious and easy explanation for this would be that there is a significant loss of NO in the sampling system by some unspecified mechanism. While not ruling this out completely it appears not to be the explanation. Although the sampling system has never been calibrated under complete simulation of diesel conditions it has been satisfactorily checked against high pressure calibration gases. However, the possibility of carbon contamination of the valve remains an open question.

Without obtaining further data at different probe locations it is impossible to be definitive in providing an explanation for the observed behavior. However, it is possible to construct a variety of plausible explanations which could represent the actual situation. For example, as suggested above it may be that late in the cycle the probe is sampling relatively "young" zones where the fuel came into the system late in the injection period. As a consequence such a zone would experience rather rich combustion early in its history with attendant low NO levels. Subsequently such a zone experiences dilution by air entrainment to lean conditions but the temperatures are too low at that time to produce significant NO. A necessary condition for this or any other mechanistic explanation to be valid is that there exists considerable unmixdeness late into the expansion stroke. Otherwise the late sample measurements would have to reflect the entire cylinder content and hence the exhaust value. Now the measured fuel/air ratios (deduced from the excess oxygen) confirm that this unmixedness does indeed exist. Sample equivalence ratios at the exhaust valve opening point are presented in Figures C-4, 5, 6, and C-7. The mass average of these values must be 0.5 (the exhaust value).

The distribution of equivalence ratio with crank angle is presented in Figures C-8 and C-9 for several swirl levels and at two valve insertions. An interesting peculiarity is the dip in equivalence ratio after the initial spike followed by a period of growing richer and then a final dilution period. A possible explanation again rests on the concept of "younger" and previously richer zones appearing in the neighborhood of the valve later in the cycle. Another explanation might be that this behavior reflects a jet interaction phenomenon where at approximately 25° ca the sample position begins to experience the presence of a neighboring jet. Figure C-7 provides additional evidence that unmixedness persists late into the cycle. Data is presented there for different valve insertion depths. Substantial gradients exist at $\theta = 150^{\circ}$ in both NO and equivalence ratios.

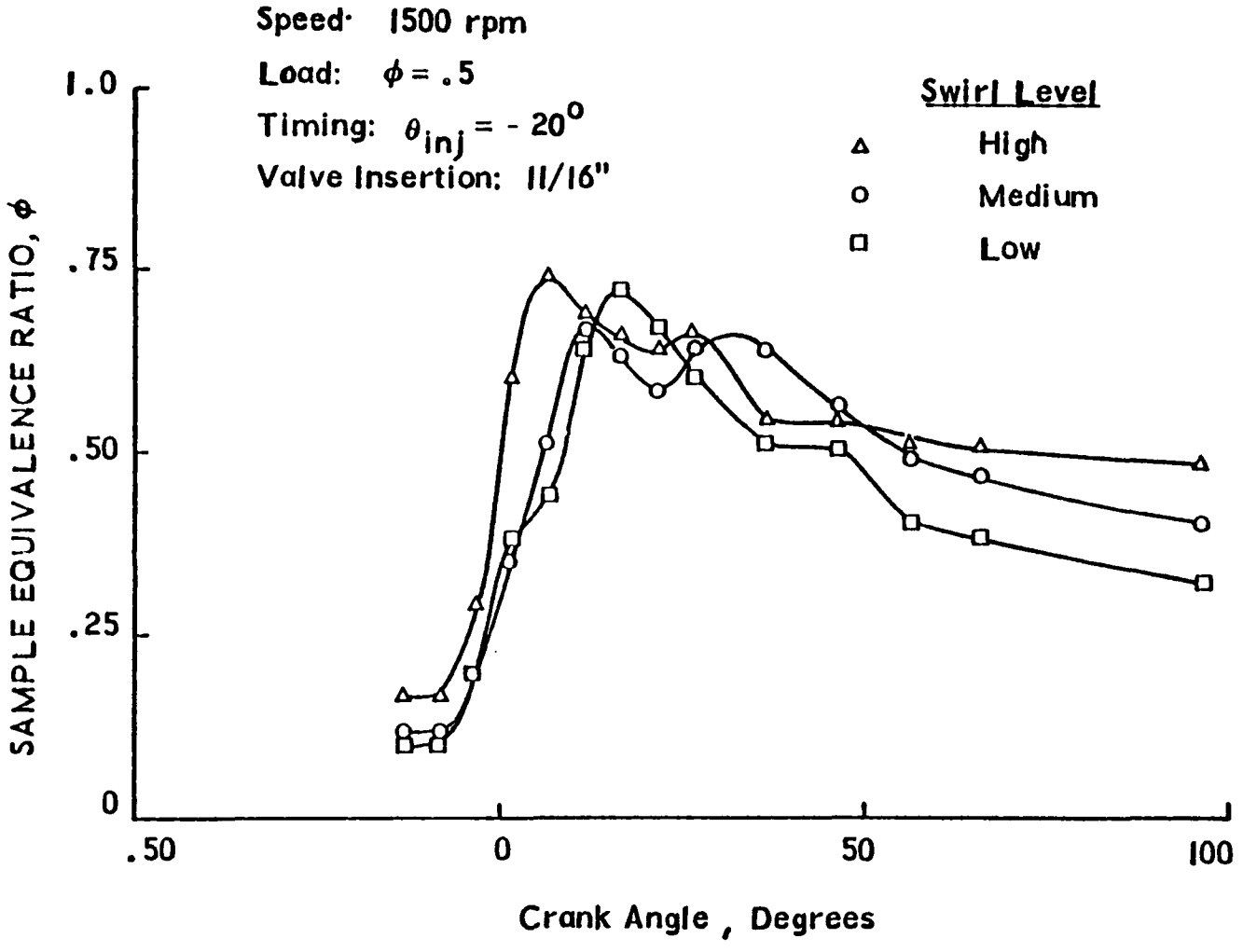

Figure C-8. Dependence of Sample Equivalence Ratio on Swirl - 11/16" Valve Insertion

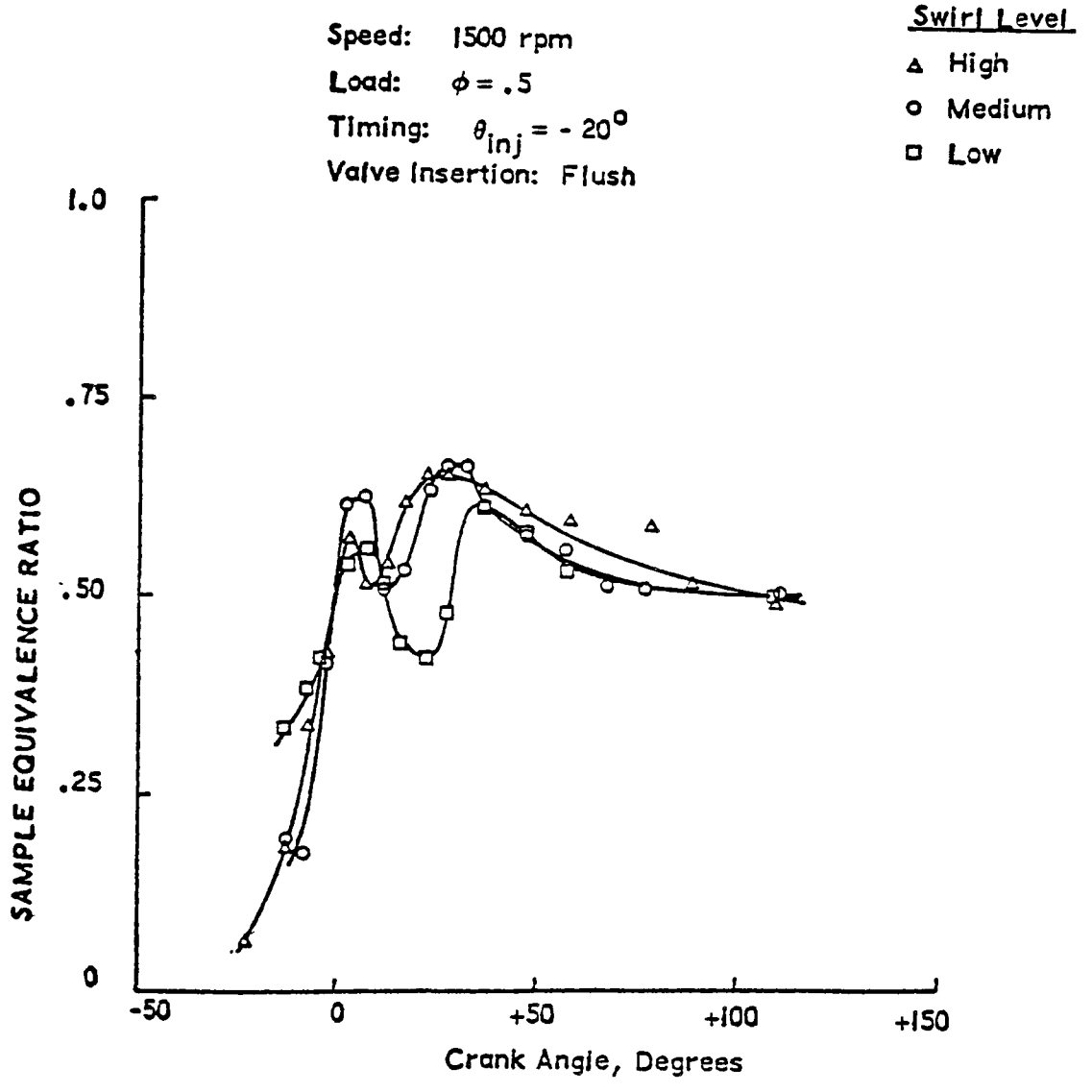

Figure C-9. Dependence of Sample Equivalence Ratio on Swirl - Flush Valve Position

C-5. CONCLUSIONS

Experience gained from in cylinder sampling suggests, that if properly applied, this technique could provide valuable information which would aid in the development of improved mathematical models. However, certain questions regarding sample integrity remain to be answered. The tentative conclusions suggested by the data are:

- Significant unmixedness persists throughout the cycle
- It does appear that the mixing process cannot be described by a random homogeneous turbulence field with variations of species concentration occurring in a random fashion in space and time. The mixing process appears well ordered and repeatable, that has its origins in the well-ordered jet mixing patterns occurring only in the cycle.
- There is considerable need to generate much more data, particularly with the sample valve inserted to cover the total free volume. Data obtained with the valve flush with the cylinder head is of limited value because of the significant vertical gradients.

REFERENCES

1. Wilson, R.P. Jr., Waldman, C.H., and Muzio, L.J., "Foundation for Modelling NO_x and Smoke Formation in Diesel Flames," Ultrasystems Final Report, APRAC Project CAPE 20-17, (1974).

2. Nightingale, D.R., "A Fundamental Investigation into the Problem of NO Formation in Diesel Engines," Paper presented at the SAE Off. Highway Vehicle Meeting Milwaukee, Sept. 8-11 (1975), SAE 750848.

APPENDIX D

SAMPLING VALVE DATA TEST SERIES 3

Sampling value data test series 3 are presented in this appendix under the following order.

No. of points	Speed (rpm)	Load ϕ	Timing (ATDC)	Swirl Level	Fuel Injector
8	1500	0.6	-20	Medium	6
7	1500	0.6	-20	High	6
7	1500	0.6	-20	Low	6
8	1500	0.6	-12	Medium	6
7	1500	0.6	-28	Medium	6
8	1500	0.35	-20	Medium	6
4	1500	0.35	-20	Low	6
1	1500	0.75	-20	Medium	6
1	2100	0.6	-20	Medium	6
4	1500	0.6	-20	Medium	4

Input Conditions		Exhaust Concentrations	
Speed	1500 rpm	NO_x	2460 ppm
Equivalence Ratio (nominal)	0.6	CO	0.005 percent
Timing (ATDC)	-20.	UHC	0
Swirl Level	Medium	CO_2	8.6 percent
Fuel Injector	6	O_2	8.7 percent

Sample Valve Location

R = 2.7 cms

θ = 0° from jet axis

Z = 0 depth (cms)

Sampling Time (°)	NO_x ppm	CO %	UHC ppm	CO_2 %	O_2 %
-22	137	.003	730	0.50	19.3
-12	90	.080	950	0.50	19.0
- 7	600	.430	1250	2.95	15.8
- 2	1560	.500	900	3.90	12.0
3	2146	.450	420	3.70	8.5
8	2688	.900	350	7.20	10.0
13	2937	.400	0	7.50	8.5
23	3650	.180	0	8.10	8.0
33	4240	.150	0	8.00	8.1
43	4070	.360	0	9.00	6.8

Input Conditions		Exhaust Concentrations	
Speed	1500 rpm	NO_x	2411 ppm
Equivalence Ratio (nominal)	0.6	CO	0.006 percent
Timing (ATDC)	-20.	UHC	0
Swirl Level	Medium	CO_2	7.8 percent
Fuel Injector	6	O_2	8.3 percent

Sample Valve Location

R = 2.7 cms

θ = 30° from jet axis

Z = 0 depth (cms)

Sampling Time (o)	NO_x ppm	CO %	UHC ppm	CO_2 %	O_2 %
-22	139	0.001	360	0.30	19.2
-12	123	0.003	5400	0.58	14.5
- 7	660	5.10	9500	6.70	4.1
- 2	820	5.50	12500	6.40	2.9
3	1489	4.50	2500	6.10	7.5
8	2090	0.70	950	7.00	9.3
13	2188	0.65	850	8.00	8.3
23	3150	0.66	650	7.70	8.5
33	3800	0.60	0	7.20	6.0
43	4120	0.50	0	7.10	5.5

Input Conditions		Exhaust Concentrations	
Speed	1500 rpm	NO_x	2431 ppm
Equivalence Ratio (nominal)	0.6	CO	0.007 percent
Timing (ATDC)	-20.0	UHC	0
Swirl Level	Medium	CO_2	9.1 percent
Fuel Injector	6	O_2	8.7 percent

Sample Valve Location

R = 3.9 cms

θ = 0° from jet axis

Z = 0 depth (cms)

Sampling Time ($^{\circ}$)	NO_x ppm	CO %	UHC ppm	CO_2 %	O_2 %
-22	140	0.005	500	0.7	19.5
-12	143	0.004	1250	0.4	20.0
- 7	1370	0.4	650	4.9	14.0
- 2	3542	2.7	500	8.4	7.0
3	3280	2.5	0	8.9	6.3
8	3980	1.9	0	9.3	5.8
13	3950	1.6	0	9.1	6.5
23	4035	0.86	0	9.4	7.1
33	4039	0.94	0	9.6	6.1
43	3300	0.6	0	9.4	6.5

Input Conditions		Exhaust Concentrations	
Speed	1500 rpm	NO_x	2435 ppm
Equivalence Ratio (nominal)	0.6	CO	0.01 percent
Timing (ATDC)	-20.	UHC	0
Swirl Level	Medium	CO_2	8.5 percent
Fuel Injector	6	O_2	8.6 percent

Sample Valve Location

R = 3.9 cms

θ = 15° from jet axis

Z = 0 depth (cms)

Sampling Time (°)	NO_x ppm	CO %	UHC ppm	CO_2 %	O_2 %
-22	77	0.005	1500	0.47	20.0
-12	84	0.65	6500	0.8	16.5
- 7	350	0.65	8000	1.0	13.5
- 2	1480	1.6	4000	2.1	10.3
3	2190	1.7	1700	4.6	7.8
8	2730	1.55	1200	6.0	7.1
13	2880	1.5	1200	7.4	6.9
23	3170	1.15	1050	8.1	6.5
33	3840	0.86	0	8.9	6.2
43	3890	0.8	0	9.3	5.6

Input Conditions		Exhaust Concentrations	
Speed	1500 rpm	NO_x	2383 ppm
Equivalence Ratio (nominal)	0.6	CO	0.2 percent
Timing (ATDC)	-20.	UHC	0
Swirl Level	Medium	CO_2	8.1 percent
Fuel Injector	6	O_2	8.7 percent

Sample Valve Location

R = 3.9 cms

θ = 30° from jet axis

Z = 0 depth (cms)

Sampling Time (°)	NO_x ppm	CO %	UHC ppm	CO_2 %	O_2 %
-22	315	0.12	130	0.9	18.9
-12	327	1.1	400	3.6	15.0
- 7	680	2.6	1600	4.2	11.8
- 2	2546	4.5	1000	7.0	7.0
3	3440	4.2	220	9.0	5.5
8	2360	6.6	200	8.1	3.5
13	3570	2.0	160	9.1	5.5
23	2940	1.4	130	9.5	5.3
33	2750	0.6	110	9.0	6.6
43	2027	0.9	90	8.1	9.5

Input Conditions		Exhaust Concentrations	
Speed	1500 rpm	NO_x	2426 ppm
Equivalence Ratio (nominal)	0.6	CO	0.1 percent
Timing (ATDC)	-20.	UHC	0
Swirl Level	Medium	CO_2	8.5 percent
Fuel Injector	6	O_2	8.8 percent

Sample Valve Location

R = 3.9 cms

θ = 30° from jet axis

Z = 0 depth (cms)

Sampling Time (°)	NO_x ppm	CO %	UHC ppm	CO_2 %	O_2 %
-22	133	0.2	600	0.61	19.5
-12	123	1.9	1050	1.55	16.5
- 7	890	10.0	5750	6.50	2.7
- 2	1112	6.6	3000	7.00	4.9
3	2100	5.4	2000	7.00	5.5
8	2950	2.2	1050	8.60	6.4
13	3300	1.4	900	8.80	6.8
23	3800	0.8	700	9.10	6.9
33	4018	0.8	0	9.50	6.0
43	3700	0.8	0	9.20	6.0

Input Conditions		Exhaust Concentrations	
Speed	1500 rpm	NO_x	2396 ppm
Equivalence Ratio (nominal)	0.6	CO	0.006 percent
Timing (ATDC)	-20.	UHC	0
Swirl Level	Medium	CO_2	8.5 percent
Fuel Injector	6	O_2	8.8 percent

Sample Valve Location

R = 3.9 cms

θ = 45° from jet axis

Z = 0 depth (cms)

Sampling Time ($^{\circ}$)	NO_x ppm	CO %	UHC ppm	CO_2 %	O_2 %
-22	280	0.15	820	1.35	18.0
-12	300	0.28	920	1.50	17.5
- 7	2220	2.35	660	9.10	5.3
- 2	2980	3.80	600	9.40	3.9
3	3015	3.40	0	9.00	4.5
8	3007	2.00	0	9.00	5.7
13	3800	1.35	0	9.00	6.3
23	4118	0.80	0	8.00	6.1
33	3700	0.45	0	9.50	6.2
43	3590	0.60	0	9.00	6.2

Input Conditions		Exhaust Concentrations	
Speed	1500 rpm	NO_x	2300 ppm
Equivalence Ratio (nominal)	0.6	CO	0.15 percent
Timing (ATDC)	-20.	UHC	0
Swirl Level	Medium	CO_2	8.8 percent
Fuel Injector	6	O_2	8.8 percent

Sample Valve Location

R = 5.6 cms

θ = 30° from jet axis

Z = 0 depth (cms)

Sampling Time (°)	NO_x ppm	CO %	UHC ppm	CO_2 %	O_2 %
-22	92	0.005	100	0.67	19.4
-12	75	0.35	100	0.65	19.1
- 7	821	10.00	100	6.50	1.3
- 2	370	10.00	120	4.00	0.4
3	1160	10.00	0	6.40	1.2
8	2140	9.00	0	7.40	1.9
13	2170	5.00	0	8.00	4.0
23	2733	1.80	0	8.40	6.1
33	2800	1.30	0	9.60	5.0
43	3050	1.20	0	9.90	4.7

Input Conditions		Exhaust Concentrations	
Speed	1500 rpm	NO_x	2100 ppm
Equivalence Ratio (nominal)	0.6	CO	0.005 percent
Timing (ATDC)	-20.	UHC	0
Swirl Level	High	CO_2	8.5 percent
Fuel Injector	6	O_2	8.6 percent

Sample Valve Location

R = 2.7 cms

θ = 0^{o} from jet axis

Z = 0 depth (cms)

Sampling Time (°)	NO_x ppm	CO %	UHC ppm	CO_2 %	O_2 %
-22	115	0.002	320	0.40	19.8
-12	143	0.45	1200	1.85	17.0
- 7	1560	0.75	1500	5.50	12.3
- 2	3400	2.20	400	8.60	6.0
3	3419	8.80	0	8.40	1.0
8	2280	10.00	0	8.40	0.1
13	1312	10.00	0	8.50	0.0
23	1581	7.00	0	10.10	0.0
33	2233	3.80	0	11.60	0.3
43	2355	2.00	0	11.80	1.3

Input Conditions		Exhaust Concentrations	
Speed	1500 rpm	NO_x	2450 ppm
Equivalence Ratio (nominal)	0.6	CO	0.2 percent
Timing (ATDC)	-20.	UHC	0
Swirl Level	High	CO_2	8.6 percent
Fuel Injector	6	O_2	8.9 percent

Sample Valve Location

R = 2.7 cms

θ = 30° from jet axis

Z = 0 depth (cms)

Sampling Time (°)	NO_x ppm	CO %	UHC ppm	CO_2 %	O_2 %
-22	112	0.05	1600	0.6	20.5
-17	40	0.40	4500	0.8	19.0
-12	180	5.40	9200	5.0	9.2
- 7	860	9.00	10200	7.8	2.6
- 2	2010	10.00	14000	6.6	1.2
3	3000	4.40	2600	9.9	2.7
8	3220	6.50	1100	10.0	0.8
13	2210	8.00	1000	9.9	0.2
28	2250	4.00	1000	12.0	0.6
38	950	2.40	770	12.0	1.2

Input Conditions		Exhaust Concentrations	
Speed	1500 rpm	NO_x	2534 ppm
Equivalence Ratio (nominal	0.6		
Timing (ATDC)	-20.0	CO	0.25 percent
Swirl Level	High	UHC	0
Fuel Injector	6	CO_2	8.0 percent
		O_2	8.4 percent

Sample Valve Location

R = 3.9 cms

θ = 0° from jet axis

Z = 0 depth (cms)

Sampling Time ($^{\circ}$)	NO_x ppm	CO %	UHC ppm	CO_2 %	O_2 %
-22	264	0.08	160	0.8	18.6
-12	330	0.17	180	1.5	17.6
- 7	1518	0.46	180	5.1	12.4
- 2	1354	3.8	150	6.1	8.4
3	2360	4.3	150	6.9	7.0
8	4300	1.7	130	9.0	6.4
13	3234	1.8	130	9.3	4.6
23	3340	1.4	130	10.5	3.7
33	2900	1.0	-0	11.0	3.5
43	2248	1.0	60	11.0	3.6

Input Conditions		Exhaust Concentrations	
Speed	1500 rpm	NO_x	2200 ppm
Equivalence Ratio (nominal)	0.6	CO	0.25 percent
Timing (ATDC)	-20.	UHC	0
Swirl Level	High	CO_2	8.6 percent
Fuel Injector	6	O_2	8.6 percent

Sample Value Location

R = 3.9 cms

θ = 15° from jet axis

Z = 0 depth (cms)

Sampling Time (°)	NO_x ppm	CO %	UHC ppm	CO_2 %	O_2 %
-22	265	0.14	190	0.8	19.4
-12	227	0.36	450	1.0	18.9
- 7	1968	2.2	1700	5.6	11.5
- 2	1852	1.2	500	6.1	10.9
3	1936	8.6	400	7.4	2.1
8	3637	2.0	380	8.9	6.1
13	3419	2.3	280	7.9	6.6
23	2324	1.3	230	8.1	7.5
33	1800	1.0	170	7.0	9.1
43	1385	0.8	150	6.0	9.6

Input Conditions		Exhaust Concentrations	
Speed	1500 rpm	NO_x	2200 ppm
Equivalence Ratio (nominal)	0.6	CO	0.3 percent
Timing (ATDC)	-20.	UHC	0
Swirl Level	High	CO_2	8.4 percent
Fuel Injector	6	O_2	8.6 percent

Sample Valve Location

R = 3.9 cms

θ = 45° from jet axis

Z = 0 depth (cms)

Sampling Time (°)	NO_x ppm	CO %	UHC ppm	CO_2 %	O_2 %
-22	152	0.05	58	1.3	19.5
-12	350	0.60	78	3.4	15.2
- 7	410	1.00	120	3.2	15.2
- 2	1085	5.20	240	5.2	8.8
3	2130	1.20	95	5.8	11.2
8	1745	2.20	86	7.0	8.6
13	1530	1.40	80	6.8	9.4
23	1490	1.20	90	7.2	9.6
33	1470	0.55	80	7.2	9.5
43	1140	0.45	60	6.8	10.4

Input Conditions		Exhaust Concentrations	
Speed	1500 rpm	NO_x	2190 ppm
Equivalence Ratio (nominal)	0.6	CO	0.3 percent
Timing (ATDC)	-20.	UHC	0
Swirl Level	High	CO_2	8.7 percent
Fuel Injector	6	O_2	9.0 percent

Sample Valve Location

R = 5.6 cms

θ = 30° from jet axis

Z = 0 depth (cms)

Sampling Time (o)	NO_x ppm	CO %	UHC ppm	CO_2 %	O_2 %
-22	170	0.20	900 .	0.69	19.5
-12	256	0.50	1250	2.10	17.5
- 7	344	0.70	1600	2.60	16.9
- 2	660	7.00	1250	4.60	8.2
3	1750	5.40	1000	7.70	6.0
8	1705	2.60	800	6.50	9.5
13	1650	1.50	740	5.90	11.2
23	1414	0.73	470	6.00	12.5
33	1036	0.45	0	4.90	13.2
43	650	0.15	0	2.30	14.0

Input Conditions		Exhaust Concentrations	
Speed	1500 rpm	NO_x	2190 ppm
Equivalence Ratio (nominal)	0.6		
Timing (ATDC)	-20.	CO	0.05 percent
Swirl Level	Medium	UHC	0
Fuel Injector	4	CO_2	8.9 percent
		O_2	9.0 percent

Sample Valve Location

R = 5.6 cms

θ = 0° from jet axis

Z = 0 depth (cms)

Sampling Time (°)	NO_x ppm	CO %	UHC ppm	CO_2 %	O_2 %
-22	67	0.04	120	0.3	20.5
-12	72	1.50	150	0.8	18.3
- 7	190	5.00	7500	3.2	12.5
- 2	470	1.10	3000	2.3	17.2
3	1206	3.00	600	6.0	10.0
8	2025	6.00	400	8.5	4.0
13	2140	3.40	390	9.0	4.4
23	1902	1.50	300	9.5	6.0
33	2045	0.65	260	9.6	7.2
43	1925	0.60	200	9.4	7.0

Input Conditions		Exhaust Concentrations	
Speed	1500 rpm	NO_x	1685 ppm
Equivalence Ratio (nominal)	0.6	CO	0.1 percent
Timing (ATDC)	-20.	UHC	0
Swirl Level	Low	CO_2	8.2 percent
Fuel Injector	6	O_2	8.3

Sample Valve Location

R = 2.7 cms

θ = 0° from jet axis

Z = 0 depth (cms)

Sampling Time (°)	NO_x ppm	CO %	UHC ppm	CO_2 %	O_2 %
-22	135	0.05	300	0.50	19.3
-12	70	0.80	2500	1.02	17.9
- 7	188	1.80	4000	2.80	14.1
- 2	432	1.70	4000	3.30	13.5
3	718	0.60	800	4.30	13.4
8	770	0.23	500	3.60	14.8
13	916	0.15	0	3.70	15.0
23	917	0.10	0	3.80	14.7
33	1038	0.08	0	3.90	14.5
43	980	0.09	0	4.20	14.2

Input Conditions		Exhaust Concentrations	
Speed	1500 rpm	NO_x	1830 ppm
Equivalence Ratio (nominal)	0.6	CO	0.1 percent
Timing (ATDC)	-20.	UHC	0
Swirl Level	Low	CO_2	8.6
Fuel Injector	6	O_2	9.0

Sample Vavle Location

R = 2.7 cms

θ = 30° from jet axis

Z = 0 depth (cms)

Sampling Time (°)	NO_x ppm	CO %	UHC ppm	CO_2 %	O_2 %
-22	91	0.05	540	0.45	20.0
-12	360	1.05	1400	3.20	16.0
- 7	800	1.00	900	4.30	13.5
- 2	856	0.85	900	4.40	13.5
3	1010	0.30	700	4.40	14.0
8	1113	0.10	440	4.00	15.5
13	1200	0.11	450	3.90	15.7
28	1223	0.11	350	4.00	15.9
38	1190	0.10	-0	3.90	15.5

Input Conditions		Exhaust Concentrations	
Speed	1500 rpm	NO_x	1805 ppm
Equivalence Ratio (nominal)	0.6	CO	0.15 percent
Timing (ATDC)	-20.0	UHC	0
Swirl Level	Low	CO_2	8.5 percent
Fuel Injector	6	O_2	8.8 percent

Sample Valve Location

R = 3.9 cms

θ = 0° from jet axis

Z = 0 depth (cms)

Sampling Time (°)	NO_x ppm	CO %	UHC ppm	CO_2 %	O_2 %
-22	130	0.1	210	.56	19.5
-12	172	3.4	2000	2.3	14.3
- 7	663	6.0	2500	5.2	8.0
- 2	767	4.4	1500	5.0	8.9
3	1460	2.6	400	6.0	9.5
8	1800	1.5	300	6.3	10.1
13	1817	0.95	250	6.7	10.5
23	1830	0.50	200	6.2	11.0
33	1590	0.30	200	5.9	11.8
43	1370	0.25	200	4.3	14.0

Input Conditions		Exhaust Concentrations	
Speed	1500 rpm	NO_x	1780 ppm
Equivalence Ratio (nominal)	0.6	CO	0.15 percent
Timing (ATDC)	-20.	UHC	0
Swirl Level	Low	CO_2	8.6 percent
Fuel Injector	6	O_2	8.8 percent

Sample Valve Location

R = 3.9 cms

θ = 15° from jet axis

Z = 0 depth (cms)

Sampling Time (°)	NO_x ppm	CO %	UHC ppm	CO_2 %	O_2 %
-22	135	0.13	350	0.43	20.1
-12	224	8.5	4000	4.6	7.0
- 7	760	10.0	8000	6.5	2.0
- 2	1245	7.0	3000	7.2	4.5
3	1295	3.6	1200	7.5	7.2
8	1935	1.1	750	6.8	11.0
13	1880	0.8	650	6.0	11.9
23	1790	0.4	450	6.0	12.5
33	1750	0.36	400	6.0	12.5
43	1684	0.4	210	6.0	13.0

Input Conditions		Exhaust Concentrations	
Speed	1500 rpm	NO_x	1555 ppm
Equivalence Ratio (nominal)	0.6	CO	0.1 percent
Timing (ATDC)	-20.	UHC	0
Swirl Level	Low	CO_2	8.6 percent
Fuel Injector	6	O_2	8.8 percent

Sample Valve Location

R = 3.9 cms

θ = 30° from jet axis

Z = 0 depth (cms)

Sampling Time (°)	NO_x ppm	CO %	UHC ppm	CO_2 %	O_2 %
-22	173	0.05	200	0.75	19.8
-12	198	0.25	260	1.25	18.5
- 7	1681	3.4	400	7.4	8.4
- 2	2005	3.8	350	7.2	7.4
3	2390	2.4	240	7.6	9.5
8	2160	1.4	200	6.8	10.9
13	2142	0.7	200	5.8	11.8
23	1867	0.2	170	5.1	13.0
33	1493	0.14	110	5.0	13.3
43	1380	0.13	100	4.3	14.5

Input Conditions		Exhaust Concentrations	
Speed	1500 rpm	NO_x	1717 ppm
Equivalence Ratio (nominal)	0.6	CO	0.15 percent
Timing (ATDC)	-20.	UHC	0
Swirl Level	Low	CO_2	8.6 percent
Fuel Injector	6	O_2	8.8 percent

Sample Valve Location

R = 3.9 cms

θ = 45° from jet axis

Z = 0 depth (cms)

Sampling Time (°)	NO_x ppm	CO %	UHC ppm	CO_2 %	O_2 %
-22	150	0.08	240	0.66	19.7
-12	185	0.26	400	0.9	19.3
- 7	350	1.2	550	3.2	15.5
- 2	290	3.6	460	5.5	8.5
3	1136	4.0	360	7.2	6.5
8	1410	2.0	310	7.5	7.5
13	1220	1.5	160	6.8	8.5
23	1250	0.4	110	4.3	5.2
33	1040	0.2	48	4.0	6.0
43	755	0.2	40	3.6	6.1

Input Conditions		Exhaust Concentrations	
Speed	1500 rpm	NO_x	1670 ppm
Equivalence Ratio (nominal)	0.6	CO	0.1 percent
Timing (ATDC)	-20.	UHC	0
Swirl Level	Low	CO_2	8.5 percent
Fuel Injector	6	O_2	8.6 percent

Sample Valve Location

R = 5.6 cms

θ = 30° from jet axis

Z = 0 depth (cms)

Sampling Time (°)	NO_x ppm	CO %	UHC ppm	CO_2 %	O_2 %
-22	120	0.20	5000	0.61	19.5
-12	109	0.17	7300	0.52	19.8
- 7	200	0.46	9500	1.50	18.5
- 2	471	4.50	8100	2.60	13.2
3	1011	7.20	6700	5.40	6.7
8	1790	3.80	5700	6.60	7.5
13	1690	2.50	4700	6.20	9.3
23	1580	1.60	4100	6.20	10.5
33	1100	1.10	3100	5.60	12.0
43	1100	0.50	2600	4.80	12.8

Input Conditions		Exhaust Concentrations	
Speed	1500 rpm	NO_x	1300 ppm
Equivalence Ratio (nominal)	0.6	CO	0.06 percent
Timing (ATDC)	-12.	UHC	0
Swirl Level	Medium	CO_2	8.0 percent
Fuel Injector	6	O_2	8.4 percent

Sample Valve Location

R = 2.7 cms

θ = 0° from jet axis

Z = 0 depth (cms)

Sampling Time (o)	NO_x ppm	CO %	UHC ppm	CO_2 %	O_2 %
-12	80	0.04	300	0.48	19.1
- 7	90	0.06	500	0.40	19.1
- 2	280	0.84	1300	2.30	16.2
3	800	0.80	2000	4.10	13.3
8	1195	0.83	600	4.60	12.5
13	1330	1.00	350	4.90	12.0
23	1760	0.46	0	6.20	10.9
33	2074	0.47	0	6.80	9.5
43	1948	0.30	0	7.00	8.9

Input Conditions		Exhaust Concentrations	
Speed	1500 rpm	NO_x	1300 ppm
Equivalence Ratio (nominal)	0.6	CO	0.05 percent
Timing (ATDC)	-12	UHC	0
Swirl Level	Medium	CO_2	8.4 percent
Fuel Injector	6	O_2	8.6 percent

Sample Valve Location

R = 2.7 cms

θ = 30° from jet axis

Z = 0 depth (cms)

Sampling Time (o)	NO_x ppm	CO %	UHC ppm	CO_2 %	O_2 %
-22	56	0.05	420	0.7	20.0
-17	94	0.25	480	1.2	19.5
-12	155	1.50	500	2.5	18.2
- 7	280	2.00	1800	3.4	14.2
- 2	820	5.00	2300	8.0	4.8
3	890	4.20	3000	7.2	6.0
8	990	6.50	7100	7.0	6.0
13	850	2.50	1200	6.0	9.5
28	1160	0.35	580	5.4	13.0
38	1250	0.20	400	5.3	13.5

Input Conditions		Exhaust Concentrations	
Speed	1500 rpm	NO_x	1254 ppm
Equivalence Ratio (nominal)	0.6	CO	0.1 percent
Timing (ATDC)	-12.	UHC	0
Swirl Level	Medium	CO_2	7.9 percent
Fuel Injector	6	O_2	8.6 percent

Sample Valve Location

R = 3.9 cms

θ = 0° from jet axis

Z = 0 depth (cms)

Sampling Time (o)	NO_x ppm	CO %	UHC ppm	CO_2 %	O_2 %
-12	102	.06	175	0.35	19.5
- 7	58	.09	250	0.36	19.0
- 2	70	.25	700	0.60	18.2
3	238	.35	400	1.20	17.5
8	984	.60	150	3.40	14.7
13	1094	.30	150	3.60	15.1
23	1394	.20	85	4.50	13.2
33	1350	.15	-0	6.00	12.0
43	1290	.23	-0	6.40	11.0

Input Conditions		Exhaust Concentrations	
Speed	1500 rpm	NO_x	1412 ppm
Equivalence Ratio (nominal)	0.6	CO	0.15 percent
Timing (ATDC)	-12.	UHC	0
Swirl Level	Medium	CO_2	8.0 percent
Fuel Injector	6	O_2	8.4 percent

Sample Valve Location

R = 3.9 cms

θ = 15^{o} from jet axis

Z = 0 depth (cms)

Sampling Time (°)	NO_x ppm	CO %	UHC ppm	CO_2 %	O_2 %
-12	200	0.10	300	0.4	19.5
- 7	108	4.00	4500	1.6	14.0
- 2	236	7.60	8000	3.8	7.0
3	280	5.20	7000	3.5	9.5
8	370	3.70	3900	3.8	11.9
13	1014	1.20	1100	4.2	12.5
23	923	0.40	500	3.2	15.1
33	718	0.28	320	3.4	15.0
43	737	0.19	210	3.3	15.2

Input Conditions		Exhaust Concentrations	
Speed	1500 rpm	NO_x	1395 ppm
Equivalence Ratio (nominal)	0.6	CO	0.1 percent
Timing (ATDC)	-12.	UHC	0
Swirl Level	Medium	CO_2	8.0 percent
Fuel Injector	6	O_2	8.8 percent

Sample Valve Location

R = 3.9 cms

θ = 30^{o} from jet axis

Z = 0 depth (cms)

Sampling Time (o)	NO_x ppm	CO %	UHC ppm	CO_2 %	O_2 %
-12	197	0.05	200	0.54	19.5
- 7	201	0.15	220	0.60	19.4
- 2	852	4.60	300	7.40	5.2
3	2160	2.80	250	8.50	5.5
8	1880	2.50	200	7.70	8.0
13	1470	1.70	190	7.00	9.5
23	1150	0.28	190	5.00	12.9
33	976	0.15	160	4.40	13.9
43	912	0.15	110	4.40	13.9

Input Conditions		Exhaust Concentrations	
Speed	1500 rpm	NO_x	1085 ppm
Equivalence Ratio (nominal)	0.6	CO	0.01 percent
Timing (ATDC)	-12.	UHC	0
Swirl Level	Medium	CO_2	8.5 percent
Fuel Injector	6	O_2	8.6 percent

Sample Valve Location

R = 3.9 cms

θ = 45° from jet axis

Z = 0 depth (cms)

Sampling Time (°)	NO_x ppm	CO %	UHC ppm	CO_2 %	O_2 %
-22	83	0.05	94	0.7	19.6
-12	56	0.05	100	0.7	19.8
- 7	56	0.05	120	0.8	19.6
- 2	72	0.05	130	1.2	19.5
3	1055	0.50	110	4.8	13.5
8	1730	0.40	100	5.4	13.0
13	1328	0.40	100	5.0	13.5
23	1015	0.20	88	5.5	12.5
33	785	0.10	55	4.4	14.5
43	560	0	52	0	0

Input Conditions		Exhaust Concentrations	
Speed	1500 rpm	NO_x	1230 ppm
Equivalence Ratio (nominal)	0.6	CO	0.008 percent
Timing (ATDC)	-12.	UHC	0
Swirl Level	Medium	CO_2	8.2 percent
Fuel Injector	6	O_2	9.2 percent

Sample Valve Location

R = 5.6 cms

θ = 0^{o} from jet axis

Z = 0 depth (cms)

Sampling Time (o)	NO_x ppm	CO %	UHC ppm	CO_2 %	O_2 %
-12	88	0.005	30	0.3	20.5
- 7	77	0.15	100	0.3	19.2
- 2	231	4.80	4000	4.2	9.5
3	430	4.30	850	5.2	8.5
8	980	3.40	150	7.7	6.1
13	1440	7.80	60	8.0	1.8
23	2080	3.60	0	9.5	3.8
33	1900	1.90	0	8.5	7.2
43	1830	0.70	0	8.0	7.9

Input Conditions		Exhaust Concentrations	
Speed	1500 rpm	NO_x	1209 ppm
Equivalence Ratio (nominal)	0.6	CO	0.1 percent
Timing (ATDC)	-12.	UHC	0
Swirl Level	Medium	CO_2	8.2 percent
Fuel Injector	6	O_2	9.2 percent

Sample Valve Location

R = 5.6 cms

θ = 30° from jet axis

Z = 0 depth (cms)

Sampling Time (o)	NO_x ppm	CO %	UHC ppm	CO_2 %	O_2 %
-12	72	0.09	560	0.35	19.8
- 7	70	0.09	540	0.30	19.9
- 2	230	0.65	560	1.80	17.8
3	199	10.00	460	3.80	5.8
8	735	6.80	900	5.40	6.9
13	1330	3.80	800	6.10	8.7
23	1130	1.15	420	5.80	10.9
33	957	0.50	370	4.60	13.7
43	730	0.40	240	4.00	16.3

Input Conditions		Exhaust Concentrations	
Speed	1500 rpm	NO_x	4440 ppm
Equivalence Ratio (nominal)	0.6	CO	0.06 percent
Timing (ATDC)	-28.	UHC	0
Swirl Level	Medium	CO_2	7.9 percent
Fuel Injector	6	O_2	8.1 percent

Sample Valve Location

R = 2.7 cms

θ = 0° from jet axis

Z = 0 depth (cms)

Sampling Time (°)	NO_x ppm	CO %	UHC ppm	CO_2 %	O_2 %
-32	291	0.04	200	0.4	19.5
-22	201	0.10	600	0.5	19.0
-12	322	1.70	2500	3.2	14.2
- 7	1880	1.15	600	5.9	11.0
- 2	2722	0.55	300	6.5	10.5
3	3580	0.26	300	6.6	10.7
8	4400	0.16	250	7.0	10.0
13	4785	0.35	225	8.0	8.2
23	5400	0.24	-0	8.8	7.5
33	5664	0.15	-0	8.9	7.3
43	5500	0.16	-0	8.7	7.0

Input Conditions		Exhaust Concentrations	
Speed	1500 rpm	NO_x	3640 ppm
Equivalence Ratio (nominal)	0.6	CO	0.05 percent
Timing (ATDC)	-28.	UHC	0
Swirl Level	Medium	CO_2	8.3 percent
Fuel Injector	6	O_2	8.9 percent

Sample Valve Location

R = 2.7 cms

θ = 30° from jet axis

Z = 0 depth (cms)

Sampling Time (°)	NO_x ppm	CO %	UHC ppm	CO_2 %	O_2 %
-22	240	0.15	500	0.6	20.0
-17	250	1.50	580	2.2	16.2
-12	580	6.20	1400	6.2	6.2
- 7	905	7.00	4000	6.2	5.0
- 2	1750	1.00	700	5.2	11.7
3	2460	0.35	640	5.8	12.0
8	3800	0.40	520	6.5	11.2
13	4000	0.40	440	7.4	9.8
28	4150	0.25	280	8.0	8.8
38	4200	0.35	240	8.1	8.8

Input Conditions		Exhaust Concentrations	
Speed	1500 rpm	NO_x	3710 ppm
Equivalence Ratio (nominal)	0.6	CO	0.15 percent
Timing (ATDC)	-28.	UHC	0
Swirl Level	Medium	CO_2	8.0 percent
Fuel Injector	6	O_2	8.6 percent

Sample Valve Location

R = 3.9 cms

θ = 0° from jet axis

Z = 0 depth (cms)

Sampling Time (°)	NO_x ppm	CO %	UHC ppm	CO_2 %	O_2 %
-27	440	0.06	96	0.8	18.6
-17	460	0.30	400	1.3	17.5
- 7	2940	0.60	170	5.5	11.1
- 2	2490	0.45	160	5.8	12.9
3	2670	0.60	170	6.0	11.9
8	3400	0.45	160	6.0	11.9
13	3988	0.25	-0	6.7	11.1
23	4720	0.23	-0	8.0	9.0
33	5485	0.18	-0	8.4	8.5
43	5120	0.12	-0	7.9	9.0

Input Conditions		Exhaust Concentrations	
Speed	1500 rpm	NO_x	3245 ppm
Equivalence Ratio (nominal)	0.6	CO	0.1 percent
Timing (ATDC)	-28.	UHC	0
Swirl Level	Medium	CO_2	8.2 percent
Fuel Injector	6	O_2	8.8 percent

Sample Valve Location

R = 3.9 cms

θ = 15° from jet axis

Z = 0 depth (cms)

Sampling Time (°)	NO_x ppm	CO %	UHC ppm	CO_2 %	O_2 %
-27	325	0.23	190	0.7	19.2
-17	221	3.50	270	2.6	12.3
-12	644	5.20	3000	4.8	8.5
- 7	1322	4.60	1000	5.5	9.6
- 2	1681	5.50	570	6.5	6.7
3	2317	3.20	460	6.0	8.2
8	2731	1.30	420	6.6	10.0
13	3521	1.20	360	7.0	9.0
23	3571	0.60	250	6.4	10.6
33	2490	0.45	200	5.8	11.3
43	2360	0.40	180	5.0	13.0

Input Conditions		Exhaust Concentrations	
Speed	1500 rpm	NO_x	3540 ppm
Equivalence Ratio (nominal)	0.6	CO	0.1 percent
Timing (ATDC)	-28.	UHC	0
Swirl Level	Medium	CO_2	8.0 percent
Fuel Injector	6	O_2	8.6 percent

Sample Valve Location

R = 3.9 cms

θ = 30° from jet axis

Z = 0 depth (cms)

Sampling Time (°)	NO_x ppm	CO %	UHC ppm	CO_2 %	O_2 %
-32	560	0.15	100	1.0	18.3
-12	1830	3.20	300	7.4	7.0
- 7	2370	3.40	350	7.8	6.6
- 2	2760	2.00	240	7.3	7.9
3	2440	0.76	200	6.0	10.0
8	3070	0.70	160	6.6	10.6
13	3840	0.46	140	7.0	10.2
23	3645	0.30	130	6.7	9.8
33	3300	0.34	90	7.4	10.0
43	2820	0.26	80	6.4	10.8

Input Conditions		Exhaust Concentrations	
Speed	1500 rpm	NO_x	3600 ppm
Equivalence Ratio (nominal)	0.6	CO	0.1 percent
Timing (ATDC)	-28.	UHC	0
Swirl Level	Medium	CO_2	8.7 percent
Fuel Injector	6	O_2	8.5 percent

Sample Valve Location

R = 3.9 ppm

θ = 45° from jet axis

Z = 0 depth (cms)

Sampling Time (°)	NO_x ppm	CO %	UHC ppm	CO_2 %	O_2 %
-27	215	0.06	70	0.66	19.5
-17	322	1.10	100	0.71	19.4
- 7	2336	1.15	100	5.80	11.5
- 2	2340	1.00	90	5.50	12.0
3	2360	0.40	90	5.20	12.7
8	2188	0.25	80	4.80	13.5
13	2525	0.40	70	5.60	12.0
23	2804	0.25	60	5.70	11.2
33	2560	0.20	60	5.90	11.9
43	2020	0.15	60	5.00	13.1

Input Conditions		Exhaust Concentrations	
Speed	1500 rpm	NO_x	3823 ppm
Equivalence Ratio (nominal)	0.6	CO	0.1 percent
Timing (ATDC)	-28.	UHC	0
Swirl Level	Medium	CO_2	8.5 percent
Fuel Injector	6	O_2	8.8 percent

Sample Valve Location

R = 5.6 cms

θ = 30° from jet axis

Z = 0 depth (cms)

Sampling Time (°)	NO_x ppm	CO %	UHC ppm	CO_2 %	O_2 %
-27	180	0.21	240	0.65	19.7
-17	260	0.25	360	0.65	20.2
-12	1635	5.20	450	6.80	6.8
- 7	1600	9.00	540	6.00	4.8
- 2	1555	6.20	570	6.60	6.6
3	2500	2.30	490	6.70	8.9
8	3507	0.90	440	6.70	11.1
13	3499	0.60	370	6.40	10.8
23	2590	0.50	240	5.60	12.5
33	1711	0.40	180	4.70	14.0
43	1430	0.25	180	2.40	14.6

Input Conditions		Engine Concentration	
Speed	1500 rpm	NO_x	1880 ppm
Equivalence Ratio (nominal)	0.35	CO	0.05 percent
Timing (ATDC)	-20.	UHC	0
Swirl Level	Medium	CO_2	5.4 percent
Fuel Injector	6	O_2	13.2 percent

Sample Valve Location

R = 2.7 cms

θ = 0° from jet axis

Z = 0 depth (cms)

Sampling Time ($^{\circ}$)	NO_x ppm	CO %	UHC ppm	CO_2 %	O_2 %
-22	72	0.01	250	0.05	20.5
-12	75	0.05	2000	0.15	20.2
- 7	500	1.70	2600	3.80	14.0
- 2	1190	1.15	900	6.00	11.2
3	1285	0.65	550	5.30	12.0
8	1070	0.20	500	4.40	15.5
13	1370	0.07	400	5.00	14.5
28	2280	0.03	250	6.00	13.2
38	2420	0.03	-0	5.80	13.1

Input Conditions		Exhaust Concentrations	
Speed	1500 rpm	NO_x	2000 ppm
Equivalence Ratio (nominal)	.35	CO	0.05 percent
Timing (ATDC)	-20.0	UHC	850 ppm
Swirl Level	Medium		
Fuel Injector	6	CO_2	5.2 percent
		O_2	13.1 percent

Sample Valve Location

R = 2.7 cms

$\theta = 30^{\circ}$ from jet axis

Z = 0 depth (cms)

Sampling Time (o)	NO_x ppm	CO %	UHC ppm	CO_2 %	O_2 %
-22	105	0.05	280	0.30	19.8
-17	80	0.10	700	0.40	19.8
-12	95	1.50	2800	1.80	17.0
- 7	580	8.00	6000	6.20	5.0
- 2	715	2.00	1100	5.00	13.0
3	905	0.35	600	3.60	15.0
8	1350	0.20	500	4.50	14.5
13	1472	0.15	450	4.50	14.0
18	1810	0.10	0	4.50	14.0
23	2100	0.15	0	4.60	13.7
28	2030	0.15	280	5.80	12.5
38	2420	0.15	250	5.20	13.0

Input Conditions		Exhaust Concentrations	
Speed	1500 rpm	NO_x	1840 ppm
Equivalence Ratio (nominal)	.35	CO	0.10 percent
Timing (ATDC)	-20.0	UHC	0
Swirl Level	Medium		
Fuel Injector	6	CO_2	5.5 percent
		O_2	12.3 percent

Sample Valve Location

R = 3.9 cms

$\theta = 0^{\circ}$ from jet axis

Z = 0 depth (cms)

Sampling Time (o)	NO_x ppm	CO %	UHC ppm	CO_2 %	O_2 %
-22	154	0.06	1400	0.03	19.5
-12	163	0.15	1500	0.40	19.0
-7	234	0.50	1300	1.40	17.8
-2	1715	0.65	840	4.60	13.1
3	1730	1.00	900	5.40	12.6
8	1830	0.60	780	5.40	12.5
13	1570	0.17	760	4.50	14.0
23	1630	0.10	600	4.20	14.5
33	2012	0.10	400	4.70	13.5
43	2250	0.60	300	5.10	13.2

Input Conditions		Exhaust Concentrations	
Speed	1500 rpm	NO_x	1718 ppm
Equivalence Ratio (nominal)	.35	CO	0.10 percent
Timing (ATDC)	-20.0	UHC	0
Swirl Level	Medium	CO_2	5.2 percent
Fuel Injector	6	O_2	12.7 percent

Sample Valve Location

R = 3.9 cms

θ = 15° from jet axis

Z = 0 depth (cms)

Sampling Time (o)	NO_x ppm	CO %	UHC ppm	CO_2 %	O_2 %
-22	180	0.05	170	0.25	19.6
-12	139	5.40	240	2.30	11.2
- 7	519	7.60	6800	4.60	7.0
- 2	475	2.00	1100	3.60	13.0
3	895	1.00	570	4.00	15.1
8	1304	0.50	450	3.60	14.7
13	1347	0.30	370	3.40	15.7
23	911	0.15	120	3.00	16.0
33	1160	0.16	100	2.40	17.5
43	1048	0.15	100	3.20	16.5

Input Conditions		Exhaust Concentrations	
Speed	1500 rpm	NO_x	1765 ppm
Equivalence Ratio (nominal)	.35	CO	0.06 percent
Timing (ATDC)	-20.0	UHC	0
Swirl Level	Medium	CO_2	5.1 percent
Fuel Injector	6	O_2	13.2 percent

Sample Valve Location

R = 3.9 cms

$\theta = 30^{\circ}$ from jet axis

Z = 0 depth (cms)

Sampling Time (o)	NO_x ppm	CO %	UHC ppm	CO_2 %	O_2 %
-22	150	0.06	170	0.40	19.8
-12	158	1.10	240	2.40	16.0
- 7	1700	4.20	500	8.00	5.5
- 2	2020	4.80	600	7.80	5.0
3	1373	1.40	300	7.10	8.8
8	1017	0.53	280	4.40	13.5
13	970	0.24	240	3.80	14.5
23	1140	0.18	210	3.40	15.2
33	1045	0.18	150	3.70	15.2
43	1000	0.16	140	3.40	15.6

Input Conditions		Exhaust Concentrations	
Speed	1500 rpm	NO_x	1824 ppm
Equivalence Ratio (nominal)	.35	CO	0.07 percent
Timing (ATDC)	-20.0	UHC	0
Swirl Level	Medium	CO_2	5.0 percent
Fuel Injector	6	O_2	13.2 percent

Sample Valve Location

R = 3.9 cms

$\theta = 45^{o}$ from jet axis

Z = 0 depth (cms)

Sampling Time (o)	NO_x ppm	CO %	UHC ppm	CO_2 %	O_2 %
-22	147	0.05	100	0.30	19.8
-12	148	0.70	120	0.33	19.8
- 7	825	0.60	125	3.80	14.5
- 2	2145	1.00	105	7.00	9.7
3	2268	2.00	98	7.40	8.3
8	1600	1.00	95	5.60	11.5
13	1300	0.30	80	4.00	14.0
23	1430	0.10	70	4.10	14.5
33	1400	0.08	70	4.00	15.0
43	1275	0.07	70	3.70	15.2

Input Conditions		Exhaust Concentrations	
Speed	1500 rpm	NO_x	2156 ppm
Equivalence Ratio (nominal)	.35	CO	0.15 percent
Timing (ATDC)	-20.0	UHC	0
Swirl Level	Medium	CO_2	5.3 percent
Fuel Injector	6	O_2	12.0 percent

Sample Valve Location

R = 5.6 cms

θ = 0° from jet axis

Z = 0 depth (cms)

Sampling Time (o)	NO_x ppm	CO %	UHC ppm	CO_2 %	O_2 %
-22	211	0.20	50	0.65	19.5
-12	270	1.00	125	1.40	17.8
- 7	183	2.00	550	2.60	15.8
- 2	620	1.20	200	2.00	17.1
3	940	2.70	150	4.80	11.2
8	2150	4.00	95	7.50	5.5
13	2647	2.20	80	7.70	7.0
23	2976	0.55	0	8.00	8.2
33	2704	0.30	0	7.00	9.0
43	2530	0.25	0	6.60	9.4

Input Conditions		Exhaust Concentrations	
Speed	1500 rpm	NO_x	2200 ppm
Equivalence Ratio (nominal)	.35	CO	0.09 percent
Timing (ATDC)	-20.0	UHC	0
Swirl Level	Medium	CO_2	6.0 percent
Fuel Injector	6	O_2	12.2 percent

Sample Valve Location

R = 5.6 cms

θ = 30° from jet axis

Z = 0 depth (cms)

Sampling Time (o)	NO_x ppm	CO %	UHC ppm	CO_2 %	O_2 %
-22	160	0.11	250	0.32	20.0
-12	132	0.15	400	0.32	20.1
- 7	887	4.00	360	6.60	8.1
-2	570	10.00	1000	4.60	4.1
3	1200	5.20	310	6.60	6.5
8	1694	1.05	280	6.50	11.4
13	1860	0.65	240	5.80	12.5
23	1540	0.30	160	4.60	13.8
33	880	0.20	70	3.40	17.2
43	928	0.20	90	4.40	17.0

Input Conditions		Exhaust Concentrations	
Speed	1500 rpm	NO_x	1570 ppm
Equivalence Ratio (nominal)	.35	CO	0.10 percent
Timing (ATDC)	-20.0	UHC	800 ppm
Swirl Level	Low	CO_2	5.4 percent
Fuel Injector	6	O_2	13.0 percent

Sample Valve Location

R = 2.7 cms

$\theta = 30^{\circ}$ from jet axis

Z = 0 depth (cms)

Sampling Time (o)	NO_x ppm	CO %	UHC ppm	CO_2 %	O_2 %
-22	115	0.00	310	0.60	20.0
-17	90	0.00	480	0.30	20.0
-12	96	0.60	1700	1.00	18.5
- 7	410	1.70	2500	4.40	13.5
- 2	745	1.00	900	4.60	13.5
3	708	0.30	640	4.00	15.2
8	690	0.15	500	3.80	16.0
13	710	0.15	460	3.30	16.2
18	720	0.15	380	3.20	16.2
28	760	0.10	300	3.00	16.5
38	840	0.15	240	3.20	16.7

Input Conditions		Exhaust Concentrations	
Speed	1500 rpm	NO_x	1539 ppm
Equivalence Ratio (nominal)	.35	CO	0.10 percent
Timing (ATDC)	-20.0	UHC	0
Swirl Level	Low		
Fuel Injector	6	CO_2	5.6 percent
		O_2	12.8 percent

Sample Valve Location

R = 3.9 cms

$\theta = 0^{\circ}$ from jet axis

Z = 0 depth (cms)

Sampling Time (o)	NO_x ppm	CO %	UHC ppm	CO_2 %	O_2 %
-22	76	0.06	500	0.35	19.9
-12	155	3.00	5000	2.10	15.0
-7	622	7.00	5500	6.00	6.0
-2	930	4.40	1700	6.70	8.5
3	1489	1.80	770	6.10	11.1
8	1618	0.75	660	5.40	13.1
13	1537	0.30	610	5.10	13.8
23	1623	0.18	500	5.00	14.2
33	1540	0.10	0	4.40	14.2
43	1255	0.12	0	4.00	14.8

Input Conditions		Exhaust Concentrations	
Speed	1500 rpm	NO_x	1463 ppm
Equivalence Ratio (nominal)	.35	CO	0.01 percent
Timing (ATDC)	-20.	UHC	0
Swirl Level	Low	CO_2	5.1 percent
Fuel Injector	6	O_2	13.4 percent

Sample Valve Location

R = 3.9 cms

θ = 15° from jet axis

Z = 0 depth (cms)

Sampling Time (o)	NO_x ppm	CO %	UHC ppm	CO_2 %	O_2 %
-22	163	0.06	200	0.31	20.1
-12	138	5.40	240	2.80	11.5
- 7	462	10.00	7600	5.00	3.8
- 2	1120	5.20	1800	6.20	7.3
3	1203	1.30	540	5.20	11.5
8	1153	0.70	420	4.40	13.5
13	1178	0.28	320	4.20	14.7
23	950	0.20	250	4.00	15.2
33	960	0.18	150	4.00	15.1
43	1110	0.20	110	3.80	15.5

Input Conditions		Exhaust Concentrations	
Speed	1500 rpm	NO_x	1620 ppm
Equivalence Ratio (nominal)	.35	CO	0.06 percent
Timing (ATDC)	-20.0	UHC	0
Swirl Level	Low	CO_2	5.1 percent
Fuel Injector	6	O_2	13.2 percent

Sample Valve Location

R = 3.9 cms

θ = 30° from jet axis

Z = 0 depth (cms)

Sampling Time (o)	NO_x ppm	CO %	UHC ppm	CO_2 %	O_2 %
-22	242	0.04	200	0.45	19.9
-12	255	0.20	250	0.66	19.1
- 7	1455	1.40	310	6.60	10.5
- 2	1620	1.60	330	7.20	9.5
3	1550	1.00	280	6.80	9.8
8	1292	0.27	240	5.00	12.9
13	1250	0.10	200	4.60	14.0
23	1100	0.07	180	4.20	14.5
33	1080	0.08	140	3.60	15.2
43	1100	0.08	130	3.60	15.6

Input Conditions		Exhaust Concentrations		
Speed	1500 rpm	NO_x	2420	ppm
Equivalence Ratio (nominal)	.75			
Timing (ATDC)	-20.0	CO	0.35	percent
Swirl Level	Medium	UHC	0	
Fuel Injector	6	CO_2	10.8	percent
		O_2	4.5	percent

Sample Valve Location

R = 5.6 cms

θ = 0° from jet axis

Z = 0 depth (cms)

Sampling Time (o)	NO_x ppm	CO %	UHC ppm	CO_2 %	O_2 %
-22	300	0.46	35	1.2	19.5
-12	260	7.10	1250	4.5	7.2
-7	711	10.0	1000	6.2	1.2
-2	1080	10.0	800	6.6	0.1
3	1570	10.0	250	7.0	0.3
8	1870	7.0	140	8.5	2.5
13	1950	4.7	0	9.3	4.0
23	2640	2.5	0	10.5	3.2
33	2884	2.2	0	11.4	2.3
43	2920	2.6	0	11.6	1.3

Input Conditions		Exhaust Concentrations	
Speed	2100 rpm	NO_x	2440 ppm
Equivalence Ratio (nominal)	.60	CO	0.35 percent
Timing (ATDC)	-20.0	UHC	0
Swirl Level	Medium	CO_2	8.5 percent
Fuel Injector	6	O_2	8.3 percent

Sample Valve Location

R = 5.6 cms

$\theta = 0^{\circ}$ from jet axis

Z = 0 depth (cms)

Sampling Time (o)	NO_x ppm	CO %	UHC ppm	CO_2 %	O_2 %
-22	133	0.006	500	0.40	20.2
-12	680	0.200	500	1.20	19.0
- 7	1457	2.300	1700	7.90	7.4
-2	1366	5.700	550	8.70	3.9
3	1740	10.000	450	7.50	0.4
8	1370	5.000	300	8.50	5.0
13	1560	0.800	0	9.00	7.0
23	3080	1.070	0	11.00	4.2
33	3500	0.760	0	11.50	3.8
43	4020	0.500	0	11.3	4.2

Input Conditions		Exhaust Concentrations	
Speed	1500 rpm	NO_x	2253 ppm
Equivalence Ratio (nominal)	0.6	CO	0.05 percent
Timing (ATDC)	-20.	UHC	0
Swirl Level	Medium	CO_2	8.9 percent
Fuel Injector	4	O_2	8.9 percent

Sample Valve Location

R = 2.7 cms

θ = 0° from jet axis

Z = 0 depth (cms)

Sampling Time (°)	NO_x ppm	CO %	UHC ppm	CO_2 %	O_2 %
-22	153	.06	250	1.0	19.5
-12	130	.40	600	0.8	19.9
- 7	300	.65	1000	1.3	19.1
- 2	1080	.10	4000	3.5	16.8
3	1640	.20	1700	4.3	15.0
8	2100	.93	150	6.0	11.5
13	2340	.85	150	6.4	11.0
23	2411	.25	120	5.7	12.5
33	2600	.04	100	5.9	12.2
43	2722	.20	95	7.2	11.5

Input Conditions		Exhaust Concentrations	
Speed	1500 rpm	NO_x	2450 ppm
Equivalence Ratio (nominal)	0.6	CO	0.05 percent
Timing (ATDC)	-20.	UHC	0
Swirl Level	Medium	CO_2	8.5 percent
Fuel Injector	4	O_2	8.4 percent

Sample Valve Location

R = 2.7 cms

θ = 54° from jet axis

Z = 0 depth (cms)

Sampling Time (o)	NO_x ppm	CO %	UHC ppm	CO_2 %	O_2 %
-22	131	0.05	125	0.6	19.9
-12	402	0.80	150	4.0	15.0
- 7	1500	2.50	300	7.0	9.0
- 2	1600	5.00	900	7.0	6.0
3	1000	4.00	1000	4.8	8.8
8	1566	0.60	200	3.0	15.0
13	1840	0.20	150	4.9	13.2
23	2692	0.20	120	7.1	11.0
33	3500	0.30	100	8.1	9.5
43	3250	0.20	75	8.1	8.9

Input Conditions		Exhaust Concentrations	
Speed	1500 rpm	NO_x	2100 ppm
Equivalence Ratio (nominal)	0.6	CO	0.07 percent
Timing (ATDC)	-20.	UHC	0
Swirl Level	Medium	CO_2	8.9 percent
Fuel Injector	4	O_2	8.6 percent

Sample Valve Location

R = 3.9 cms

θ = 0° from jet axis

Z = 0 depth (cms)

Sampling Time (°)	NO_x ppm	CO %	UHC ppm	CO_2 %	O_2 %
-22	106	0.04	200	0.4	20.3
-12	91	0.38	750	0.5	20.0
- 7	124	0.55	850	0.7	19.5
- 2	1333	0.15	300	3.5	15.9
3	2240	1.20	280	5.4	12.0
8	2258	0.75	250	6.6	11.0
13	2440	0.60	210	6.0	11.9
23	2140	0.55	210	6.5	11.0
33	1519	0.30	160	5.4	12.5
43	1360	0.20	140	5.0	13.5

Input Conditions		Exhaust Concentrations	
Speed	1500 rpm	NO_x	2120 ppm
Equivalence Ratio (nominal)	0.6	CO	0.05 percent
Timing (ATDC)	-20.	UHC	0
Swirl Level	Medium	CO_2	8.7 percent
Fuel Injector	4	O_2	8.8 percent

Sample Valve Location

R = 3.9 cms

θ = 33° from jet axis

Z = 0 depth (cms)

Sampling Time (°)	NO_x ppm	CO %	UHC ppm	CO_2 %	O_2 %
-22	80	0.1	260	1.0	20.0
-12	156	3.0	900	3.2	14.0
- 7	435	8.0	2200	5.5	7.5
- 2	350	6.0	2800	4.3	9.2
3	290	3.8	700	4.4	11.0
8	1008	0.6	380	4.4	14.0
13	1540	0.5	240	4.5	13.8
23	2000	0.6	200	7.5	9.5
33	1730	0.7	120	9.2	6.8
43	1670	0.7	120	9.5	6.5

Input Conditions		Exhaust Concentrations	
Speed	1500 rpm	NO_x	2364 ppm
Equivalence Ratio (nominal)	0.6	CO	0.1 percent
Timing (ATDC)	-20.	UHC	0
Swirl Level	Medium	CO_2	8.6 percent
Fuel Injector	4	O_2	8.5 percent

Sample Valve Location

R = 5.6 cms

θ = 45° from jet axis

Z = 0 depth (cms)

Sampling Time (°)	NO_x ppm	CO %	UHC ppm	CO_2 %	O_2 %
-22	197	0.9	110	0.9	18.8
-12	357	3.0	160	3.8	13.5
- 7	362	10.0	380	4.4	1.8
- 2	477	10.0	1600	3.8	1.2
3	1040	10.0	5000	5.2	2.1
8	1450	4.8	1000	6.8	7.1
13	1640	1.3	360	5.8	11.2
23	2620	1.4	300	7.5	8.2
33	2734	1.0	120	8.4	8.1
43	2380	1.1	100	8.5	8.5

TECHNICAL REPORT DATA
(Please read Instructions on the reverse before completing)

1. REPORT NO.	2.	3. RECIPIENT'S ACCESSION NO.
EPA-460/3-76-008-a		

4. TITLE AND SUBTITLE
Study of the Oxides of Nitrogen and Carbon Formation in Diesel Engines

5. REPORT DATE
Issued May 1976

6. PERFORMING ORGANIZATION CODE

7. AUTHOR(S)
C. J. Kau, T. J. Tyson, M. P. Heap

8. PERFORMING ORGANIZATION REPORT NO.

9. PERFORMING ORGANIZATION NAME AND ADDRESS
Ultrasystems, Inc.
2400 Michelson Drive
Irvine, California 92715

10. PROGRAM ELEMENT NO.

11. CONTRACT/GRANT NO.
68-01-0436

12. SPONSORING AGENCY NAME AND ADDRESS
U.S. Environmental Protection Agency
Office of Air and Waste Management
Office of Mobile Source Air Pollution Control
Ann Arbor, Michigan 48105

13. TYPE OF REPORT AND PERIOD COVERED
Final Report June '73-June '76

14. SPONSORING AGENCY CODE

15. SUPPLEMENTARY NOTES
Co-sponsor: Coordinating Research Council, 30 Rockefeller Plaza, New York, New York, 10020

16. ABSTRACT

A mathematical model describing heat release and pollutant formation in direct injection diesel engines has been developed and tested. The model includes several empirical constants which can be tuned to fit the requirements of a particular engine. Sensitivity studies indicate that the model is most responsive to those constants which control fuel/air mixing. Numerical experiments strongly suggest that diffusion flames modelled by spherical droplet flames are unsuitable for this type of system. The model has been tested against results obtained with a single cylinder diesel engine. Reasonable predictions of the influence of engine design and operation parameters on NO_x emissions were obtained. However, predictions of smoke emissions were not satisfactory.

17. KEY WORDS AND DOCUMENT ANALYSIS

a. DESCRIPTORS		b. IDENTIFIERS/OPEN ENDED TERMS	c. COSATI Field/Group
Diffusion Flames	Mathematical Modeling	Mobile Sources	21-07 (Reciprocating Engines)
Air Pollution	Soot	Exhaust Gas Recirculation	21-02 (Combustion)
Diesel Engines	Computer Program	Divided Chamber Engine	
Combustion	Fuel Sprays		
Emission	Internal Combustion Eng		
Nitric Oxide (NO)	Fuel Comsumption		
Nitrogen Oxides			
Smoke			

18. DISTRIBUTION STATEMENT	19. SECURITY CLASS *(This Report)*	21. NO. OF PAGES
Release Unlimited		206
	20. SECURITY CLASS *(This page)*	22. PRICE

EPA Form 2220-1 (9-73)